INFLAMMASOMES AND GASDERMINS IN IMMUNE DEFENSE AND PATHOLOGY

Stephen Bela Kovacs

A dissertation submitted to the faculty at the University of North Carolina at Chapel Hill in partial fulfillment of the requirements for the degree of Doctor of Philosophy in the Department of Microbiology and Immunology.

Chapel Hill
2021

Approved by:

Edward Miao

Zhi Liu

Mohanish Deshmukh

Jenny Ting

Helen Lazear

ABSTRACT

Stephen Bela Kovacs: Inflammasomes and gasdermins in immune defense and pathology
(Under the direction of Edward Miao)

Pyroptosis is a form of programmed cell death that effectively defends against intracellular pathogens by lysing an infected cell, thereby removing the pathogens' replicative niche, and by releasing danger-associated molecular patterns and the pro-inflammatory cytokines interleukin (IL)-1β and IL-18, thereby promoting an immune response. However, when activated at the incorrect time or in excess, pyroptosis can cause significant pathology.

Pyroptosis was traditionally considered to primarily occur in monocytes and macrophages and, as a result, most studies of pyroptosis to date utilized monocytes and macrophages. Recently, the role of pyroptosis in defending non-immune cells, most notably intestinal epithelial cells, has been appreciated. Furthermore, with the recent discovery that gasdermin D was the direct mediator of pyroptosis in macrophages and monocytes, we now know that there is an entire gasdermin family with similar pore-forming and lytic capabilities, each with a specific expression pattern in different tissue compartments. Consequently, it is essential to improve our understanding about how inflammasomes and various members of the gasdermin family trigger pyroptosis and interface with immune responses not just in macrophages, but also in other cell types and tissues as well.

To explore this concept, we first compared the role of inflammasomes and gasdermin D in neutrophils versus macrophages during infection with the environmental pathogen

Burkholderia thailandensis. Second, we completed the first steps for generating a cell-specific knockout line of gasdermin D. Third, we explored the gasdermin family by specifically focusing on the keratinocyte-specific gasdermin A, and by performing a molecular evolutionary analysis of the gasdermin family as a whole.

TABLE OF CONTENTS

LIST OF TABLES

LIST OF FIGURES

LIST OF ABBREVIATIONS

BFA	Brefeldin A
BP	Bullous pemphigoid
Gsdma	Gasdermin A
Gsdmb	Gasdermin B
Gsdmc	Gasdermin c
Gsdmd	Gasdermin d
Gsdme	Gasdermin e
IFN-γ	Interferon-γ
IL-1β	Interleukin-1β
IL-18	Interleukin-18
LPS	Lipopolysaccharide
Pjvk	Pejvakin
WT	Wild-type

CHAPTER 1: INTRODUCTION[1]

Intrinsic and extrinsic cell death pathways defend against pathogens

The immune system actively surveys the extracellular space with phagocytes, including macrophages and neutrophils, that phagocytose bacteria, fungi, and parasites. Many pathogens invade host cells and, consequently, avoid phagocytes. The host engages cell intrinsic defenses to kill intracellular pathogens, such as autophagy to return cytosolic pathogens into lysosomes where they can be degraded. Having evolved in this context, successful intracellular pathogens evade these defenses. The continued existence of the infected host cell as a permissive niche threatens the host. The solution is that this infected cell must be killed.

Killing of infected cells can be accomplished through either cell-intrinsic or cell-extrinsic mechanisms. If the cell itself can identify its compromised state, it will activate cell-intrinsic death mechanisms that include cell-intrinsic apoptosis, necroptosis, and pyroptosis. However, many intracellular pathogens evade or inhibit cell-intrinsic programmed cell death. Our last lines of defense are cytotoxic cells in the innate and adaptive immune systems, including natural killer cells and cytotoxic T lymphocytes, that can induce cell-extrinsic apoptosis of infected cells. Our laboratory compared these forms of cell death in a recent review[1]. Recently, gasdermin D was discovered to form a pore and act as the effector for pyroptosis, (cell-intrinsic programmed

[1]This chapter was adapted from a review published in *Trends in Cell Biology*. The original citation is as follows: Kovacs SB, Miao EA. Gasdermins: Effectors of Pyroptosis. Trends Cell Biol. 2017 Sep;27(9):673-684. SBK wrote and edited this review under the guidance of EAM.

lysis). Gasdermin D is one of six gasdermin proteins, most of which have now been shown to have pore-forming activity.

Inflammasomes survey the cytosol for contamination or perturbation

Inflammasomes are innate immune sensors that survey the cytosol for contamination or cellular perturbation, and in response they trigger pyroptosis. For example, the NAIP/NLRC4 inflammasome detects bacterial type III and type IV secretion systems when they aberrantly inject rod, needle, or flagellin protein into the cytosol[2]. Once activated, the NAIP/NLRC4 inflammasome activates the protease caspase-1, which in turn cleaves the inflammatory cytokines pro-IL-1β and pro-IL-18 to their mature forms and also triggers pyroptotic membrane rupture. Other caspase-1-activating inflammasomes respond to cytosolic contamination by DNA (AIM2) or proteases (NLRP1), to perturbations within the Rho GTPases (Pyrin), or to catastrophic disruption of cellular physiology (NLRP3)[2].

In parallel, murine caspase-11, and its humans orthologs caspase-4 and -5, independently activate pyroptosis but cannot directly cleave pro-IL-1β and pro-IL-18. Unlike all other caspases, caspase-11/4/5 are activated by direct interaction with cytosolic LPS[2].

Inflammasomes defend against numerous pathogens, although many pathogens evade detection. However, when aberrantly activated, inflammasomes drive immunopathology and sepsis.

Pyroptosis defends against intracellular infection

Pyroptosis can defend against intracellular infection by eliminating the compromised cell, thereby removing the pathogen's protective niche, and simultaneously eliciting an inflammatory

response. The utility of pyroptosis against intracellular pathogens can be studied by engineering normally evasive bacteria to be detected by inflammasomes. For example, *Salmonella* Typhimurium and *Listeria monocytogenes,* which evade inflammasomes during systemic infection by repressing flagellin, among other strategies[1], have been engineered to force flagellin expression during the intracellular phase of infection. These modified bacteria reveal that pyroptosis kills the compromised host cell but does not kill the intracellular bacteria[1]. These bacteria remain trapped within the corpse of the pyroptotic cell in a structure we term the pore-induced intracellular trap (PIT)[3] (Figure 1). The PIT holds the bacteria in place and simultaneously elaborates neutrophil chemoattractants[3,4] including DAMPs and eicosanoids[5]. Neutrophils, or perhaps ROS-producing macrophages[6], then engulf and kill the trapped bacteria when they efferocytose the PIT[3,4].

Pyroptosis is perhaps most effective in defense against bacteria that never evolved in the context of hosts with inflammasomes. *Chromobacterium violaceum* and *Burkholderia thailandensis* are two environmental bacteria with the strongest known phenotypes of infection in inflammasome-deficient mice[7,8] (reviewed further in [9]). Pyroptosis is implicated as a major defense mechanism against these ubiquitous environmental pathogens.

Gasdermin D pores are the effectors of pyroptosis

Cleaved gasdermin D oligomerizes to form the pyroptotic pore

Cleavage of gasdermin D was recently discovered to be the mechanism by which Caspase-1 and -11 trigger pyroptosis[10-12]. Gasdermin D is expressed in immune cells and in intestinal epithelial cells[13,14]. In humans, gasdermin D is composed of a 242 amino acid (aa) amino-terminal domain (also called N-domain, NT, or gasdermin domain) connected by a 43 aa

linker to a 199 aa carboxy-terminal domain (also called C-domain or CT) (Figure 2). The amino-terminal domain forms a gasdermin pore[15,16], and thus we propose to term it the "pore-forming domain" (PFD). This pyroptotic pore forming activity has been demonstrated for most gasdermins[10,15]. However, this activity is held in check by the carboxy-terminal domain[10], which we propose to term as the "repressor domain" (RD). After the linker is cleaved, the RD separates from the PFD. The liberated PFD then integrates into the cell membrane, where an estimated 16 PFD monomers oligomerize to form a large 10-15 nm diameter pore[15-17]; another group suggests 21 nm[18].

The predicted structure of gasdermin D, based on the crystal structure of full length gasdermin A3 (discussed below) and more recently supported by the crystal structure of the C-terminal domain of gasdermin D, reveals an interesting mechanism of autoinhibition. The PFD and RD interact by a large surface area between these domains. The linker domain ties the two domains together at one end of the structure, while the α4 helix of the PFD extends far across the C-domain to the opposite end, where it binds to a pocket in the RD[15,19]. Upon activation, either caspase-1 or -11 cleaves the linker after amino acid 275 at a conserved (F/L)LTD motif[10,11]. Of note, the C-terminal domain contains an interface that interacts with caspase-1 (caspase-11 was not tested) to increase caspase-1- gasdermin D interactions and improve cleavage efficiency[20]. Presumably, when the linker is cleaved, the interface dissociates, the α4 helix is released from its pocket, and the PFD is released from the RD (Figure 2). Interestingly, gasdermin D can also be cleaved by caspase-3 within the PFD[21], which should inactivate the PFD and thus prevent pyroptosis once caspase-3 initiates apoptosis.

The gasdermin D pore has affinity for liposomes containing lipids with double phosphates on the glycerol scaffold (cardiolipin) or phosphorylated head groups

(phosphatidylinositol phosphate PIP_1 and PIP_2 species), and it may have a lower affinity for triple-phosphorylated PIP_3 and the zwitterion head group phosphatidylserine (PS)[15,16]. Gasdermin D does not bind the non-charged head group lipid phosphatidylinositol (PI) or the positively charged head group lipids phosphatidylcholine (PC) or phosphatidylethanolamine (PE)[15,16]. Thus, gasdermin D has greatest affinity for lipid species whose head groups have negative charge. Since PIP species and PS are restricted to the cytosolic leaflet of the plasma membrane, gasdermin D can only form pores from the cytosolic face. Neighboring cells are thus protected from gasdermin D arising from adjacent cells[16]. Cardiolipin is a component of the inner mitochondrial membrane and bacterial membranes; it is unclear whether gasdermin D has access to the inner leaflet of the mitochondria.

Gasdermin D pore formation mediates pyroptosis

The open gasdermin D pore breaks the normal permeability barrier of the plasma membrane. The most catastrophic effect is disruption of the normal separation of sodium and potassium across the plasma membrane. Normally, the cytosol has a low concentration of sodium and a high concentration of potassium, which is reversed in extracellular fluid. This concentration gradient exists in the context of the electrical gradient across the plasma membrane that draws positive ions into the relatively negative cytosol. Consequently, when a pore opens in the plasma membrane, the forces created by the concentration gradient driving potassium out of the cell are roughly counterbalanced by the electrical forces that pull potassium into the cytosol, resulting in a minimal net potassium flux initially. In contrast, sodium is drawn into the cell by both its concentration gradient and the electrical gradient, resulting in a large inward sodium

flux. As sodium flows into the cytosol, it brings its hydrating water, causing the cell volume to increase.

If few gasdermin pores are present, the cell should react by initiating compensatory mechanisms to decrease volume, called the regulatory volume decrease. Among these are swelling-activated K^+, Cl^-, and organic osmolyte (e.g. taurine) channels that export these solutes and their accompanying water[22]. If the number of pores in the plasma membrane remains small, normal emergency exocytic membrane fusion events can patch out the pore-containing membrane. Indeed, the ESCRT machinery has been shown to remove gasdermin D pores, as well as the MLKL pores that trigger necroptosis[23-26]. One can also imagine a hypothetical cell where the quantity of gasdermin D is pre-set to such a low concentration that it never exceeds the regulatory volume decrease capacity and therefore never undergoes pyroptosis. Indeed, instances of sub-lytic activation of gasdermin D have been described by others[27]. Lack of lysis does not mean lack of consequence, though, as sub-lytic pore formation could lead to extracellular release of activated IL-1β and IL-18, as well as leakage of mitochondrial DNA into the cytoplasm with subsequent activation of the cGAS pathway of immune activation[27].

On the other hand, if gasdermin pores are present in numbers exceeding the cell's compensatory capabilities, cell volume inexorably increases. Once the volume exceeds membrane capacity, the plasma membrane separates from the cortical cytoskeleton in large fluid-filled "balloons". These "balloons" are distinct from apoptotic "blebs" by morphology and composition. Shortly thereafter, a membrane rupture event occurs that releases soluble cytosolic contents. This tear is large enough to immediately dissipate soluble proteins like LDH, but organelles are retained[3]. After the rupture event, we presume that osmotic pressure equalizes, stopping further volume increases.

In summary, two membrane-breaching events occur after caspase-1/11 activation: 1) the gasdermin D pore opens; and soon thereafter 2) the membrane ruptures (Figure 2). We use the term "pyroptosis" as synonymous with the membrane rupture event resulting from gasdermin pores[10]. Inflammasome activation has also been implicated in expulsion of intestinal epithelial cells (IECs) from the intestinal epithelium prior to pyroptosis in response to microbial infection. While gasdermin D is required for pyroptosis but dispensable for expulsion of IECs[28], the possibility remains that other gasdermins (discussed below) may play a role in IEC expulsion, either alone or with redundancy.

Gasdermin D pore as the IL-1β and IL-18 release mechanism

During pyroptosis, caspase-1 cleaves IL-1β and IL-18 to generate the mature cytokines prior to membrane rupture. As IL-1β and IL-18 lack a normal secretion signal, they are cytosol-restricted proteins. The possibility that pyroptotic membrane rupture was the release mechanism was at odds with observations of IL-1β release in the absence of pyroptosis[29-33]. Thus, whether these cytokines were actively secreted from cells or whether they were instead released by pyroptotic membrane rupture had remained confusing.

Remarkably, the 10-15 nm diameter of the gasdermin pore is large enough to allow passage of IL-1β (4.5 nm)[15,16] and IL-18 (5.0 nm). This explains the mechanism by which these proteins are released from cells prior to lysis. Importantly, the gasdermin pore is small enough to restrict larger molecules; 25-30 nm diameter ribosomes and larger organelles will not pass through the pore[3].

How can a cell release IL-1β/IL-18 through a gasdermin pore without lysing soon after? Theoretically, a cell with few gasdermin pores could shut off the inflammasome[34], remove the

pores through exocytic patching mechanisms[23,24,26], and thus survive. This would release IL-1β and IL-18 though a transient gasdermin pore without killing the cell[29-33]. An additional layer of complexity arises from the membrane patching event itself, which should release a membrane-bound exosome that contains not only the gasdermin pore, but also any processed IL-1β that is nearby, perhaps explaining IL-1β observed in microparticles[35,36].

Gasdermin pores may also target other membranes

The gasdermin D pore can insert into the bacterial membranes, which are rich in cardiolipin, and kill the bacteria, at least in vitro[16]. However, since bacteria survive pyroptosis[3,37], the physiologic relevance of bacterial membrane-targeting remains unclear. For vacuolar bacteria, the PFD would require passing through an existing gasdermin pore in the vacuole to oligomerize on the bacterial membrane; thus, vacuolar bacteria may have minimal exposure to the gasdermin pore. Indeed, we have shown that *S.* Typhimurium that has been engineered to trigger pyroptosis survives the pyroptotic event in vivo. Interestingly, while these bacteria survive, they are damaged during the process of pyroptosis[3]. This damage might be caused by the gasdermin D pore[16], but equally valid hypotheses include damage from rapid volume (and presumably pressure) shifts during pyroptosis or from ROS generated from mitochondria during pyroptosis[38]. For cytosolic bacteria, the gasdermin D pore should have direct access to bacterial membranes. This has been suggested to be toxic to *L. monocytogenes* in vitro[16], although *L. monocytogenes* and another cytosol-invasive bacterium survive pyroptosis in vitro in our hands[3]. Thus, bacteria remain alive in vivo after pyroptosis, but it remains unclear if pyroptosis damages bacteria to accelerate killing by secondary phagocytes that efferocytose these PIT-trapped bacteria.

Many organelles have cytosolic leaflets that are composed of lipids similar to the inner leaflet of the plasma membrane. If the gasdermin pore inserts into the endoplasmic reticulum, it would release calcium stores into the cytosol. This likely contributes to the calcium flux observed after caspase-1 activation but prior to pyroptosis[5,39]. The cytoplasmic leaflet of vacuoles also resembles the cytoplasmic leaflet of the plasma membrane. However, vacuolar fluid contents likely reflect the extracellular fluid. Therefore, insertion of the gasdermin pore into the vacuolar membrane would allow ionic flux that in theory should cause sodium to flow from the vacuole into the cytosol, thereby shrinking the vacuole. Thus, vacuolar bacteria may remain doubly trapped: first within the membrane-bound and compressed vacuole, and second within the PIT.

Gasdermin family

Gasdermin D is a member of a family of conserved proteins that includes gasdermin A, B, C, D, E, and DFNB59[10,40] (Table 1). Previously, gasdermin E and DFNB59 were proposed to be excluded from the gasdermin family, and instead called gasdermin-related proteins[14]; however, we prefer to simplify the nomenclature by including all six genes in a single gasdermin family, given recent advances[21,41]. Most family members maintain the same domain structure with significant similarity between the PFD and RD, but divergent linkers[10]. DFNB59 is an exception with a divergent, shorter C-terminal domain. The PFD of most members can induce cell death[10,11,15,21] (not yet examined for DFNB59). Whereas humans and most other mammals have one copy of each gasdermin, mice have triplicated gasdermin A (gasdermin A1-3), deleted gasdermin B, and quadruplicated gasdermin C (gasdermin C1-4). Each gasdermin member has a distinct and restricted pattern of expression as discussed below.

Gasdermin A

Gasdermin A is expressed in epithelial cells of the skin, tongue, esophagus, stomach, mammary glands, and umbilical cord[40,42,43]. In mice, gasdermin A1 is expressed primarily in suprabasal epidermis, hair follicles, and forestomach[14,43-45]; gasdermin A2 is expressed primarily in glandular stomach[40]; and gasdermin A3 is expressed primarily in suprabasal epidermis[14,43,44,46,47]. Multiple spontaneous mutations in gasdermin A3 have been associated with spontaneous alopecia and hyperkeratosis[44,46-50]. Histologically, inflammation and a resulting depletion of skin bulge stem cells have been observed in mice with *Gsdma3* mutations[49,51]. Additionally, one *Gsdma3* mutation causes defective of mammary gland development[52]. In contrast, gasdermin A3 knockout mice are phenotypically normal[43]. The alopecia phenotypes therefore likely result from gain-of-function mutations. Indeed, in vitro, these disease-causing mutations in gasdermin A3 result in an inability of the RD to effectively inhibit the PFD, causing increased spontaneous pore formation in the absence of linker cleavage[10]. These mutations therefore suggest that gasdermin A may play a role in causing inflammation within the skin. In humans, single nucleotide polymorphisms (SNPs) in *GSDMA* have been associated with asthma[53]. Only one study has suggests gasdermin A expression in the lung[54], consequently, the mechanism by which gasdermin A contributes to asthma remains unclear.

Gasdermin B

Like *GSDMA*, *GSDMB* SNPs are also associated with asthma in multiple populations[53,55-57]. Gasdermin B expression has been detected in lymphocytes, esophagus, stomach, liver, and colon[40,42]. While one group did not observe significant expression of gasdermin B in the lung[54], another group did observe gasdermin B in the lung and implicated it in influencing expression of

genes related to airway remodeling and hyper-responsiveness[58]. Furthermore, one disease-associated SNP causes an alteration in the conformational flexibility and surface charge of a region in the RD[59]. The *GSDMB* SNPs and the *GSDMB* region of chromosome 17q21 have been associated with several other immune diseases as well[60-67]. Since *GSDMA* and *GSDMB* are genetically linked to each other as well as ORMDL3 (a gene encoding a sphingolipid biosynthesis regulator with SNPs also associated with asthma) within chromosome 17q12-21, it may be that the linkage with asthma is either due to one or some combination of these genes. The study of gasdermin B in vivo will be more difficult because mice naturally lack the gene.

A recent report shows that gasdermin B can be cleaved by granzyme A[68], suggesting that gasdermin B promotes pyroptotic cell death downstream of cytotoxic immune cells including NK cells and $CD8^+$ cytotoxic T lymphocytes (CTLs). Therefore, NK or CTL attack can result in a cell dying by pyroptosis if granzyme A activates gasdermin B, or the cell may die by apoptosis if granzyme B activates caspase-8. It remains unclear how this decision is made, whether it is driven by the gasdermin expression in the target cell or the granzyme expression in the NK/CTL, and whether there is communication between the cells to change these expression patterns. This discovery suggests that gasdermin B may be particularly useful against viruses. However, mice lack gasdermin B, thereby limiting the ability to assess the function of gasdermin B using in vivo models. The physiologic relevance of this pathway during infections consequently remains unknown.

Gasdermin B has also reported to be cleaved by caspase-3, -6, and -7, but within the PFD[59], similar to PFD cleavage of gasdermin D[21]. Thus, both gasdermin B and gasdermin D may be inactivated during apoptosis to prevent pyroptosis after caspase-3 activates. However, this idea is must be reconciled with caspase-3 activating gasdermin E (see below), and with

gasdermin B being simultaneously activated by granzyme A and inactivated by granzyme B-activated caspase-3.

Gasdermin C

Little is known about the function of gasdermin C. Gasdermin C is expressed in esophagus, stomach, trachea, spleen, intestines, bladder, and skin[40,42]. Gasdermin C expression is increased in metastatic melanoma[69] but suppressed in esophageal and gastric cancer[13]. Furthermore, gasdermin C has recently been proposed to be activated by caspase-8 downstream of PD-L1 activation to promote pyroptosis of cancer cells. In mice, gasdermin C1, C2, and C4 are expressed in stomach, large and small intestines, bladder, and prostate while C3 is restricted to bladder, prostate, and large intestines[42].

Gasdermin E (DFNA5)

Mutations in *GSDME* are associated with development of heritable, nonsyndromal deafness (thus the original name: deafness autosomal dominant 5, DFNA5)[70-72]. *GSDME* is expressed in placenta, brain, heart, kidney, cochlea, intestines, and IgE-primed mast cells[40,42]. Deafness associated with *GSDME* is characterized by an autosomal dominant inheritance and gradual loss of hearing, typically starting at high frequency by age fifteen[73]. All known mutations in *GSDME* associated with deafness are characterized by skipping of exon 8, resulting in frameshifts and the formation of truncated gasdermin E protein[70-72]. The truncated RD fails to repress the PFD, resulting in a gain-of-function[41]. Knocking out *GSDME* in mice does not result in deafness[74].

Caspase-3 was recently shown to specifically cleave gasdermin E, which then forms pores in the plasma membrane and triggers lytic cell death in response to caspase-3 activators such as chemotherapeutic drugs, TNF, and viral infection[21,41]. Rogers et al. proposed that gasdermin E is the effector of secondary necrosis[21]; that is lysis of apoptotic cells after prolonged time if apoptotic cells are not efferocytosed. On the other hand, Wang et al. demonstrated that only specific cells express gasdermin E, and proposed that in such cells, caspase-3 activation is switched from driving an apoptotic program to causing pyroptosis[41]. Thus, certain cells may be programmed to undergo pyroptosis instead of apoptosis, at least under certain circumstances. *Gsdme*-knockout mice were shown to be resistant to the toxicity of chemotherapy drugs such as cisplatin[41].

It is reasonable to expect that gain-of-function mutations in gasdermin E could lead to progressive deafness by increasing susceptibility for cells within the auditory system to undergo programmed cell death. However, why hair cells in the ear are uniquely susceptible to this is unclear. Transcription of *GSDME* increases in response to p53 activation, and its expression is silenced in colorectal, gastric, and breast cancer, suggesting a possible role of gasdermin E in suppressing cancer[73]. To date, most of the research into gasdermin E has focused on its role in tumor immunology and chemotherapy cytotoxicity.

Pejvakin (DFNB59)

PJVK (also called *DFNB59*) encodes the protein pejvakin, which, like gasdermin E, is associated with deafness[75,76]. If pejvakin is later shown to form a pore, it may be appropriate to re-name it as “gasdermin F”. DFNB59 has been detected in hair cells of the inner ear and other cells of the auditory system, but it is also broadly expressed[75]. In humans, mutations in *PJVK* are

associated with autosomal recessive nonsyndromic sensorineural hearing loss with or without cochlear dysfunction[75,76]. Unlike *GSDME* mutations, *PJVK* mutations are heterogeneous, including both truncations and missense mutations (p.T54I or p.R183W). The Petit group observed that functional pejvakin in mice was necessary to allow existing peroxisomes to proliferate and protect cochlear sensory hair cells and auditory neurons from noise-induced generation of reactive oxidative species[77]. This same group later suggested that pejvakin is directly activated by the oxidation of cysteines on its C-terminal domain, thereby allowing pejvakin to detect ROS[78]. The ability of pejvakin to form pores and the possible role of pejvakin pore formation in mediating proliferation of peroxisomes remains unknown. One possibility is that pejvakin forms a pore to transport proteins into the peroxisomes necessary for peroxisome proliferation in response to increased ROS. Indeed, several PEX proteins are already known to mediate import of large proteins into peroxisomes through the formation of transient pores[79]. Alternatively, Defourney et al. suggest that pejvakin promotes peroxisome proliferation downstream of promoting autophagy of older peroxisomes[78], though this could also plausibly reflect activation of autophagy machinery in response to leakage secondary to pore formation. Another group has suggested that pejvakin instead functions through interactions with cytoskeletal proteins or through a structural role in hair cells[80].

Cell-specific roles of inflammasomes and gasdermins

Traditionally, pyroptosis was believed to occur predominantly in macrophages. As a result, most studies have been conducted using macrophages and most of our understanding of the pyroptotic pathways have thus been restricted to macrophages. However, it is now appreciated that pyroptosis does in fact occur not just in other immune cells, but even non-

immune cells like intestinal epithelial cells[28]. Furthermore, this discovery that gasdermin D triggers pyroptosis is particularly remarkable because the human genome encodes six proteins with the potential to form pores in the membrane and cause lysis, each with their own specific expression pattern and most of which are in fact not expressed in immune cells. Thus, we need to improve our understanding of the function of pyroptotic pathways in the diverse array of cell-types that we now know exhibit pyroptotic potential. The goal of my thesis was to expand our understanding of inflammasomes and gasdermins in various cell types, first by exploring the role of gasdermin D in other cell types and then by exploring the gasdermin family beyond gasdermin D.

Human gene	Alternate names	Mouse gene	Expression[a]	Activated by	Major disease associations
GSDMA	gasdermin (GSDM) gasdermin1 (GSDM1)	*Gsdma1* *Gsdma2* *Gsdma3*	Skin, tongue, esophagus, stomach, mammary glands, and umbilical cord	Unknown	Alopecia (GOF) Asthma
GSDMB	PRO2521, gasdermin-like (GSDML)	Absent	Lymphocytes, esophagus, stomach, liver, and colon	Granzyme A	Asthma and other immune diseases
GSDMC	MLZE	*Gsdmc1* *Gsdmc2* *Gsdmc3* *Gsdmc4*	Esophagus, stomach, trachea, spleen, intestines, bladder, and skin	Unknown	Unknown
GSDMD	GSDMDC1, DFNA5L	*Gsdmd*	Immune cells, stomach, esophagus, intestines	Caspase-1/11/4/5	Sepsis
DFNA5	gasdermin E (*GSDME*)	*Dfna5*	Placenta, brain, heart, kidney, cochlea, intestines, and IgE-primed mast cells	Caspase-3	AD congenital deafness (GOF)
DFNB59	Pejvakin, (PJVK)	*Dfnb59*	Inner ear hair cells, auditory system, broadly expressed in other tissues	Unknown	AR congenital deafness (LOF)

Table 1. Gasdermin family nomenclature and expression pattern.

[a]Expression data taken from [39-41 75]

[b]AD = autosomal dominant; AR = autosomal recessive; GOF = gain-of-function; LOF = loss-of-function

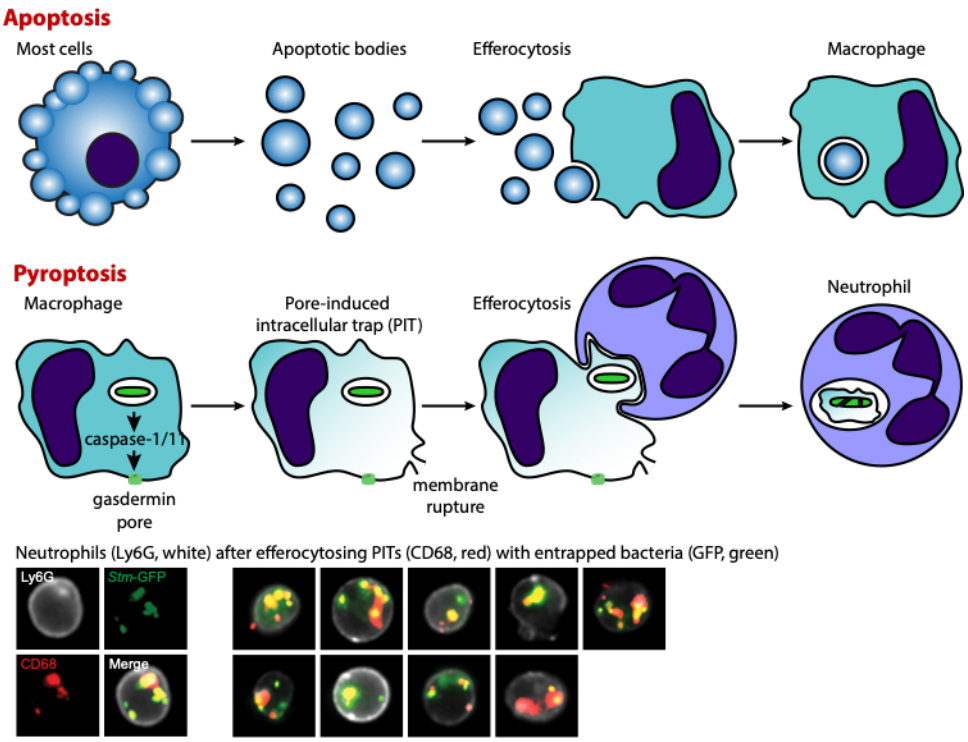

Figure 1. Pyroptosis converts cells into pore-induced intracellular traps (PITs). Whereas apoptosis converts cells into apoptotic bodies, pyroptosis converts cells into PITs. The membrane rupture event that defines pyroptosis immediately disperses soluble cytosolic contents. However, although torn, the plasma membrane remains largely intact such that organelles and live intracellular bacteria remain trapped within. This is different from the image of cellular debris, where all cellular contents are dispersed. Efferocytosis is the process whereby one cell phagocytoses another. Apoptotic bodies are typically efferocytosed by macrophages. In contrast, PITs are efferocytosed by neutrophils. These neutrophils then kill the previously intracellular, now PIT-trapped, bacteria. Pictures of neutrophils (marked by Ly6G, white) that have efferocytosed macrophage PITs (marked by CD68, red) that entrap intracellular bacteria (GFP, green) after the engineered bacteria are prompted to express flagellin and trigger pyroptosis of macrophages in vivo[3].

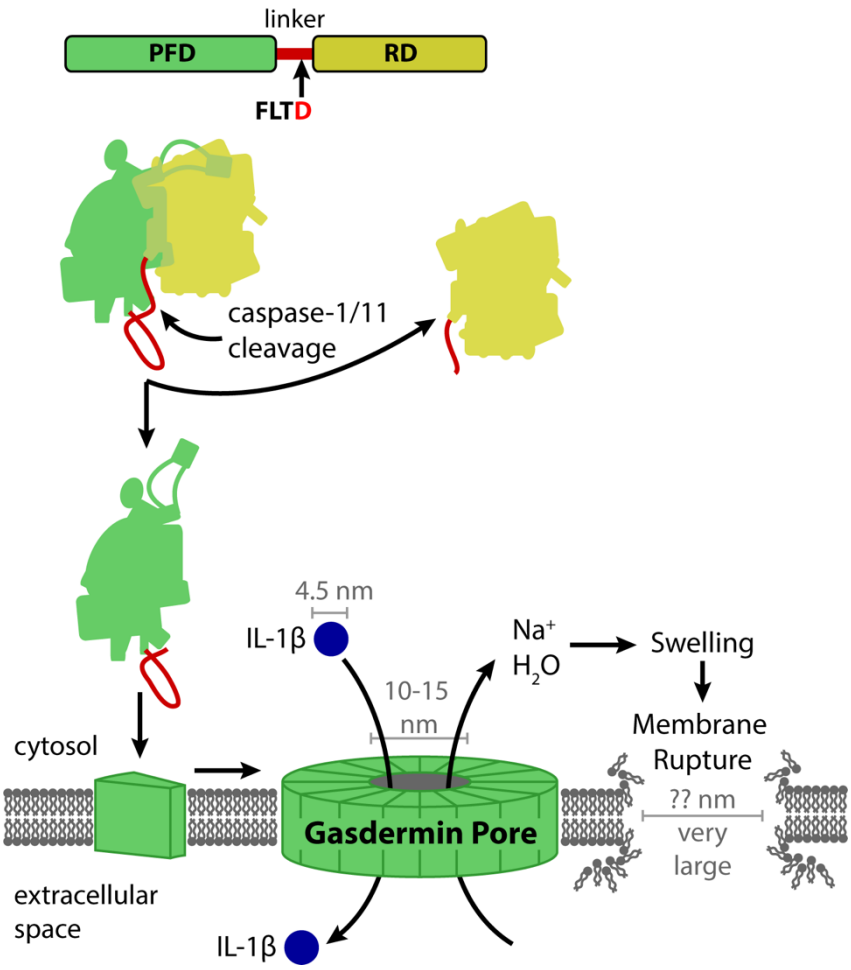

Figure 2. Caspase-1/11 activate the gasdermin D pore to cause pyroptosis. Caspase-1 is activated by various inflammasomes in response to contamination of the cytosol or perturbation of basic cellular homeostasis. Caspase-11 (mice) and caspase-4 and -5 (humans) activate by direct sensing of cytosolic LPS. Upon activation, these caspases cleave pro-IL-1β, pro-IL-18, and gasdermin D. Gasdermin D is composed of an amino-terminal pore-forming domain (PFD, green), a linker (red), and a carboxy-terminal repression domain (RD). The amino-terminal pore-forming domain (PFD) of gasdermin D then interacts with the plasma membrane and approximately 16 monomers oligomerize to form a gasdermin pore. The diameter of this pore is estimated in the range of 10-15 nm, which is large enough to release small proteins, including mature IL-1β (4.5 nm diameter), probably at a relatively slow rate. Simultaneously, sodium

enters the cell, bringing with it water that causes the cell volume to increase. This can rapidly exceed the volume capacity of the membrane, resulting in membrane rupture that is larger in size than the gasdermin pore, but smaller or on par with most organelles and intracellular bacteria. Upon membrane rupture, all remaining soluble cytosolic contents are released so rapidly as to be essentially instantaneous.

CHAPTER 2: EVALUATING CYTOKINE PRODUCTION BY FLOW CYTOMETRY USING BREFELDIN A IN MICE[2]

Introduction

Activation of inflammasome pathways often requires two signals: a priming signal, and an activating signal. The priming signal is important for ensuring that an inflammasome is only activated in the context of infection, thereby reducing the risk of damage due to aberrant activation. Priming both promotes transcription of components of the inflammasome pathways and post-translational modifications of existing proteins to allow the inflammasomes to activate[81]. For example, signaling downstream of any TLR can prime the NLRP3 inflammasome for activation[81]. Caspase-11, on the other hand, has stricter priming requirements. In vivo defense against the cytosol invasive bacterium *Burkholderia thailandensis* requires priming by IFN-γ[8]. This stricter priming may be due to the fact that the LPS sensed by caspase-11 is a ubiquitous molecule that can aberrantly be introduced into the cytosol even when the infecting pathogen lacks the virulence capacity to invade the cytosolic compartment. Therefore, identifying the source of IFN-γ during infection is significant.

During infection with *Burkholderia thailandensis*, IFN-γ production is induced by IL-18 within a day of infection to prime caspase-11, resulting in complete clearance of infection[8]. Given the swift kinetics of this IFN-γ production, we wanted to identify which cells were

[2]This chapter was adapted from a protocol previously published in *STAR Protocols*. The original citation is as follows: Kovacs, S. B., Oh, C., Aachoui, Y., & Miao, E. A. (2020). Evaluating cytokine production by flow cytometry using brefeldin A in mice. *STAR Protocols*, *2*(1), 100244. SBK optimized the protocol and wrote this entire section himself under the guidance of EAM and YA.

responding to IL-18 to produce this IFN-γ. Consequently, we needed to optimize a methodology to accurately identify cells producing IFN-γ in situ in a mouse model of infection. Cytokine reporter mice are limited by the need to cross markers into various knockout backgrounds, and by availability of reporters of interest. To overcome this, we utilize injection of brefeldin A into mice to enable flow cytometric analysis of in situ cytokine production during a bacterial infection. While we evaluate IFN-γ production during *Burkholderia thailandensis* infection, this protocol can be applied to other cytokines and other mouse models.

For complete details on the use and execution of this protocol, please refer to Kovacs et al. [82], as well as Liu et al.[83], the original publication from which we adapted this protocol.

Before you Begin

The investigator should be comfortable with any procedures involved with their particular in vivo model. Additionally, investigators should be proficient with injecting mice via the intravenous route, and the use of a flow cytometer with large multi-parameter capabilities (eg. LSR II).

Table 2: Key Resources Table

REAGENT or RESOURCE	SOURCE	IDENTIFIER
Antibodies		
Alexa Fluor (AF) 488 rat anti-mouse CD127 (clone A7R34)	BioLegend	Cat# 135017
Brilliant Violet (BV) 570 rat anti-mouse CD3 (clone 17A2)	BioLegend	Cat# 100225
APC-Cy7 rat anti-human/mouse CD45R (clone RA3-6B2)	BioLegend	Cat# 103223

APC-Cy7 rat anti-mouse Ly6G (clone 1A8)	BioLegend	Cat# 127623
PE-Cy7 rat anti-mouse CD90.2 (clone 53-2.1)	BioLegend	Cat# 140309
BV650 mouse anti-mouse NK1.1 (clone PK136)	BioLegend	Cat# 108735
BV421 Armenian hamster anti-mouse TCRγδ (clone GL3)	BioLegend	Cat# 118119
AF594 rat anti-mouse CD4 (clone GK1.5)	BioLegend	Cat# 100446
PE rat anti-mouse CD8 (clone 53-6.7)	BioLegend	Cat# 100708
APC rat anti-mouse IFN-γ (clone XMG1.2)	BioLegend	Cat# 505810
Bacterial and Virus Strains		
Burkholderia thailandensis, strain E264-1 (ATCC® 700388™ strain E264 that was previously passaged through *Casp1*$^{-/-}$*Casp11*$^{-/-}$ mice)	Aachoui et al., 2015	N/A
Chemicals, Peptides, and Recombinant Proteins		
LIVE/DEAD™ Fixable Blue Dead Cell Stain Kit	ThermoFisher Scientific	Cat# L23105
Experimental Models: Organisms/Strains		
Mouse: Wild type (WT): C57BL/6J	The Jackson Laboratory	JAX# 000664
Software and Algorithms		
FlowJo (we used version 9.9.6 for all figures in this protocol but recommend the most recent version, version 10.7)	TreeStar	N/A
Other		

Fixation/Permeabilization Solution kit	BD Biosciences	554714
Brilliant Stain Buffer	BD Biosciences	563794
UltraComp eBeads™ Compensation Beads	ThermoFisher Scientific	Cat# 01-2222

Materials and Equipment

Table 3: Extracellular antibody master mix

Antibody	**Dilution factor**
BV650 anti-mouse NK1.1	1:80
BV570 anti-mouse CD3	1:40
BV421 anti-mouse TCRγδ	1:40
AF488 anti-mouse CD127	1:320
PE-Cy7 anti-mouse CD90	1:400
APC-Cy7 anti-mouse Ly6G	1:1280
APC-Cy7 anti-human/mouse CD45R	1:320
AF594 anti-mouse CD4 (optional)	1:400
PE anti-mouse CD8 (optional)	1:160
Diluent	**Volume per sample**
Brilliant Stain Buffer	50 μL
FACS Buffer	Add until total volume is 100 μL

Note 1: CD4 and CD8 antibodies are included as optional because while these antibodies did provide adequate delineation of CD4 and CD8 T cell populations, the fluorophore-marker

combinations were not optimized, resulting in minor compensation issues. See Expected Outcomes for more details.

Note 2: All sample data included in figures in this protocol used FACS buffer as diluent without Brilliant Stain Buffer added. However, we recommend using Brilliant Stain Buffer in this panel or any other panel that utilizes multiple Brilliant Violet dyes to avoid potential nonspecific staining due to aggregation of these dyes that could affect your interpretation of your data. FACS buffer should be used when your panel includes one or fewer Brilliant Violet or other polymer-based dyes.

Table 4: Intracellular antibody master mix

Antibody	**Dilution factor**
APC anti-mouse IFN-γ	1:400
Diluent	BD Biosciences Perm/Wash buffer
Total volume (per sample)	100 µL

Table 5: ACK lysis buffer recipe

Reagent	**Final Concentration**	**Amount**
NH_4Cl	150 mM	4.01 g
$KHCO_3$	10 mM	0.5 g
Na_2EDTA	0.1 mM	18.6 mg
H_2O	N/A	500 mL
Total	**N/A**	**500 mL**
Titrate pH to 7.2-7.4; Store at room temperature (25-27°C)		

Table 6: FACS buffer

Reagent	**Final Concentration**	**Amount**
EDTA (0.5 M)	4 mM	4 mL
Bovine Serum Albumin (BSA)	0.5%	2.5g
PBS	N/A	496 mL
Total	**N/A**	**500 mL**
		Store at 4°C

Step-by-Step Method Details

Prepare bacterial inoculum

For this protocol, we will describe staining for in situ cytokine production by lymphocytes during *Burkholderia thailandensis* infection. The inoculation protocol should be adjusted to fit the infection or treatment protocol of interest. Figure 3 summarizes the protocol.

Timing: 2-3 days

1. Grow a bacterial culture.
    a. Two to three days prior to infection, streak out *Burkholderia thailandensis* from frozen stock onto a Luria-Bertani (LB) plate, and grow for one to two days at 37°C.

    Note: Plates of streaked *B. thailandensis* can be stored for up to a week at 4°C.

b. Inoculate a 1.5 mL liquid LB culture with a single colony and grow for 16 hours at 37°C in a shaking incubator to achieve stationary phase.

Pause point: If mice will not be infected immediately at the end of this 16 hour incubation, place the bacteria on ice until ready to infect mice.

2. Prepare the inoculum.
    a. Pellet the 1.5 mL liquid culture of bacteria by spinning in a microcentrifuge at 3000xg for 1 minute.
    b. Remove the supernatant and resuspend in 1 mL PBS to wash the bacteria. Spin at 3000xg for 1 minute. Repeat for a total of two PBS washes. Resuspend in 1 mL PBS.
    c. Estimate the concentration of bacteria using an OD_{600} as determined using a spectrometer.
        i An OD_{600} of 1.00 is approximately $1x10^9$ CFU/mL of *B. thailandensis*. The relationship between OD_{600} and CFU is approximately linear below OD_{600} of 1.00. Dilute the bacteria until its OD_{600} is less than 1.00.
        ii Calculate concentration using the following equation:

            Concentration (in CFU/mL) = OD_{600} x $1x10^9$ CFU/mL x dilution factor
    d. Dilute the inoculum with PBS to $2x10^7$ CFU per 200 μL (the volume for each inoculum injection).
    e. Verify inoculum via spot dilution plating.
        i Create a total of eight (including undiluted) 1:10 serial dilutions of the inoculum in PBS.

ii Plate 10 μL of each dilution in triplicate on an LB plate using a spot plating method (or plate 100 μL if using a whole plate method).

iii Incubate overnight (14-16hrs) at 37°C.

iv Looking at the dilution which has approximately 10-50 colonies per spot, count and average the number of colonies per spot.

v Calculate actual inoculum using the following formula:

Inoculum (in CFU/mouse) = average # colonies x dilution factor x 20

Infect and treat mice with brefeldin A

We next infect the mice and, after waiting enough time to allow immune responses to establish, treat mice with the Golgi blocker brefeldin A (BFA). Since most cytokines are processed and secreted through the classical secretory pathway that passes through the Golgi apparatus, BFA prevents the secretion of cytokines, causing their accumulation within the immune cells for eventual detection by flow cytometry. Thus, treating mice with BFA allows for the evaluation of in situ cytokine production without requiring the use of reporter mice. Consequently, mice of any genetic background can be used, allowing the evaluation of the effects of knocking out genes on cytokine production without prior crossing of knockout mice onto a reporter background. For example, we successfully evaluated cytokine production in both wild type and *Rag1*$^{-/-}$ mice[82].

Our timings for this experiment were based on known kinetics of *B. thailandensis* infection in wild type mice. The time point in each mouse model will vary, but the timing of injecting BFA 6 hours prior to euthanizing the mice is important to allow for adequate accumulation of cytokines within cells.

Timing: 1 day

3. Inject mice intraperitoneally with 200 µL of the inoculum created in step 2. Uninfected control mice should be injected with 200 µL of PBS as a mock infection.
4. Twelve hours after infection, treat mice with BFA.
    a. Dilute BFA stock.
        i BFA stock should be reconstituted in DMSO to a concentration of 20 mg/mL.

        Note: BFA stock can safely be stored at -20°C for at least a year.

        ii Further dilute working solution to 0.5 mg/mL in PBS. Keep this solution at room temperature (RT; 25-27°C) in order to avoid injecting a large volume of cold liquid into the mice. Do not reuse working solution.
    b. Inject 500 µL of working solution of BFA intravenously into the tail vein of both infected and uninfected mice.
        i **Note:** This volume was used in the original publication by Liu et al. [83]. We did not attempt to optimize the injection volume, as this volume worked for our studies. Considerations include whether the volume used enhances BFA exposure throughout the body or reduces cytotoxic effects by dilution of BFA (Troubleshooting 2).
5. Six hours after injecting BFA, euthanize mice and promptly harvest spleens per your institution's animal guidelines. Keep spleens in PBS and on ice until all samples are ready to process.

    Alternative: While keeping the spleens in PBS is sufficient over a short duration when harvesting spleens and immediately proceeding to the next steps, consider keeping

spleens in serum-free media such as DMEM for longer durations to avoid loss of cell viability. Cells can be maintained in this media until RBC lysis.

Note: Until cells have been fixed, cells are still alive and actively producing cytokines, albeit in a manner no longer reflective of the in situ setting. While the cell populations and their cytokine productions are likely stable at this point for a short period, it is advisable to proceed to the next steps through cell fixation (step 27) as soon as possible.

CRITICAL: The exact timing of these injections will depend on the infection and model being tested. In this case, we have optimized the time points of our infection (18 hour total infection time) to view cytokine production during innate immune responses to *B. thailandensis* with a infective dose of $2x10^7$ CFU. Indeed, if the inoculum of *B. thailandensis* is lowered to $1x10^4$ CFU in wild type mice, the infection is cleared faster and we think that cytokine production returns to baseline by 18 hours post-infection, resulting in a lack of staining (Figure 4, compared to robust IFN-γ signal in Figure 5). Thus, it is important to optimize the timing of your BFA injections and tissue harvests for your specific model (Troubleshooting 1).

Create a single cell suspension of splenocytes

We next need to create a single cell suspension so that we can stain them for flow cytometry.

Timing: 2 hours

6. Place the spleen on a 70 micron cell strainer fitted on top of a 50 mL conical tube.
7. Using the plunger of a 1 mL syringe, gently press the spleen against the strainer to mechanically disrupt the tissue. Continue until the only remaining tissue on the strainer is

white and fatty in texture, occasionally adding PBS to ensure that the tissue and cells do not dry out.

8. Wash the remaining cells off the strainer and into the underlying 50 mL conical using 10 mL of PBS. Dispose of the strainer and add PBS to the conical for a total volume of 30 mL.

   Alternatives: If you are interested in immune cells present in other organs, the processing protocol may differ. Analogous procedures can be used for immune cell-dense organs like lymph nodes; however, more fibrous organs will likely require additional steps such as more intense physical manipulations and/or treatment with proteases like collagenase. For example, see the methods section of [84] for descriptions of how to process mouse liver and lungs.

9. Spin the cells at 800xg**,** 4°C, for 10 minutes using a standard centrifuge
10. Discard the supernatant and resuspend in 5 mL of ACK RBC lysis buffer. Incubate on ice for 5 minutes

    Critical: The timing of incubating your cells for five minutes is important to avoid potential loss of cell viability (Troubleshooting 1).

11. Add 35 mL of PBS to stop lysis. Spin at 800xg, 4°C, for 10 minutes using a standard centrifuge.
12. Discard the supernatant and resuspend in 5 mL of PBS.
13. Filter through a new 70 micron cell strainer fitted on top of a new 50 mL conical to remove aggregates of dead cells that formed after lysis.

14. **Key Step:** Count cells using a cell counter or hemocytometer and record the data. These counts will be used to aliquot for staining in the next steps as well as for calculating absolute counts of subsets in the final analyses.

Alternative: If you desire to localize the cells that are producing cytokine within the organ, you can instead fix the spleen in 4% PFA and perform immunofluorescent staining using an analogous protocol published by Mazet et al[85].

Stain splenocytes and perform flow cytometric analysis

We next stain our cells for flow cytometry. Under normal circumstances (without BFA treatment), most cytokines are synthesized and promptly secreted by the cell. This causes the total pool of cytokine protein within the cell to be very low, despite high transcription and translation. Brefeldin A halts intracellular vesicle formation and transportation of proteins from the endoplasmic reticulum to the Golgi apparatus, inhibiting the secretory pathway and resulting in accumulation of translated proteins within the cell. This greatly increases the sensitivity of detection with antibodies specific for the cytokine of interest.

Timing: 2 days

15. Plate 1-2x10^6 cells in 200 μL PBS for each mouse into a well on a polypropylene, round-bottom 96-well plate.
16. Prepare a well for a live/dead (L/D) compensation tube.
    a. Take 1 to 2 million splenocytes and split into two Eppendorf tube.
    b. Heat shock one of the tubes by heating it at 55°C for 5 minutes followed by 2 minutes on ice. The other tube should remain on ice the entire time.

c. Mix the cells from the two Eppendorf tubes together and plate onto the sample plate. This ensures that the compensation tube will have sizable populations of both live and dead cells to serve as positive and negative compensation controls.

Alternative: Instead of using cells for L/D compensation, you can use amine reactive beads (for example, see Arc™ Amine Reactive Compensation Bead Kit (cat# A10628) from Thermo Fischer). If using these beads, you can make this compensation tube alongside the other compensation tubes in step 34.

17. Centrifuge the plate at 450xg, RT, for 5 minutes. Discard supernatant.
18. Resuspend each well with 200 μL of PBS. Centrifuge the plate at 450xg, RT, for 5 minutes and discard supernatant.
19. Resuspend each well with 100 μL of L/D stain in PBS for 20 minutes at RT in the dark
    a. To make L/D stain, add 1 μL of L/D stock per 1 mL of PBS
20. Add 100 μL FACS buffer to each well. Centrifuge the plate at 450xg, RT, for 5 minutes and discard the supernatant.
21. Resuspend each sample in 100 μL of extracellular staining master mix, and the L/D compensation well in 100 μL of PBS. Stain for 30 minutes at RT in the dark.
22. Add 100 μL of FACS buffer to each well. Centrifuge the plate at 450xg, RT, for 5 minutes and discard the supernatant.
23. Resuspend each well with 200 μL of FBS buffer. Centrifuge the plate at 450xg, RT, for 5 minutes and discard the supernatant.
24. Add 100 μL of BD Biosciences Fix/Perm to each well. Incubate at 4°C for 20 minutes in the dark.

Note: Depending on the cytokine being stained, this fix/perm step may need to be extended to 45 minutes to an hour to get optimal intracellular staining of the cytokine. For IFN-γ, we found that 20 minutes was sufficient (Troubleshooting 2).

25. Add 100 µL of BD Biosciences Perm/Wash buffer to each well. Centrifuge the plate at 1250xg, 4°C, for 5 minutes and discard the supernatant.
26. Resuspend each well with 200 µL of BD Biosciences Perm/Wash buffer. Centrifuge the plate at 1250xg, 4°C, for 5 minutes and discard the supernatant.
27. Resuspend each well with 200 µL of BD Biosciences Perm/Wash buffer.

    Pause Point: Once all cells have been fixed, samples can be stored at 4°C in the dark overnight in the Perm/Wash buffer. Intracellular staining can be resumed the following day with no significant change in staining.
28. Centrifuge plate at 1250xg, 4°C, for 5 minutes and discard the supernatant.
29. Resuspend each sample in 100 µL of intracellular staining master mix and the L/D compensation well in 100 µL of BD Biosciences Perm/Wash buffer. Stain for 1 hour at 4°C in the dark.
30. Resuspend each well with 100 µL of BD Biosciences Perm/Wash buffer. Centrifuge the plate at 1250xg, 4°C, for 5 minutes and discard the supernatant.
31. Resuspend each well with 200 µL of FBS buffer. Centrifuge the plate at 1250xg, RT, for 5 minutes and discard the supernatant.
32. Resuspend in 200 µL of FACS buffer. Transfer to a flow tube with a filter.
33. Prepare compensation tubes.
    a. Add 1 µL of antibody to 1 drop of UltraComp eBeads™ Compensation Beads.

Note: These beads can bind mouse, rat, and hamster-derived antibodies, which works with all antibodies used in the panel included in this protocol. However, if you use different antibodies in your panel, ensure that the beads are compatible with all antibodies being used. Beads compatible with antibodies derived from other species are also commercially available. Alternatively, if enough cells present the marker for the antibody, you can stain splenocytes with the antibody alone to use as a compensation tube.

b. Vortex briefly.
c. Incubate at RT in the dark for 15 minutes.
d. Add 150 μL of FACS buffer and centrifuge at 450xg.
e. Resuspend in 200 μL of FACS buffer and transfer to a flow tube.

Note: For conventional flow cytometry (such as the flow we performed using an LSRII), beads offer an easy way to generate compensation samples that usually result in accurate compensation. However, if using a full spectrum flow cytometer, then the slight differences between fluorescent spectra of fluorophores on beads compared to cells could result in unmixing errors. Thus, these users will need to determine if there are any differences between single color controls using beads and cells, and they should use cells as compensations controls if there is a difference.

34. Keep samples at 4°C in the dark until ready to run on a flow cytometer.
35. Run samples through flow cytometer.
36. Analyze results using FlowJo.

Expected Outcomes

If successful, using the gating schema displayed in Figure 5A, only minimal amounts of cytokine staining will be detected in uninfected controls, which represents the basal level of cytokine production (Troubleshooting 3). A robust signal should be detected from the infected mice where cells are strongly producing cytokine (Figure 5B). Frequency of cells can be determined directly from flow cytometry analyses. The gating schema used will enable analysis of T cells ($CD3^+$), NK cells ($CD3^-NK1.1^+CD127^-$), and ILC1s ($CD3^-NK1.1^+CD127^+CD90^+$ or $CD3^-NK1.1^-CD127^+CD90^+$) (Figure 5A-C). Gamma-delta T cells can also be identified within the $CD3^+$ population (Figure 5D).

We have also expanded the panel with CD4 and CD8 (see optional antibodies), allowing the identification of CD4 and CD8 T cells within the $CD3^+$ population. While compensation issues begin to appear since we did not optimize the fluorophore-marker combinations in the panel expanded to include CD4 and CD8, we include these antibodies in this protocol as an option since they were sufficient to delineate the CD4 and CD8 populations (Figure 5D). Further optimization of which fluorophore is assigned to each marker can be done to avoid these compensation issues.

Quantification and Statistical Analysis

Frequency is calculated using FlowJo analysis software. In addition to frequency, absolute counts for each population being examined should be calculated. This calculation is important because differences in frequency can result from either changes in that population of cells (eg. more NK cells are present in the spleen) or changes in the other populations (eg. fewer T cells will make NK cell frequency increase). Absolute counts allow determination of the causes of changes in frequencies. This can easily be performed by multiplying the total

splenocyte count determined immediately after forming the single cell suspension for each sample (see step 14) by the frequencies of each gate used to gate on the population. For example, to calculate absolute number of NK cells in the spleen that produce IFN-γ using the gating from Figure 5A, we did the following:

Absolute # of NK cells producing IFN-γ in spleen $=$

$$5.75x10^7 \textbf{ splenocytes} \times 0.976 \textbf{ (singlet freq)} \times 0.62 \textbf{ (lymphocyte freq)}$$
$$\times 0.822 \textbf{ (live cell freq)} \times 0.286 \textbf{ (non-excluded cell freq)}$$
$$\times 0.0234 \textbf{ (IFN-γ -producing cell freq)} \times 0.618 \textbf{ (NK cell freq)}$$
$$= 1.18x10^5 \text{ NK cells}$$

Using the "Frequency of Total" statistic in FlowJo for a given population, this equation can be simplified to:

Absolute count = **splenocyte count** x **Freq of Total (for given population)**

Limitations

BFA is a Golgi blocker that inhibits the secretory pathway. This has several implications. First, BFA only inhibits release of cytokines that go through the secretory pathway. Members of the IL-1 family (e.g. IL-1β, IL-18, IL-33) do not encode a secretion signal, are stored in the cytosol, and are released by cell lysis or membrane permeabilization rather than through the secretory pathway[86]. Therefore, this methodology will not assess release of these cytokines. Indeed, it would give the opposite result: positive staining would indicate the lack of release of IL-1 family members. Similarly, some cell types contain pre-formed cytokine not intended for immediate release. Notably, this includes mast cells which store pre-formed TNF until another stimulus promotes its release[87]. Neither the methodology reported here nor the use of cytokine

reporter mice will be able to differentiate the pre-formed cytokine from cytokine that is created and immediately secreted on demand.

Second, release of cytokines, chemokines, and other proteins is important for a diverse array of immune functions. Thus, adding BFA likely alters kinetics and dynamics of infections and immune responses. However, these effects of BFA could be minimized by only treating mice with BFA after the immune response to be studied has had time to establish and by limiting the treatment time with BFA to 6 hours.

In addition, as a Golgi blocker, BFA can be toxic to cells. It is therefore important to monitor for cell death using live/dead markers. In our *B. thailandensis* infection model, BFA toxicity appears minimal. However, it is possible that some populations of cells may be more sensitive to BFA in other murine models, which could result in a selective loss in that population that may be difficult to detect unless that particular cell type was specifically examined.

Finally, sensitivity for detecting a cytokine response will be limited by the robustness of the cytokine response, the size of the population being looked at, and the accessibility of the tissue to blood flow (and therefore to the BFA that is injected intravenously). Low prevalence of responding cells could be particularly apparent when examining non-lymphoid tissues. This could be rectified by enriching for immune cells and removing stromal cells. Furthermore, this is a limitation that likely affects this BFA method of assessing in situ cytokine production more than the use of a reporter mouse. The fluorophores used in reporter mice often have longer half-lives than those of cytokines, meaning that more can accumulate within individual cells[88-90]. This increases the signal and improves the sensitivity of the reporter mice compared to BFA-treated mice (at the cost of being less able to resolve cytokine secretion that occurred over shorter periods of time).

Troubleshooting

Problem 1:

Low cell number

Potential Solution:

If this is accompanied by excessive cell death per the live/dead staining, this could have resulted from lysing too long with ACK buffer. Large clumps forming after treatment with ACK buffer could suggest this as a culprit. In this case, ensure samples do not remain in ACK buffer too long. If working with many samples, lyse only a small group at once and then proceed to next group once PBS has been added to ACK-treated samples to stop reaction. Alternatively, using too high of a concentration of BFA for too long may result in cell toxicity. In this case, lower concentration of BFA used or see if treating mice with BFA for a shorter duration reduces cytotoxicity without significantly reducing the signal of your cytokine.

If low cell numbers are not accompanied by excessive cell death, this could have resulted from plating the wrong number of splenocytes per well for staining or loss of cells during washing steps (e.g. aspiration of pellet). Verify that you are correctly counting the number of splenocytes obtained and correctly calculating the volume of cell suspension to add into each well for staining.

Lastly, some mouse lines deficient in lymphocytes, such as *Rag1*$^{-/-}$, do not have many splenocytes. Therefore, a low cell count may be expected for these mouse lines. In these cases, the goal is to collect and analyze as many cells as possible.

Problem 2:

No cytokine signal

Potential Solution:

Optimization may be required for each model to determine the time point that maximizes the likelihood for capturing a cytokine signal. With the proper timing, this protocol can be easily applied to a diverse array of models. The main stipulations are that you wait a sufficient amount of time to establish an immune response prior to BFA injection to minimize the effect of BFA on the immune response (see Limitations for more details), and you treat mice with BFA for approximately 6 hours immediately prior to harvesting the mouse.

Another potential cause of a lack of cytokine signal is that BFA does not always efficiently block cytokine secretion. In these cases, another Golgi blocker, monensin, may be more successful at inhibiting secretion of the cytokine. Indeed, Sun et al. reported successfully treating mice intravenously with 0.5 mg of monensin in 500 μL of PBS instead of BFA to successfully visualize IL-10 production[91]. For reference on which cytokines are known to be efficiently inhibited by brefeldin A versus monensin, see the Cytokine Detection subsection of the Techniques section on the following website: https://www.bdbiosciences.com/us/applications/research/intracellular-flow/.

Finally, while we found 20 minute fix/perm (step 24) was sufficient for staining of IFN-γ, this duration of time may be insufficient for other cytokines. Thus, consider extending the fix/perm step up to 45 minutes or an hour.

Problem 3:

High background signal for cytokine in uninfected control

Potential Solution:

Even if you utilize the optimized dilutions suggested for antibody master mix included in this protocol, batch variation could cause increased background for a given amount of antibody used. Therefore, titrate the antibody to determine the best concentration to use. In addition, utilize a fluorescent minus one (FMO) control in which you stain with all of the antibodies in the panel except for the one with which you are having trouble. This will enable you to see if there is a compensation issue that needs to be corrected as well as improve your gating strategy by allowing more accurate discrimination between positive and negative signals.

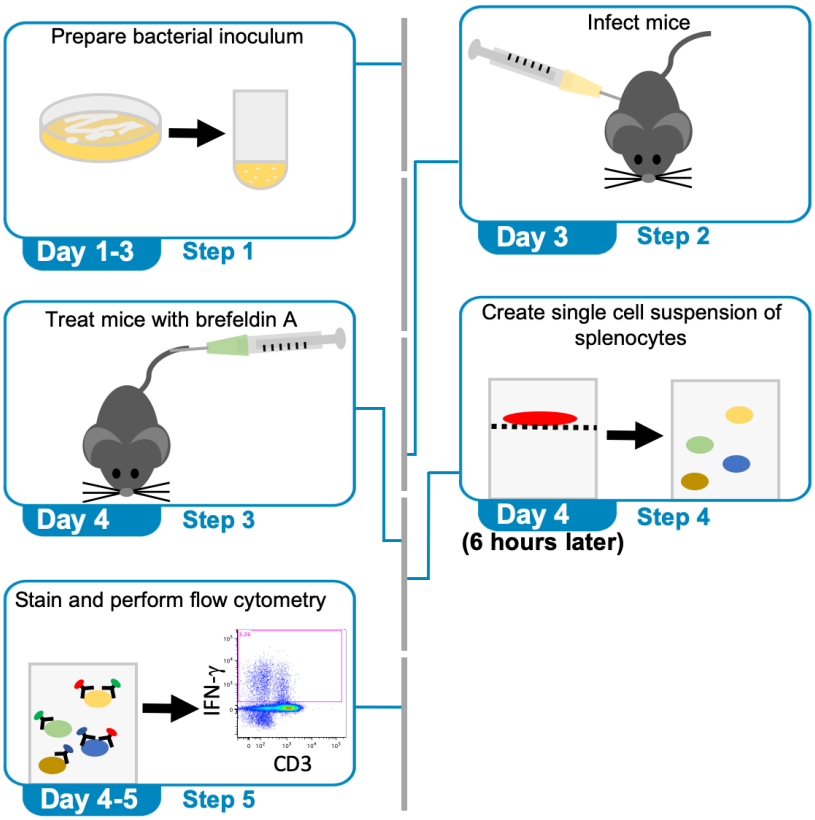

Figure 3: Graphical summary of protocol.

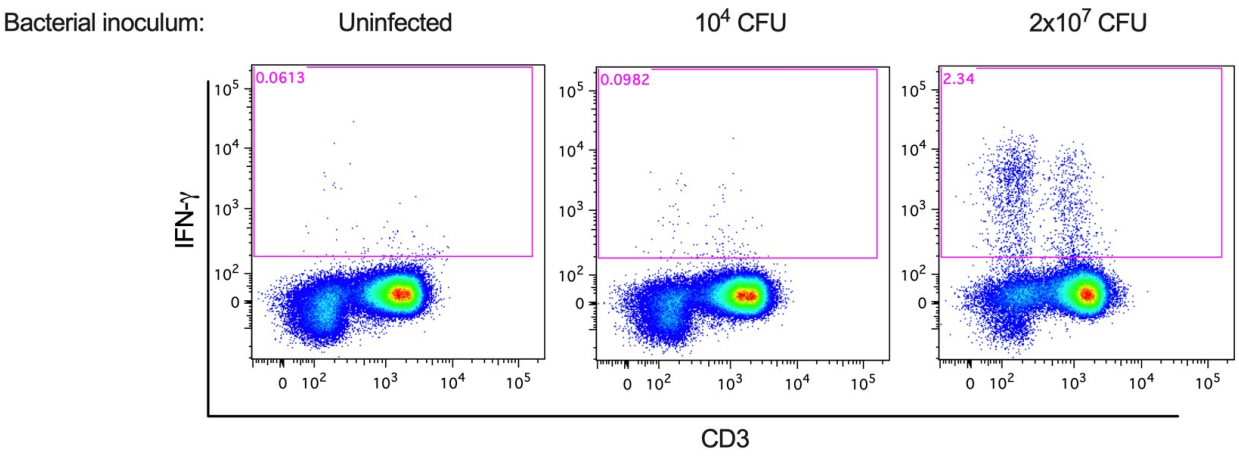

Figure 4. Choosing correct experimental conditions and timing is essential for observing robust cytokine signal. When infecting with a large bacterial inoculum ($2x10^7$ CFU), a robust IFN-γ signal is observed at 18 hours post-infection. When using smaller bacterial inoculum (10^4 CFU), IFN-γ signal is similar to background levels at 18 hours post-infection, a time point at which infection with this lower inoculum has already been cleared.

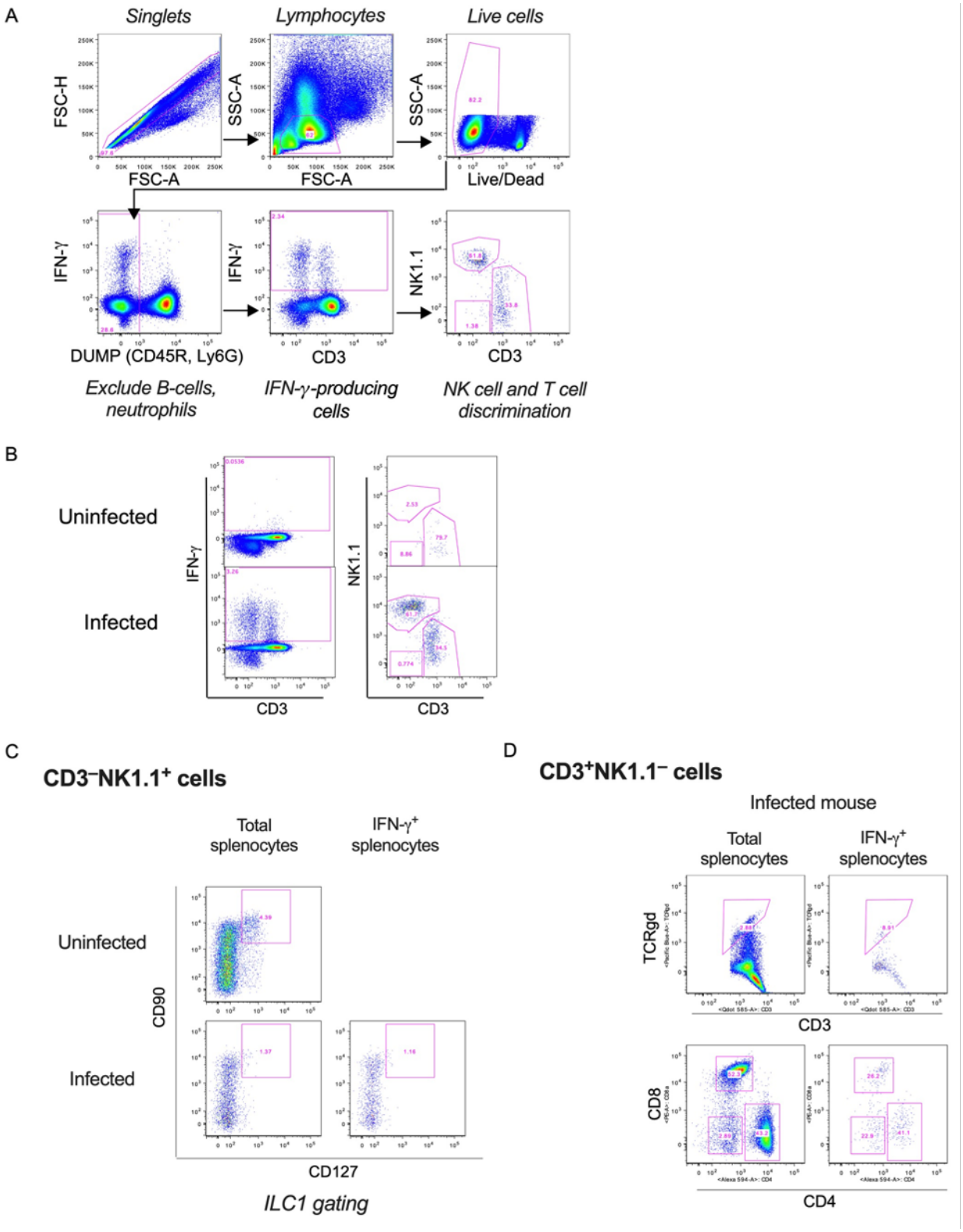

Figure 5. Analysis of flow cytometric data. A) Gating strategy used to characterize what cell

types constitute the IFN-γ-producing cells. Italicized labels indicate what cell population is being gated. B) Representative results at 18 hours post-infection with $2x10^7$ CFU *B. thailandensis*. C) Representative results demonstrating gating of ILC1s within the $CD3^{-}NK1.1^{+}$ subset. D) Representative results demonstrating TCRγδ and CD4 and CD8 subpopulations of the $CD3^{+}NK1.1^{-}$ subset when including the optional CD4 and CD8 antibodies.

CHAPTER 3: NEUTROPHIL CASPASE-11 IS ESSENTIAL TO DEFEND AGAINST A CYTOSOL INVASIVE BACTERIUM[3]

Introduction

The innate immune system includes multiple cell types that can be classified as either myeloid cells or lymphocytes that begin acting in defense against pathogens prior to the onset of adaptive responses. The myeloid lineage includes cells like macrophages and neutrophils that function to directly kill bacteria and other pathogens. The innate immune cells with lymphoid lineage include natural killer cells (NK cells), innate lymphoid cells (ILCs), and innate-like T cell lymphocytes[92,93]. Networks of cross-talk between myeloid and lymphoid lineages in innate immunity during bacterial infection is a nascent area of study.

Tissue resident macrophages are stationed in all the organs of the body in order to survey for bacterial contamination. They will typically be the first immune cells to come into contact with an infecting bacterium, and thus they are tasked with assessing the threat potential of the microbe. Cytosolic inflammasome sensors detect the virulence capabilities of pathogens, resulting in the activation of either caspase-1 or caspase-11[94]. For example, the NAIP/NLRC4 inflammasome signals to caspase-1 when it detects the activity of virulence-associated bacterial

[3]This chapter was previously published in *Cell Reports*. The original citation is as follows: Kovacs SB, Oh C, Maltez VI, McGlaughon BD, Verma A, Miao EA, Aachoui Y. Neutrophil Caspase-11 Is Essential to Defend against a Cytosol-Invasive Bacterium. Cell Rep. 2020 Jul 28;32(4):107967. doi: 10.1016/j.celrep.2020.107967. Stephen Kovacs performed experiments identifying NK cells and T cells as the IFN-producing cells during *Burkholderia thailandensis* infection. Stephen Kovacs also bred two novel mouse lines, one with myeloid-specific deletion of caspase-11 (LysM-cre) and one with neutrophil-specific deletion of caspase-11 (Mrp8-cre). Using these lines, Stephen Kovacs performed the experiments demonstrating utilizing these lines. Stephen Kovacs was also involved in planning and interpreting experiments that he did not perform, wrote the manuscript, and guided it through publication.

type III secretion systems (T3SS)[95-99]. This detection alerts the cell to the risk posed: T3SSs inject effector proteins into the host cell cytosol, where these effectors reprogram cellular physiology to benefit the pathogen. In parallel, the caspase-11 inflammasome monitors for LPS contamination as a marker for another virulence trait: cytosolic invasion (Aachoui et al., 2013a; Hagar et al., 2013; Kayagaki et al., 2013). Upon activation, either caspase-1 or caspase-11 can independently cleave and activate the pore-forming protein gasdermin D, triggering lytic cell death called pyroptosis[10,11]. Caspase-1 can also cleave and activate the cytokines IL-1β and IL-18, which are not cleaved by caspase-11[100]. Typically, in vitro studies of pyroptosis have utilized cultured macrophages.

The beneficial responses of caspase-1 and caspase-11 have been studied during infection with many bona fide human pathogens. Interpreting these studies has been complicated by the fact that bona fide pathogens have experienced intense evolutionary pressure to evade inflammasome detection, resulting in inefficient detection by the inflammasome sensors[9]. On the other hand, many environmental bacteria appear to completely fail to evade inflammasomes, and these are superb model organisms with which to study inflammasome responses[7,9]. *Burkholderia thailandensis* uses its T3SS to lyse the vacuole and escape into the cytosol, where it replicates[101]. However, *B. thailandensis* is not a bona fide mammalian pathogen, and it never evolved mechanisms to evade inflammasomes. The result is that wild type mice easily identify the extreme virulence capacity of *B. thailandensis* and can eliminate even 20,000,000 CFU systemic challenges within one day. In contrast, *Casp1*$^{-/-}$*Casp11*$^{-/-}$ mice succumb to even a 100 CFU challenge[8]. This change in the lethal dose is the strongest inflammasome-dependent defense phenotype of any infectious model as yet published[9].

Both NLRC4 and caspase-11 can detect and respond to *B. thailandensis* as well as *Burkholderia pseudomallei*, a related bacterium that causes melioidosis in humans[8,102-104]. Our laboratory previously showed that within the first day of infection, the NLRC4 inflammasome is important to limit *B. thailandensis*[8]. While the resulting caspase-1-driven pyroptosis is probably important, more important was the release of mature IL-18. This IL-18 drove as yet unidentified cells to produce IFN-γ, which was critical for priming the caspase-11 inflammasome. Caspase-11 activation then resulted in the clearance of the bacteria, and we previously hypothesized that caspase-11 clearance was mediated via pyroptosis[8]. The importance of NLRC4 and IL-18 could be overcome by persistent infection for three days, after which other cytokine responses would also trigger IFN-γ production. However, the importance of IFN-γ and caspase-11 could not be bypassed, as both *Ifng*$^{-/-}$ and *Casp11*$^{-/-}$ mice succumbed to the low 100 CFU challenge[8].

Here we continue these studies by asking several questions. First, we investigate the cell type(s) that respond to IL-18 by producing IFN-γ, effectively forming a bridge between caspase-1 and caspase-11. Second, we investigate the importance of gasdermin D downstream of caspase-1 and caspase-11. Third, we investigate why the NLRC4-caspase-1 pathway is insufficient to clear *B. thailandensis*, since either caspase-1 or caspase-11 should be competent to drive pyroptosis, and thus they should be functionally redundant.

Results

Multiple lymphocyte populations respond to *B. thailandensis* infection

We first sought to understand which cell types were responding to the IL-18 by secreting IFN-γ. In the innate immune system, there are two primary cell types that express high levels of

the IL-18 receptor (*Il18r1* and *Il18rap*): NK cells and ILCs (Figure 6). In the adaptive immune system, activated CD4 and CD8 T cells also express significant levels of the IL-18 receptor.

To assess which cells produce IFN-γ in response to *B. thailandensis* infection, mice were infected with *B. thailandensis* for 12 hours, then treated with brefeldin A[83]. Splenocytes were collected and assessed for cytokine production by flow cytometric analysis (Figure 7A-B). A majority of the cells that produced IFN-γ consisted of $NK1.1^{+}CD3^{-}$ cells, essentially all of which were conventional NK cells ($CD127^{-}$) with only a few ILC1s ($CD90^{+}CD127^{+}$) (Figure 7C-E, Figure 8A-C). A smaller but still substantial population of IFN-γ-producing cells were $CD3^{+}$ T cells (Figure 8A-C). These $CD3^{+}$ cells consisted of a variety of different T cell subsets (Figure 7F-H). While using NK1.1 as opposed to NKp46 to identify NK cells risks underestimating the NK cell population, any underestimation is likely minimal since essentially all IFN-γ-producing $NK1.1^{-}$ cells expressed CD3, which by definition cannot be NK cells.

Interestingly, in the IFN-γ-producing cells, the geometric mean fluorescence intensity (MFI) of IFN-γ was significantly higher in NK cells than T cells (Figure 8D-E), suggesting that each NK cell may be producing more IFN-γ than its $CD3^{+}$ counterpart. Remarkably, a median of 36% of the total NK cells in the spleen produced IFN-γ in response to *B. thailandensis* infection (Figure 8F). Together, these data suggest that NK cells and innately responding T cells produce the IFN-γ required to prime caspase-11, and that NK cells are exquisitely responsive in this model.

We next asked whether these populations were required to drive the IFN-γ response necessary to clear *B. thailandensis* (Figure 9). First, we examined *Rag1*$^{-/-}$ mice, which lack all T cells (as well as B cells), but remain competent for NK cells and ILCs. *Rag1*$^{-/-}$ mice remained fully resistant to *B. thailandensis* infection, surviving both high dose $2x10^{7}$ and medium dose 10^{4}

CFU challenge (Figure 9A, 9E), and sterilizing the burdens in their spleen and liver within 1 day (Figure 9B-C, 9F-G). Further, *Rag1*$^{-/-}$ mice retained their ability to produce significant levels of serum IFN-γ (Figure 9D, 9H), and flow cytometric analysis revealed that, as expected, IFN-γ-producing cells were virtually all NK cells. Therefore, we conclude that NK cells are sufficient to produce IFN-γ to resist *B. thailandensis* infection.

To study mice that genetically lack all these IFN-γ-producing lymphocytes, we used *Rag2*$^{-/-}$ mice that also lack the common γ chain (*Il2rg*), which is required for signaling through several cytokines, including IL-15 that is essential for NK and ILC development[105,106]. *Rag2*$^{-/-}$ *Il2rg*$^{-/-}$ mice were highly susceptible to *B. thailandensis* infection, succumbing to infection and failing to sterilize *B. thailandensis* organ burdens, as was also seen in *Ifng*$^{-/-}$ mice (Figure 9A-C, 9E-G). Despite having high bacterial burdens, these mice were defective in their ability to produce IFN-γ (Figure 9D, 9H). The *Rag2*$^{-/-}$*Il2rg*$^{-/-}$ mice and the *Ifng*$^{-/-}$ mice showed equivalent susceptibility during high dose infection, but in the medium dose infection the *Rag2*$^{-/-}$*Il2rg*$^{-/-}$ mice succumbed ~3 days later, and had somewhat lower spleen burdens than seen in *Ifng*$^{-/-}$ mice. This could be due to the fact that *Rag2*$^{-/-}$*Il2rg*$^{-/-}$ mice have altered splenic architecture, which could result in subtle changes in the course of the infection. Alternatively, there may be a very weak source of IFN-γ from non-lymphocytes that slows the infection, but which is not detectable by serum ELISA and ultimately is insufficient to turn the course of the infection.

Finally, we wanted to confirm that the primary role of these cells is to produce IFN-γ, and that their cytotoxic function was not involved. Mice deficient in perforin (encoded by *Prf1*), remained fully resistant to *B. thailandensis* infection and had normal levels of serum IFN-γ (Figure 10A-B). Furthermore, treatment with exogenous IFN-γ or adoptive transfer of WT NK

cells restored resistance to infection in *Rag2*$^{-/-}$*Il2rg*$^{-/-}$ mice, whereas negative controls of PBS or *Ifng*$^{-/-}$ NK cells did not (Figure 9I-K).

In summary, a variety of lymphocyte populations respond within hours of infection by producing IFN-γ. The predominant responsive cells are NK cells, which are sufficient to produce caspase-11-priming levels of IFN-γ. It is likely that IFN-γ-producing, innately responsive T cells are also sufficient.

Gasdermin D is essential for defense against *B. thailandensis*

Our laboratory previously showed that pyroptosis of bone marrow-derived macrophages (BMM) in vitro is driven in a redundant manner by both caspase-1 and caspase-11, and only doubly deficient BMM fully fail to trigger cytotoxicity in response to *B. thailandensis* infection[103]. Gasdermin D is the recently identified executioner of pyroptosis. In agreement with this, infection of BMM with *B. thailandensis* triggered gasdermin D cleavage that was dependent on caspase-1 and, to a lesser extent, caspase-11 (Figure 11A). This data would suggest that caspase-1 is more efficient than caspase-11 at cleaving gasdermin D in response to *B. thailandensis*, at least in BMMs. Gasdermin D can be cleaved to activate pore formation by either caspase-1 or caspase-11, and thus one might predict that *Gsdmd*$^{-/-}$ BMMs would resist cytotoxicity and phenocopy *Casp1*$^{-/-}$*Casp11*$^{-/-}$ BMMs. However, this was not the case, as residual LDH release was observed in *Gsdmd*$^{-/-}$ BMMs (Figure 11B). The same was true for IL-1β release as detected by ELISA (Figure 11C). This is actually in agreement with in vitro observations by others that found that *Gsdmd*$^{-/-}$ cells still achieve cytotoxicity after inflammasome activation[11,12], likely due to apoptotic bypass pathways arising either from a signaling branch point from ASC to caspase-8 (reviewed in [1]) or branching at caspase-1 itself to

BID[107], followed by secondary necrosis. While the ASC to caspase-8 pathway should still be functional in *Casp1*$^{-/-}$*Casp11*$^{-/-}$ mice, the caspase-1 to BID pathway may be faster, which could explain why *Gsdmd*$^{-/-}$ BMM have higher levels of cytotoxicity at this time point compared to *Casp1*$^{-/-}$*Casp11*$^{-/-}$ BMM. These data would suggest that loss of gasdermin D during infection in vivo could be less impactful than the combined effect of the loss of caspase-1 and -11.

We next examined the role of gasdermin D in defense against *B. thailandensis* in vivo. We previously showed that the *Casp1*$^{-/-}$ proxy mice, *Nlrc4*$^{-/-}$*Asc*$^{-/-}$, succumb only to high dose 2x10^7 CFU infection by *B. thailandensis*, and survive medium 10^4 CFU challenges[8]. We now verify that this also holds true in the clean single knockout *Casp1*$^{-/-}$ mice, whereas *Casp11*$^{-/-}$ mice were verified again to succumb (Figure 12A-B). Although caspase-1 plays a lesser role, it can also be seen to slow the course of infection; thus, the caspase-1-sufficient *Casp11*$^{-/-}$ mice succumb slower than *Casp1*$^{-/-}$*Casp11*$^{-/-}$ mice ([8] and replicated in Figure 12A-B). This is the opposite of the in vitro data where caspase-1 appeared to be more efficient in cleaving gasdermin D (in BMMs).

Gsdmd$^{-/-}$ mice succumbed to the high 2x10^7, medium 10^4, and low 10^2 CFU dose challenges, with kinetics that matched *Casp1*$^{-/-}$*Casp11*$^{-/-}$ mice but were faster than *Casp11*$^{-/-}$ mice (Figure 12A-C). We further quantitated these results by determining bacterial burdens at day 1 after high dose challenge, or at day 2 following medium dose challenge. *Gsdmd*$^{-/-}$ mice had the highest burdens on par with *Casp1*$^{-/-}$*Casp11*$^{-/-}$ mice, with *Casp11*$^{-/-}$ only slightly lower, and *Casp1*$^{-/-}$ or their proxy *Nlrc4*$^{-/-}$*Asc*$^{-/-}$ mice having lower burdens still, and wild type (WT) mice clearing both doses (Figure 12D-G). Together, these results indicate that bypass pathways to other forms of cell death cannot compensate for the loss of pyroptosis in *Casp1*$^{-/-}$*Casp11*$^{-/-}$ mice or in *Gsdmd*$^{-/-}$ mice. This is also in agreement with Wang et al., who observed that *Gsdmd*$^{-}$

$^{-/-}$ and *Casp1*$^{-/-}$*Casp11*$^{-/-}$ mice were more susceptible than WT mice to intranasal infection with *B. thailandensis*[108].

Our laboratory previously showed that the importance of NLRC4-ASC and caspase-1 is seen only in the first three days of infection when they drive IL-18 release, which in turn triggers IFN-γ production (Aachoui et al., 2015). We now asked whether gasdermin D was important for this release of IL-18. As expected, IL-18 release within the first day of infection was dependent on gasdermin D (Figure 12H-I). *Casp1*$^{-/-}$*Casp11*$^{-/-}$ control mice with equivalent burdens to *Gsdmd*$^{-/-}$ mice also did not have detectable levels of serum IL-18 (Figure 12H-I).

Interestingly, at a later time point two-day post-infection, we observed elevated serum IL-18 in *Gsdmd*$^{-/-}$ mice, and a trending elevation in *Casp1*$^{-/-}$*Casp11*$^{-/-}$ mice that did not reach statistical significance (Figure 12J-K). Notably, the ELISA kit we used to measure the IL-18 levels was specific for the cleaved, active form of IL-18 (Figure 13). Our data is consistent with that of Wang et al., who observed a delayed elevation of IL-18 levels in bronchoalveolar lavage fluid from *Gsdmd*$^{-/-}$ mice infected intranasally with *B. thailandensis*[108]. In *Gsdmd*$^{-/-}$ mice, the IL-18 is likely still cleaved by caspase-1 and is released in a delayed manner after non-pyroptotic necrosis of the cell, perhaps secondary to the backup pathways that have been observed in vitro. Alternatively, this serum IL-18 may arise from non-specific tissue damage caused by sepsis that activates caspase-1 in uninfected cells since these mice had exceptionally high, near lethal bacterial burdens (Figure 12J). Indeed, these mice are expected to succumb to the infection by the end of the day of harvest in this experiment (Figure 12B). How IL-18 is cleaved in *Casp1*$^{-/-}$ *Casp11*$^{-/-}$ mice, however, is harder to explain. One possibility is that the ASC backup pathway-mediated caspase-8 activation results in caspase-8 cleaving IL-18[109]. Indeed, consistent with this backup pathway having a subtle effect, we observed that *Casp1*$^{-/-}$ mice (in which the ASC-

caspase-8 backup pathway remains intact) survived a day longer to high dose challenge and had a small but statistically significant reduction in burdens when compared to *Nlrc4*$^{-/-}$*Asc*$^{-/-}$ mice (in which this backup pathway is deficient) (Figure 12A, D, F). Alternatively, unprocessed IL-18 may be released by non-pyroptotic necrosis, and IL-18 could then be cleaved extracellularly. Indeed, several extracellular proteases have been reported as capable of cleaving and activating IL-18, including chymase and granzyme B[110]. Regardless of the mechanism, we can conclude that the delayed release of IL-18 is inadequate to clear infection in *Gsdmd*$^{-/-}$ and *Casp1*$^{-/-}$ *Casp11*$^{-/-}$ mice.

Caspase-11, but not caspase-1, triggers pyroptosis in neutrophils

Next, we considered the apparent paradoxical separation of the phenotypes of *Casp1*$^{-/-}$ and *Casp11*$^{-/-}$ mice. Since both caspase-1 and caspase-11 should be competent to cleave gasdermin D independently of each other, one would expect redundancy in which *Casp1*$^{-/-}$ *Casp11*$^{-/-}$ mice and *Gsdmd*$^{-/-}$ mice would be equally susceptible, whereas single *Casp1*$^{-/-}$ and *Casp11*$^{-/-}$ mice both remain resistant to infection. However, this was not the case, as caspase-1 could not substitute for caspase-11 in defense (Aachoui et al., 2015; Wang et al., 2018).

In considering why NLRC4 and caspase-1 were not sufficient to clear *B. thailandensis*, we hypothesized that there was a cell type in vivo that failed to activate NLRC4, and thus a single *Casp11*$^{-/-}$ mouse would phenocopy the double knockout in that cell type. One potential candidate cell type is the neutrophil. WT mice have been shown to effectively kill *Salmonella enterica* serovar Typhimurium when engineered to over-express the NLRC4-agonist flagellin[37]. However, if neutrophils are unable to kill phagocytosed bacteria due to loss of the ability to produce reactive oxygen species (*Ncf1*$^{-/-}$ mice lacking the phagocyte oxidase), then flagellin-

engineered *S.* Typhimurium will persist and replicate inside a vacuole within neutrophils[37]. This observation suggests that neutrophils do not effectively undergo pyroptosis when exposed to NLRC4 agonists. Consistent with this concept, Chen et al. showed that treatment of neutrophils with NLRC4 agonists triggers caspase-1 activation to promote IL-1β maturation but does not result in pyroptosis[32,111]. In contrast, neutrophil exposure to cytosolic LPS drives caspase-11 activation and gasdermin D cleavage to induce pyroptosis[111]. We thus hypothesized that neutrophils were anergic to NLRC4, but would undergo pyroptosis in response to caspase-11 activation during *B. thailandensis* infection.

First, we wanted to compare macrophage and neutrophil responsiveness to NLRC4 and caspase-11 agonists. To activate NLRC4, we treated BMM and bone marrow neutrophils with the well characterized NLRC4 agonist PrgJ-Tox[112]. To activate caspase-11, we transfected LPS into the cytoplasm of the cells. Treatment with PrgJ-Tox and cytoplasmic LPS resulted in gasdermin D cleavage in both macrophages and neutrophils, showing that both NLRC4 and caspase-11 activation produce active gasdermin D (Figure 14A-B). Caspase-11 activation with cytoplasmic LPS induced caspase-11-dependent cell death as well as IL-1β release in both macrophages and neutrophils (Figure 14C-D, G-H). It is worth noting that while we did not observe significant cleavage of caspase-11 by western blot, we have historically found western blots to be an unreliable way to evaluate caspase-11 activation compared to the downstream effects of caspase-11 activation like pyroptosis or gasdermin D cleavage[113]. In contrast to caspase-11 activation, while NLRC4 activation with PrgJ-Tox induced release of IL-1β from both macrophages and neutrophils, NLRC4 activation induced significant levels of cell death in macrophages, but not in neutrophils (Figure 14E-F, I-J).

We next wanted to evaluate inflammasome responses of neutrophils to *B. thailandensis* infection in vitro. We infected neutrophils from WT, *Casp1*$^{-/-}$ and *Casp11*$^{-/-}$ mice with *B. thailandensis*. Consistent with our data with PrgJ-Tox and cytoplasmic LPS, WT, *Casp1*$^{-/-}$, and *Casp11*$^{-/-}$ neutrophils all exhibited comparable levels of gasdermin D cleavage, demonstrating that caspase-1 and caspase-11 are both sufficient to activate gasdermin D in response to *B. thailandensis* (Figure 15A). As expected, release of IL-1β depended on caspase-1, but not caspase-11 (Figure 15B), consistent with NLRC4 being sufficient to drive caspase-1 activation. However, neutrophil cytotoxicity in response to *B. thailandensis* depended only on caspase-11 (Figure 15C), suggesting that NLRC4 activation of caspase-1 is insufficient to cause pyroptosis. This is the opposite of what we observed in macrophages, where caspase-1 was more efficient at causing gasdermin D cleavage and cell death in response to *B. thailandensis* (Figure 11A-B). These data agree with data from Chen et al. showing that NLRC4 activation triggers cytokine release but not pyroptosis in neutrophils[32,111]. However, unlike Chen et al., who found that caspase-1 inefficiently cleaved gasdermin D in neutrophils, we found that caspase-1 was similarly efficient as caspase-11 at cleaving gasdermin D in neutrophils, although we agree with Chen et al. that this did not result in pyroptosis[111]. This difference is likely attributable to PrgJ-Tox and *B. thailandensis* being more efficient at delivering the NLRC4 agonists into the cytosol than transfection of flagellin using FuGene as performed by Chen et al. The mechanism whereby neutrophils survive the gasdermin D activation downstream of caspase-1 but not caspase-11 remains to be elucidated.

Finally, to assess the effect of inflammasome activation on the ability for neutrophils to harbor *B. thailandensis*, we infected neutrophils in vitro with *B. thailandensis* and examined bacterial recovery in the presence of extracellular membrane-impermeant kanamycin, which kills

extracellular bacteria as well as those trapped in pyroptotic cells with ruptured membranes. No bacteria were recovered from WT or *Casp1*$^{-/-}$ neutrophils, whereas *Casp11*$^{-/-}$ neutrophils had significant bacterial recovery (Figure 15D). This indicates that *B. thailandensis* can survive within *Casp11*$^{-/-}$ neutrophils in vitro. This also suggests that the proposed direct bactericidal activity of cleaved gasdermin D[16,108], which forms robustly downstream of caspase-1 in these cells (Figure 15A), is insufficient to clear *B. thailandensis*, consistent with our in vivo data indicating that caspase-1 alone cannot clear *B. thailandensis* infection (Figure 12B, 12F comparing *Casp1*$^{-/-}$ to *Casp11*$^{-/-}$ mice).

Neutrophil caspase-11 is essential for survival of mice infected with *B. thailandensis*

Next, we examined the importance of neutrophil caspase-11 during *B. thailandensis* infection in vivo. To delete caspase-11 primarily in neutrophils while retaining it in most other cells, we crossed *Casp11*$^{fl/fl}$ mice with *Mrp8* promoter-driven *cre* transgene mice. *Mrp8-cre* deletes model floxed genes at 80% efficiency in splenic, peripheral blood, and bone marrow neutrophils, while deleting at 0-20% efficiency in monocyte and macrophage populations[114]. Thus, *Mrp8-cre* has been used for neutrophil-specific deletions. In contrast, *LysM-cre* deletes in both macrophages and neutrophils[114]. Both *Casp11*$^{fl/fl}$*Mrp8-cre* and *Casp11*$^{fl/fl}$*LysM-cre* mice were highly susceptible to *B. thailandensis* infection, showing bacterial burdens and survival kinetics that approached that of full body knockout controls (Figure 16A-C). This suggests that caspase-11 is absolutely essential in the neutrophil compartment.

The caveat to drawing definitive conclusions from the use of *Mrp8-cre* mice is that this *cre* line also causes a relatively smaller 0-20% deletion in monocytes and macrophages[114]. To determine if a potential deletion of caspase-11 in 20% of macrophages could account for the

phenotypes observed in *Casp11*$^{fl/fl}$*Mrp8-cre* mice, we created mixed bone marrow chimeras with a ratio of 20% of *Casp11*$^{-/-}$: 80% WT bone marrow marked with CD45.2^{+} and CD45.1^{+}, respectively. Maintenance of this ratio upon engraftment was verified by flow cytometry (Figure 17). In these mice, 20% of both macrophages and neutrophils will be completely deficient in caspase-11 and therefore could serve as intracellular niches for *B. thailandensis*. Notably, after infection with *B. thailandensis*, bacterial burdens in these mice were comparable to those of control mice engrafted with 1% *Casp1*$^{-/-}$: 99% WT bone marrow, and significantly lower than mice engrafted with 99% *Casp11*$^{-/-}$: 1% WT bone marrow (Figure 16D-E). Thus, having 20% *Casp11*$^{-/-}$ monocytes and macrophages does not cause susceptibility to *B. thailandensis* infection, arguing that the phenotype of the *Mrp8-cre* mice cannot be attributed to deletion in the monocyte/macrophage compartments. We can also conclude that having 20% *Casp11*$^{-/-}$ neutrophils was not sufficient to cause susceptibility, suggesting that the immune system can overcome a relatively small fraction of susceptible cells that harbor the infection. In summary, deletion of *Casp11* in *Mrp8-cre* marked cells, most of which are neutrophils, is sufficient to cause susceptibility to *B. thailandensis* infection. However, we do not exclude the possibility that deletion of *Casp11* in other cell types could also be sufficient to cause susceptibility.

Gasdermin D in neutrophils has recently been suggested to cause the formation of neutrophil extracellular traps (NETs)[111,115]. Typically, NET formation is dependent upon the activity of both the NADPH oxidase (which includes p47^{phox} encoded by *Ncf1*) and neutrophil elastase (encoded by *Elane*), and in some cases myeloperoxidase (MPO). We therefore infected *Elane*$^{-/-}$, *Ncf1*$^{-/-}$, and *Mpo*$^{-/-}$ mice with *B. thailandensis*. *Elane*$^{-/-}$ mice remained fully resistant, whereas *Ncf1*$^{-/-}$ mice had lower bacterial burdens than *Casp11*$^{-/-}$ mice at both medium and high doses (Figure 16F-G). The *Ncf1*$^{-/-}$ results are in agreement with our previous observation that

Ncf1$^{-/-}$ mice succumbed to *B. thailandensis* infection significantly slower than *Casp1*$^{-/-}$*Casp11*$^{-/-}$ mice (*Ncf1*$^{-/-}$ mice succumb between days 6-11, whereas *Casp1*$^{-/-}$*Casp11*$^{-/-}$ mice succumb at day 2 to a 10^4 CFU challenge[9]). The phenotype in *Ncf1*$^{-/-}$ mice could be due to the role of p47^{phox} in direct bactericidal activity via reactive oxygen species, or to its role in NETosis. Finally, *Mpo*$^{-/-}$ mice remained fully resistant to infection (Figure 16H). Thus, the genes that are traditionally required for NET formation have weaker phenotypes than caspase-11.

Discussion

We identify a coordinated innate immune defense pathway whereby initial detection of *B. thailandensis* by the NLRC4 inflammasome activates caspase-1, resulting in IL-18 release, and also likely a modestly beneficial pyroptosis. These responses occur quickly, but alone are unable to clear the infection. Next, a variety of lymphocytes, primarily NK cells and T cells, respond to the IL-18 by secreting IFN-γ, which is essential for defense. IFN-γ is required to prime caspase-11. Among caspase-11-responding cells, activation of caspase-11 in neutrophils is absolutely essential for defense. Caspase-11 activates the pyroptotic pore gasdermin D, which kills the infected neutrophil and removes an important intracellular niche for *B. thailandensis*.

We demonstrate that NK cells are the largest population that produces IFN-γ in this model. However, T cells also respond innately and produce IFN-γ. This T cell population is a conglomeration of various T cells subset, likely including both innate T cells like gamma delta T cells and NK T cells, as well as possibly conventional T cells responsive to IL-18[116]. While ILC1s were not a major producer of IFN-γ in this model likely owing to their small population in the spleen, it would be interesting to determine if resident ILC1s play a major role in other tissues where resident ILC1s are more prominent.

Why is the immune system organized in such a way that caspase-1 must respond first, then lymphocytes must assess the total caspase-1 response via monitoring for IL-18, and only then will the resulting IFN-γ prime caspase-11? We propose that because caspase-11 detects LPS, a ubiquitous component of both commensal and pathogenic gram-negative bacteria, it is more prone to false positive responses than NLRC4, which more directly detects virulence in the form of T3SS activity. False positives can result in aberrant pyroptosis that is damaging to tissues and can lead to sepsis[113,117,118]. Therefore, caspase-11 is placed behind a priming firewall designed to only be opened only when the immune system has reason to "believe" that it is likely that a cytosol-invasive pathogen is present. This likelihood arises from detection of T3SS activity in the case of *B. thailandensis*, and the judgement is made by NK cells and T cells.

Most work on inflammasomes has been done in macrophages. Indeed, despite the fact that neutrophils are quickly recruited in copious numbers to sites of early infection, it is unclear to what extent inflammasomes are activated in neutrophils or what role this activation could play in neutrophil function. We have now bridged that gap by characterizing the importance of the neutrophil caspase-11 inflammasome in vitro and in vivo. We show that NLRC4 activation fails to clear bacteria from neutrophils, whereas caspase-11 accomplishes this task with extreme efficiency. This leads us to ask: what is the benefit of having neutrophils not respond to NLRC4 agonists with pyroptosis, and why would that be different with caspase-11? Furthermore, why would neutrophils use these inflammasomes in different ways compared to macrophages?

As tissue resident sentinel cells, macrophages are the first responders to infection. Macrophages monitor for the activity of T3SS, and trigger pyroptosis to convert an infected cell into a pore-induced intracellular trap (PIT). We previously showed that this process does not kill the bacteria, but instead detains them within the remains of the pyroptotic macrophage while

simultaneously elaborating neutrophil chemoattractants. Neutrophils then efferocytose the PIT and the bacteria contained inside and kill the bacteria through the activity of potent microbicidal effectors like NADPH oxidase[3]. In this way, macrophages have the luxury of "passing the buck" to the neutrophil, a more bactericidal cell type.

Neutrophils, however, may not have the luxury of passing a bacterium to another cell. Perhaps in most cases they do not need to do so. If a neutrophil encountered a T3SS positive bacterium, it should expect that it will phagocytose and kill the bacterium. If the neutrophil were instead to kill itself, the neutrophil might fail to kill the bacterium, especially if the bacterium was still extracellular. Thus, neutrophils might be best suited to continue to live and to fight against infection as long as the bacterium remains in the vacuole, which is the primary location for neutrophil bactericidal mechanisms. On the other hand, caspase-1-driven cytokine release would be beneficial, because a T3SS positive bacterium has a higher threat level and warrants recruitment of a greater inflammatory response.

In contrast, what would happen to a neutrophil if bacteria escape into the cytosol? *B. thailandensis* escapes to the cytosol of most cells within 15 minutes[101]. Since most bactericidal activity of the neutrophil is directed at the vacuole, the event of cytosolic invasion may represent complete evasion of the neutrophil's primary function. Hence, caspase-11-driven pyroptosis should be critical to deny cytosol-invasive bacteria a niche within neutrophils.

One major outstanding question is if NLRC4 and caspase-1 activation are sufficient to produce significant levels of cleaved gasdermin D in neutrophils, why do neutrophils not undergo pyroptosis after caspase-1 activation? Chen et al. suggested that caspase-1 was unable to cleave sufficient amounts of gasdermin D in the neutrophil[111]. In contrast, we used more efficient means of NLRC4 agonist delivery, and we now observed robust caspase-1-dependent gasdermin

D cleavage, but this still failed to cause pyroptosis. The mechanism is likely explained by a recent publication, in which Karmakar et al. observed that NLRP3-driven caspase-1 activation did not result in significant accumulation of gasdermin D on the neutrophil plasma membrane, but instead gasdermin D accumulated on the membrane of azurophilic granules[119]. Likely, the large number of granules packed in each neutrophil could serve as a membrane sink for gasdermin D. During caspase-1 activation, the ASC speck usually forms perinuclearly[120,121]. Thus, gasdermin D cleaved at the ASC speck must diffuse from the perinuclear location to the outer membrane, and it would likely encounter and insert into granule membranes instead. One idea that is raised by gasdermin D pores inserting into neutrophil granules is the possibility that this could release granule bactericidal components to the cytosol, thereby killing cytosol-invasive bacteria[119]. However, in the case of *B. thailandensis*, our data show that this hypothetical mechanism is insufficient since caspase-1-sufficient *Casp11*$^{-/-}$ mice still succumb to infection.

In contrast to caspase-1, Chen et al. and our data indicate that caspase-11 activation is sufficient to cause pyroptosis[111]. Karmarkar et al. did not study the localization of gasdermin D after caspase-11 activation; however, their model introduces concepts that may explain the difference. We speculate that caspase-11 can be activated more diffusely throughout the cell. This diffuse caspase-11 could cleave gasdermin D in closer proximity to the plasma membrane. The resulting plasma membrane pores would be more likely to cause neutrophil pyroptosis. This hypothesis will be explored in future work.

In summary, our work describes how a single pathogen, *B. thailandensis*, can be detected by apparently redundant inflammasome pathways. However, these pathways are deployed differentially in macrophages compared to neutrophils. This must be driven by the different cellular characteristics and immunologic functions of the macrophage as compared to the

neutrophil. This study illustrates the importance of studying inflammasomes in vivo where complex cellular interactions occur.

Methods

Data and code availability: Source data for Supplemental Figure 1 is available through the Immunological Genome Project (immgen.org) and can be accessed by searching through the microarray database for IL18R (probe set ID 10345807) and IL18RAP (probe set ID 10345824).

Mice

Wild type (WT) C57BL/6 (Jackson Laboratory), *Casp1*$^{-/-}$ [28], *Nlrc4*$^{-/-}$*Asc*$^{-/-}$ [8], *Casp11*$^{-/-}$ [122], *Casp1*$^{-/-}$*Casp11*$^{129mut/129mut}$ referred to as *Casp1*$^{-/-}$*Casp11*$^{-/-}$ [123], *Elane*$^{-/-}$ (Jackson # 006112), *Mpo*$^{-/-}$ (Jackson Laboratory # 004265), *Ncf1*$^{mt/mt}$ referred to as *Ncf1*$^{-/-}$ (Jackson # 004742), *Prf1*$^{-/-}$ (Jackson # 002407), *Rag1*$^{-/-}$ (Jackson # 002216), *Rag2*$^{-/-}$*Il2rg*$^{-/-}$ (Taconic # 4111), *Gsdmd*$^{-/-}$ [28], *Ifng*$^{-/-}$ (Jackson # 002287), *Casp11*$^{fl/fl}$ [124], *Mrp8-cre* (Jackson # 021614), and *LysM-cre* (Jackson # 004781) mice were used in this study. All mice were 6-12 weeks old, male or female, and housed under specific pathogen free condition facilities. All protocols were approved by the Institutional Animal Care and Use Committee at the University of Arkansas for medical Sciences at Little Rock, or Institutional Animal Care and Use Committee at the University of North Carolina at Chapel Hill.

Bacterial strains

In this study, we used a *Burkholderia thailandensis* strain that we previously passaged through *Casp1*$^{-/-}$*Casp11*$^{-/-}$ mice (*B. thailandensis,* strain E264-1); this strain displays more synchronized infection kinetics than the parental E264 [8].

Primary cells

Primary neutrophils were isolated from mouse bone marrow using Neutrophil Isolation Kit (Miltenyi Biotec) using manufacturer instruction.

Bone marrow–derived macrophages (BMM) were prepared from the femur and tibia of mice by culturing with L929 cell supernatant for 7 day at 37ºC, 5% CO_2.

METHOD DETAILS

In vivo infections

For all experiments, *Burkholderia thailandesis* were grown in Luria-Bertani medium (LB) overnight at 37°C. Bacteria were pelleted from 1 mL of culture and washed in PBS before inoculation to mice. Bacteria titer was determined by OD measurement at 600 nm and plating serial dilution on LB agar plates. For lethal challenge, mice were inoculated via the intraperitoneal (i.p.) route with the doses specified in the text. For bacterial burden measurements, spleens and livers were collected on day 1 when dose of infection used $2x10^7$ CFU, and on day 1 or 2 post-infection when dose of infection used was 10^4 CFU. All organ harvested were homogenized in sterile PBS. Viable CFUs in homogenates were enumerated by plating serial dilutions on agar plates. At the same time of organ harvest, serum was collected from blood drawn by cardiac puncture for cytokines measurement. ELISA assays were

performed per manufacturer instructions to measure serum levels of mouse IL-18 (MBL International) and IFN-γ (R&D Systems). Alternatively, in figure 2I, *Rag1*$^{-/-}$, *Rag2*$^{-/-}$*Il2rg*$^{-/-}$, or *Ifng*$^{-/-}$ mice were infected i.p. with $2x10^6$ CFU of *B. thailandensis*, and treated with recombinant murine IFN-γ (0.5 mg/mice) at the time of infection and 24 hours post-infection. Bacterial burdens in organ homogenates were determined as described above. In Figure 2J-K, *Rag1*$^{-/-}$ *Il2rg*$^{-/-}$ mice were adoptively treated (tail vain injection) at day -14 and -7 with 10^6 cells of IL-2-expanded WT or *Ifng*$^{-/-}$ NK cells. Fourteen days after first adoptive transfer, mice were infected i.p. with 10^4 CFU of *B.* thailandensis. Bacterial burdens in organs homogenates were determined 72 hours post-infection as described above.

In vitro infection and analysis of inflammasome activation

For in vitro infections, *B. thailandensis* grown as described above were pelleted from 1mL of culture were opsonized with 50 µl of mouse sera for 30 min at 37°C and then suspended in 1 ml of DMEM. BMMs were prepared as described [37]. For infections, macrophages were seeded into 96-well tissue culture treated plates at a density of $5x10^4$ cells/well. Macrophages were primed with Pam_3CSK_4 (1 µg/ml) (InvivoGen) overnight. Bacteria were added to BMMs at MOI 50, centrifuged for 5 min at 300 g, and then incubated at 37°C for 1hr. After 1 hour, extracellular bacterial growth was stopped by addition of 300 µg/ml kanamycin and supernatant samples were collected at 3 hours. For neutrophil infections, bone marrow neutrophils (isolated using Neutrophil Isolation Kit (Miltenyi Biotec)) were seeded into 96-well tissue culture treated plates at a density of $4x10^5$ cells/well. Neutrophil were primed with Pam_3CSK_4 (1 µg/ml) (InvivoGen) for 4 hours. Bacteria were added to BMMs at MOI 100, centrifuged for 5 min at 300 g, and then incubated at 37°C for 1 hour. After 1 hour, extracellular bacterial growth was

stopped by addition of 300 μg/ml kanamycin, and CFU was determined at 5 hours. Alternatively, macrophages or neutrophils were primed with IFN-γ (10 ng/ml, Peprotech) and ultra-pure LPS (50ng/ml) (*E. coli* O111:B4; InvivoGen) for 4 hours. Then, cells were treated with NLRC4 agonist PrgJ-Tox[112] (2 μg/well) or transfected with LPS (10 μg/ml) for 5 hours. Cytotoxicity was defined as the percentage of total lactate dehydrogenase released into the supernatant and was determined as described[125]. IL-1β secretion was determined by enzyme-linked immunosorbent assay (ELISA) (R&D Systems). Lysates and supernatants were combined and analyzed by Western blot for GSDMD activation (EPR19828; Abcam), caspase-1 activation (Casper-1; AdipoGen), caspase-11 (EPR18628; Abcam) and actin (ACTN05 (C4); Invitrogen)

IFN-γ intracellular cytokine staining

WT C57BL/6 or *Rag1*$^{-/-}$ mice were infected with 2x10^7 CFU of *B. thailandensis.* Twelve hours later, mice were i.v. treated with 250 μg, i.v of brefledin A (Sigma-Aldrich) as previously described[83] . Six hours later, mice were euthanized, spleens were harvested, and splenocytes were extracted by mechanical disruption. Red blood cells were lysed with ACK lysing buffer, and splenocytes were counted using a hemocytometer. 2x10^6 cells from each spleen were first stained with LIVE/DEAD™ Fixable Blue Dead Cell Stain Kit (Thermo Fisher) followed by extracellular staining for 30 minutes at room temperature. Extracellular antibodies used include: Alexa Fluor (AF) 488 anti-CD127 (clone A7R34); Brilliant Violet (BV) 570 anti-CD3 (clone 17A2); APC-Cy7 anti-CD45R (clone RA3-6B2); APC-Cy7 anti-Ly6G (clone 1A8); PE-Cy7 anti-CD90.2 (clone 53-2.1); BV650 anti-NK1.1 (clone PK136); BV421 anti-TCR □□ (clone GL3). For analyzing the distribution of CD4 and CD8 T cells, a parallel aliquot of cells was stained using the same panel as above with AF594 anti-CD4 (clone GK1.5) and PE anti-CD8

(clone 53-6.7). Cells were then fixed and permeabilized with BD Cytofix/Cytoperm for 20 minutes at 4^{o}C before being stained with APC anti-IFN-γ (clone XMG1.2; BioLegend). Cells were washed, acquired on a BD LRSII (UNC Flow Cytometry Core Facility), and analyzed using FlowJo (TreeStar; version 9.9.6). All antibodies were purchased from BioLegend. Absolute counts were determined by multiplying frequencies of population of interest determined by flow cytometry with the total number of splenocytes collected as determined by hemocytometer.

QUANTIFICATION AND STATISTICAL ANALYSIS

All statistics were performed using Prism 8 (GraphPad) using either two-way ANOVA followed by Sidak's multiple comparison test, one way ANOVA followed by Tukey's multiple comparison test, or Log-rank as specified in the figure legends. Number of mice used in each in vivo survival experiment are specified in Table 7. Flow data was analyzed using FlowJo (TreeStar; version 9.9.6).

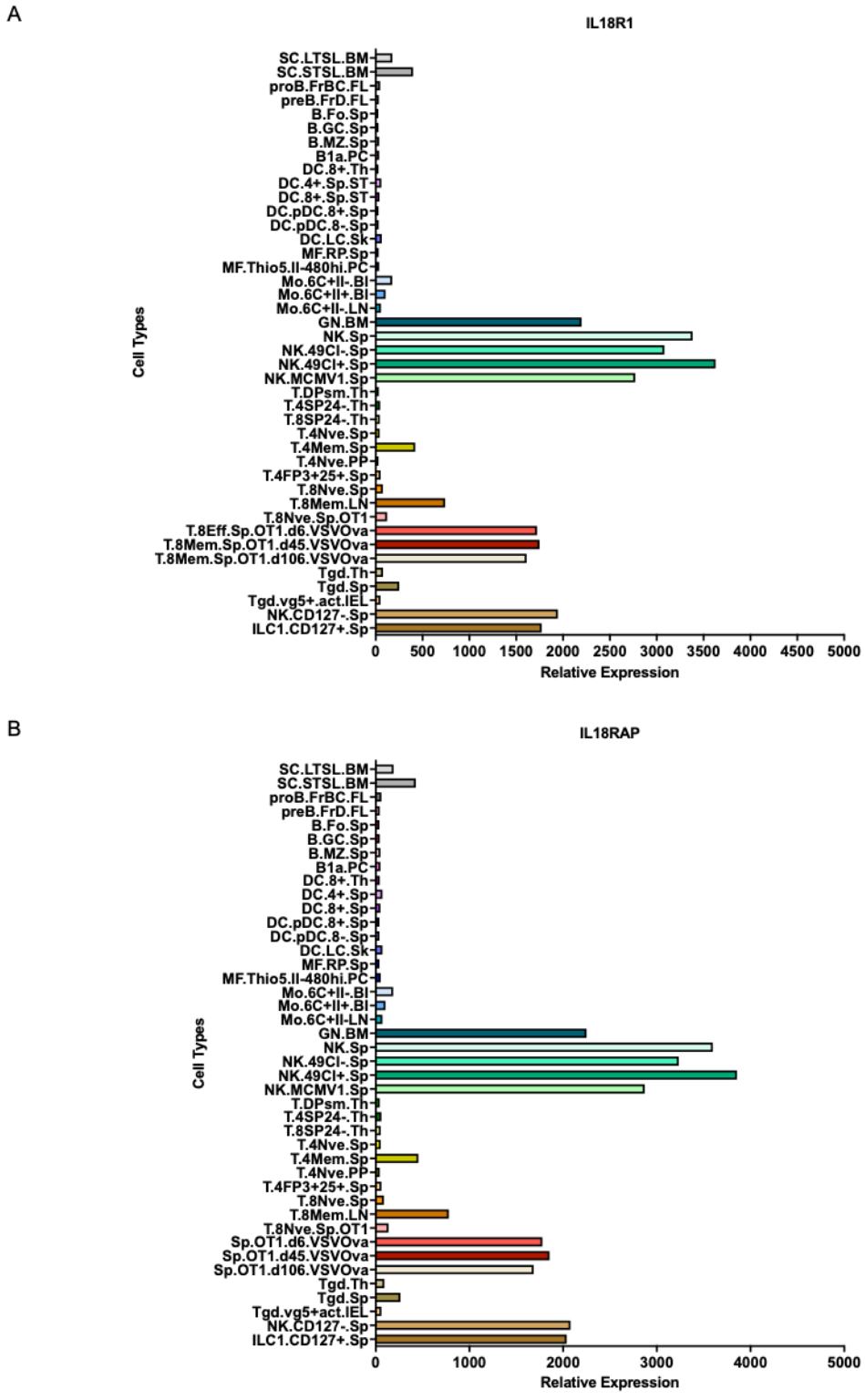

Figure 6. NK cells, ILC1 cells, and activated T cells highly express IL-18 receptor components.

(A) IL-18 Receptor 1 expression based on data from the Immunological Genome Project (immgen.org; microarray probe set ID 10345807).

(B) IL-18 Receptor Accessory Protein expression based on data from the Immunological Genome Project (immgen.org; microarray probe set ID 10345824).

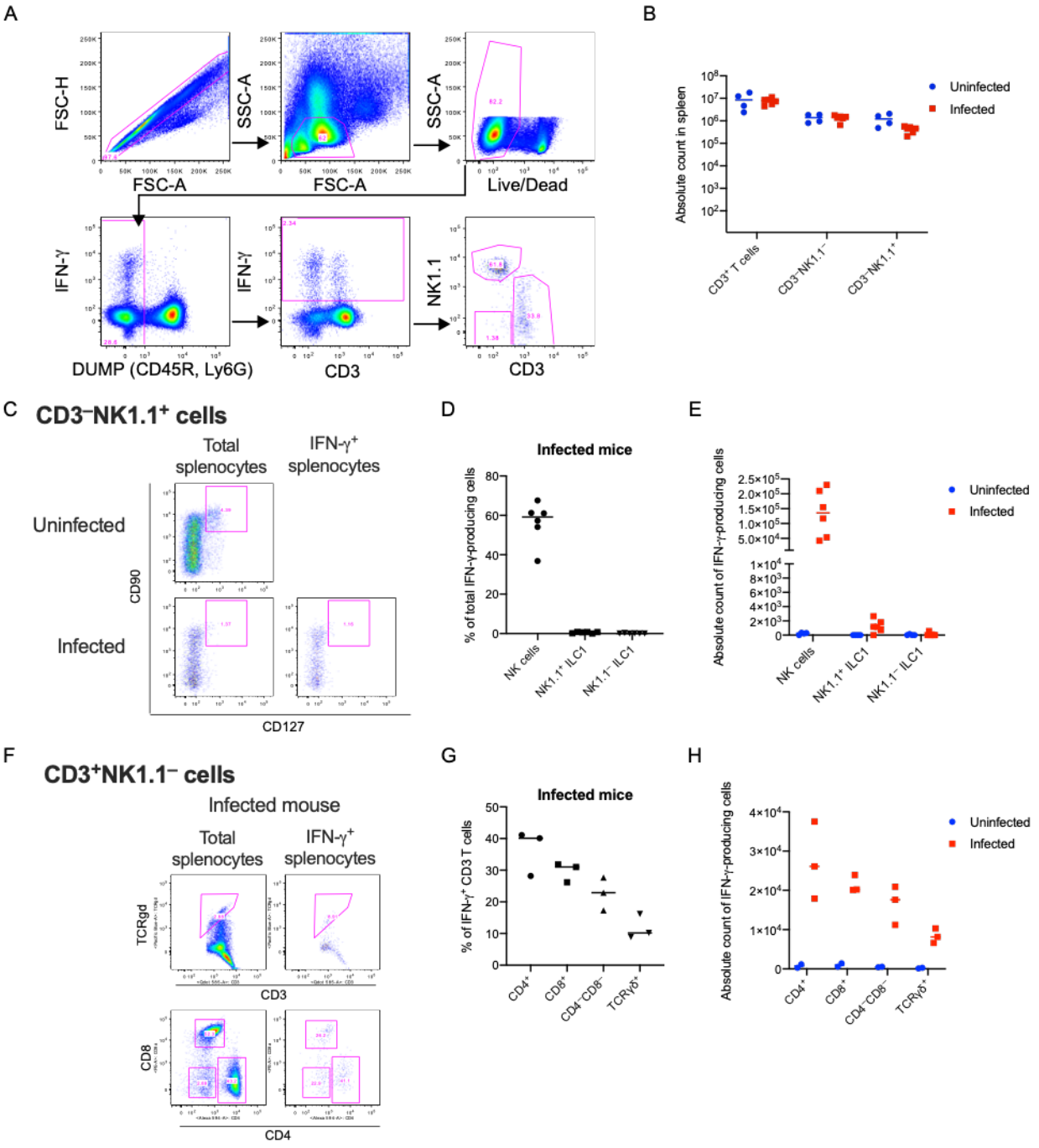

Figure 7. Gating strategy and subset analysis of IFN-γ-producing cells during *B. thailandensis* infection.

Mice were infected i.p. with $2x10^7$ CFU *B. thailandensis* for 12 hours then treated i.v. with 250 ug of brefeldin A. Six hours later, splenocytes were collected (total 18 hours post-infection) and analyzed by flow cytometry using the schema showed in (A). Absolute counts of each subset population in the spleen were determined in uninfected and infected mice (B). ILC1 cells were defined as live CD45R–Ly6G–CD3– lymphocytes that were CD90+CD127+ within either the NK1.1+ or NK1.1– populations (C). The NK cells were defined as the remainder of NK1.1+ cells that were CD127–. Cell populations were analyzed to determine determined percent of all IFN-g- producing cells that were ILC1s or NK cells (D), as well as the absolute counts of IFN-g-producing ILC1s and NK cells (E). CD3+ T cells were also analyzed for CD4, CD8, and TCR-gamma delta expression on the using the gating strategy in (F). These cells were analyzed to determined percent (G) and absolute count (H) of IFN-γ-producing CD3+ T cells that expressed these markers. Bar represents median.

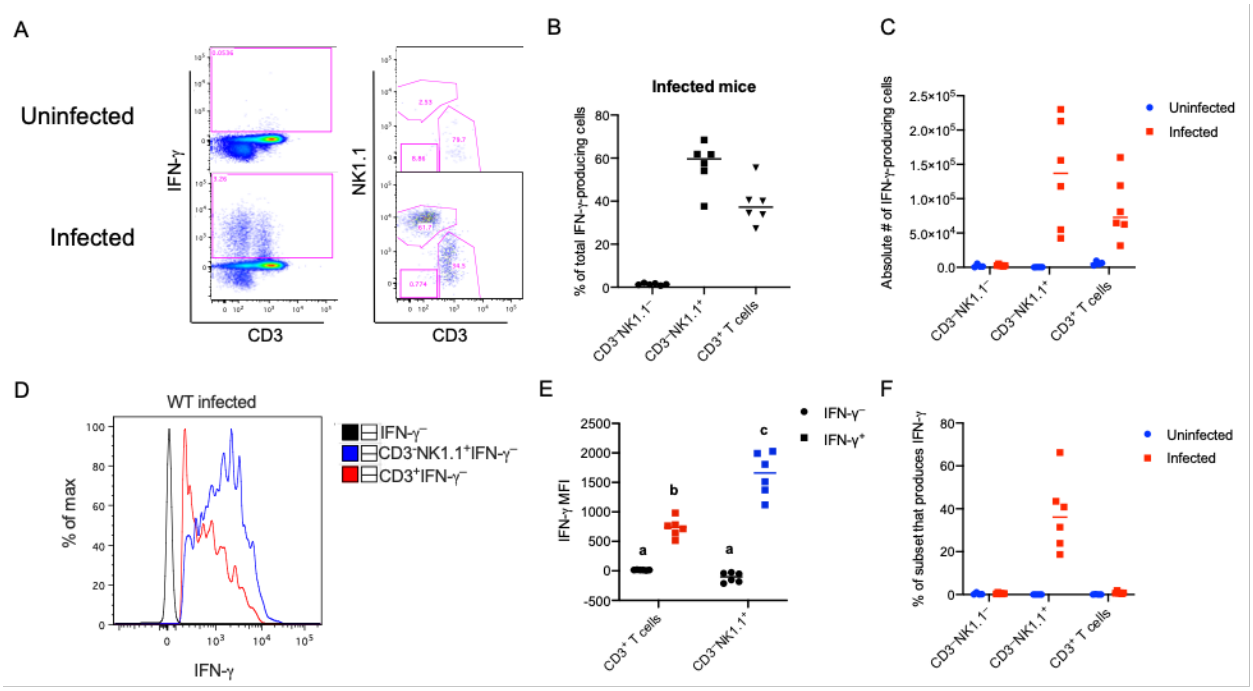

Figure 8. NK cells and T cells are the primary producers of IFN-γ during *B. thailandensis* infection.

Mice were infected i.p. with $2x10^7$ CFU *B. thailandensis*, and 12 hours later treated i.v. with 250 µg of brefeldin A. Six hours later, splenocytes were collected (total 18 hours post-infection). $Ly6G^-/CD45R^-$ live cells were analyzed by flow cytometry for IFN-γ^+ production. A representative analysis is shown in (A). IFN-γ^+ subpopulations were analyzed for percent of total IFN-γ^+ cells (B) and absolute count (C).

(D-E) Geometric mean fluorescent intensity (MFI) of IFN-γ in IFN-γ^+ and IFN-γ^- $NK1.1^+$ and $CD3^+$ subsets were compared by two-way ANOVA. Sidak's multiple comparison test was used for post-hoc pairwise comparison between MFI of $NK1.1^+$ and $CD3^+$ subsets from the same sample. Groups that do not share a letter are statistically different from each other with $p \leq 0.05$.

(F) Total spleen populations of $NK1.1^+$ and $CD3^+$ subsets were analyzed for percent that were IFN-γ^+.

All data pooled from two experiments. Bar represents median.

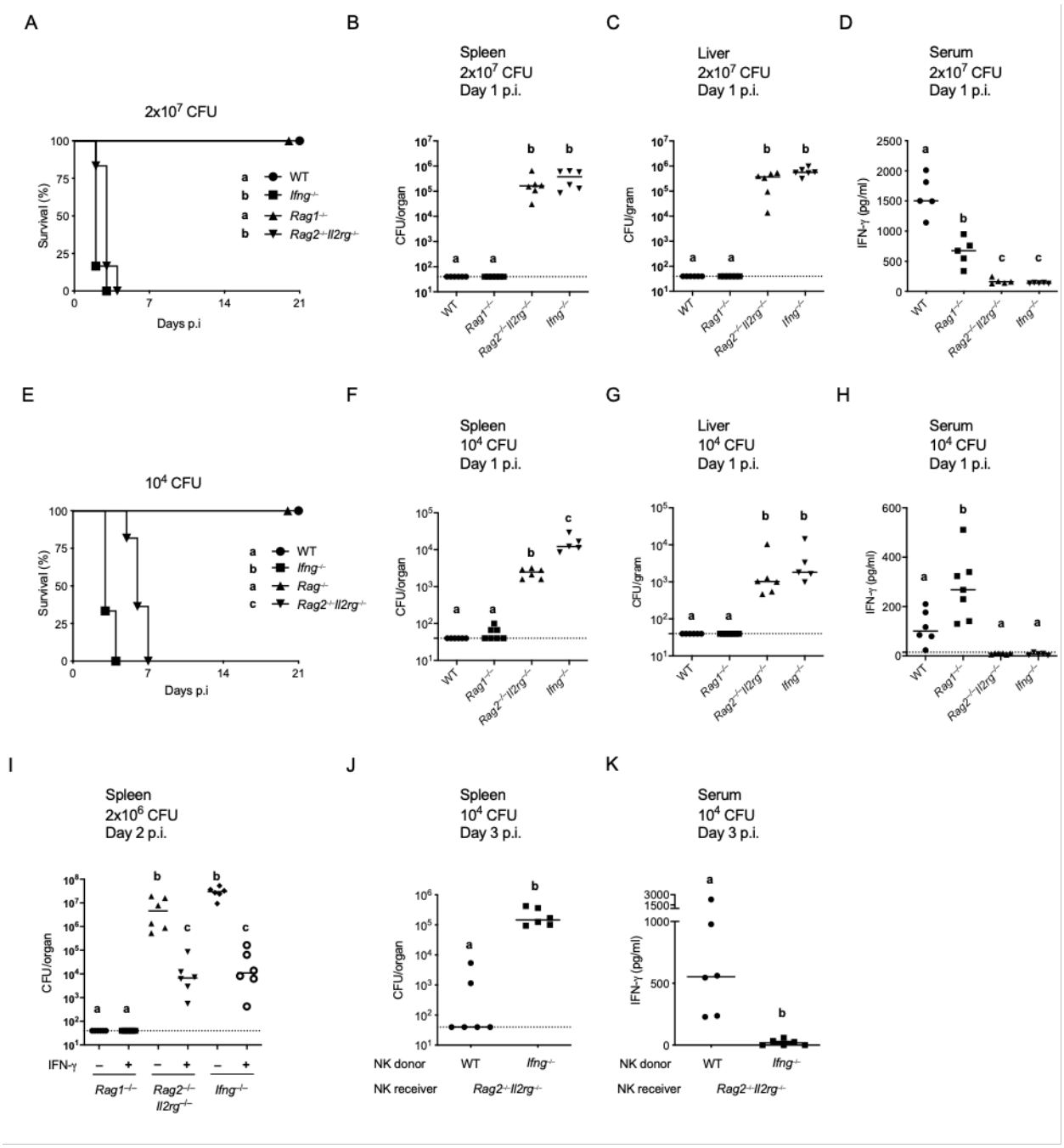

Figure 9. Innate lymphocyte production of IFN-γ is required for defense against *B. thailandensis*.

(A–H) Mice were infected i.p. with the indicated dose of *B. thailandensis*. Survival was monitored (A, E), or mice were harvested one day post infection (p.i.) and bacterial burdens in

spleens (B, F) and livers (C, G) were determined, or serum IL-18 levels were determined by ELISA (D, H).

(I) Mice were infected i.p. with $2x10^6$ CFU *B. thailandensis*, and injected i.p. with PBS or recombinant mouse IFN-γ (0.5 mg/dose) at 0 and 24 hours p.i. Splenic burdens were determined 48 hours p.i.

(J-K) Mice were adoptively treated with 10^6 NK cells at 14 and 7 days prior to infection with 10^4 CFU *B. thailandensis*. Splenic burdens (J) and serum IFN-γ levels, as determined by ELISA (K), were assessed day 3 p.i.

All data are pooled from two experiments. Bar represents median. Dashed line indicates limit of detection. For number of mice in survival panel see Table 7. Survival curves were compared using Log-rank tests using Bonferroni-corrected threshold for statistical significance of $p \leq 0.008$. Bacterial burden and IFN-γ levels were analyzed using one-way ANOVA followed by Tukey's multiple comparisons test with a statistical threshold of $p \leq 0.05$. Groups that do not share a letter are statistically different from each other.

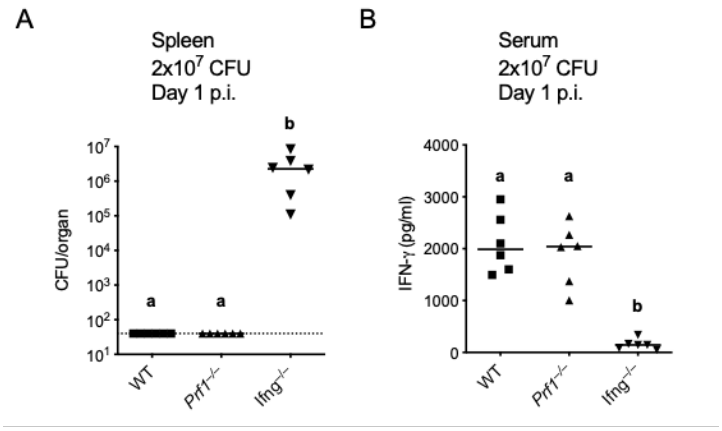

Figure 10. NK and T cell response to *B. thailandensis* infection is independent of perforin.

Mice were infected i.p. with 2x107 CFU *B. thailandensis*. We determined splenic bacterial burdens (A), and serum IFN-g levels by ELISA (B).

All data are pooled from two experiments. Bar represents median. Dashed line indicates limit of detection. Bacterial burdens and IFN-g levels were analyzed using one-way ANOVA followed by Tukey's multiple comparisons test with a statistical threshold of $p \leq 0.05$. Groups that do not share a letter are statistically different from each other.

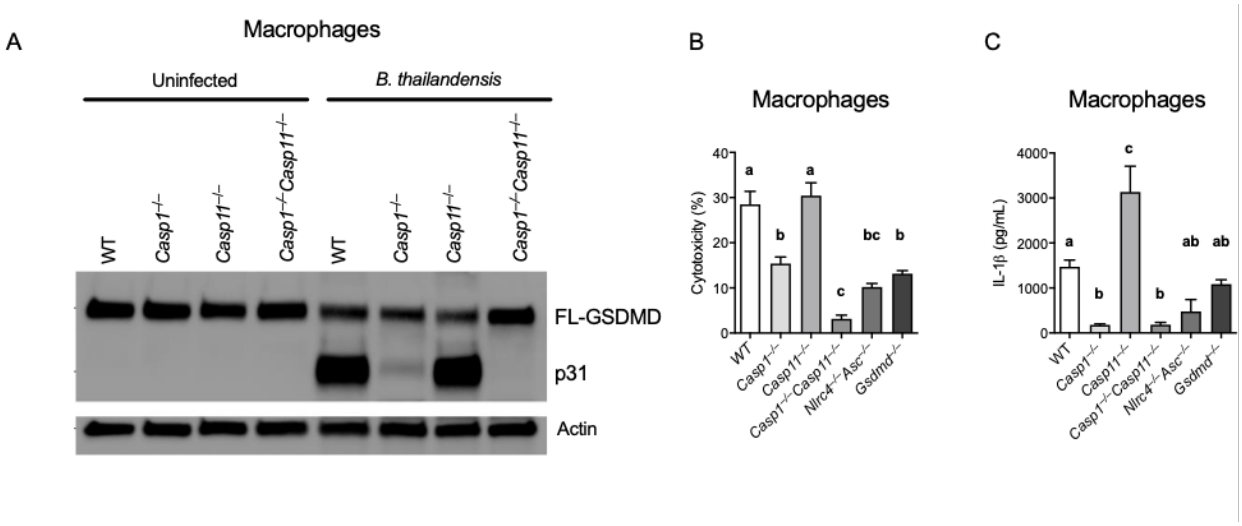

Figure 11. *B. thailandensis* induces gasdermin D-mediated pyroptosis and cytokine secretion in macrophages in vitro.

(A-C) Pam_3CSK_4-primed BMMs were infected at MOI 50 for 4 hours. Gasdermin D (GSDMD) cleavage was determined by western blot (A), cytotoxicity was determined by LDH release assay (B), and IL-1β was determined by ELISA (C).

Bar represents mean ± SEM. Data are representative of three independent experiments. Data was analyzed using one-way ANOVA followed by Tukey's multiple comparisons test. Groups that do not share a letter are statistically different from each other with $p \leq 0.05$.

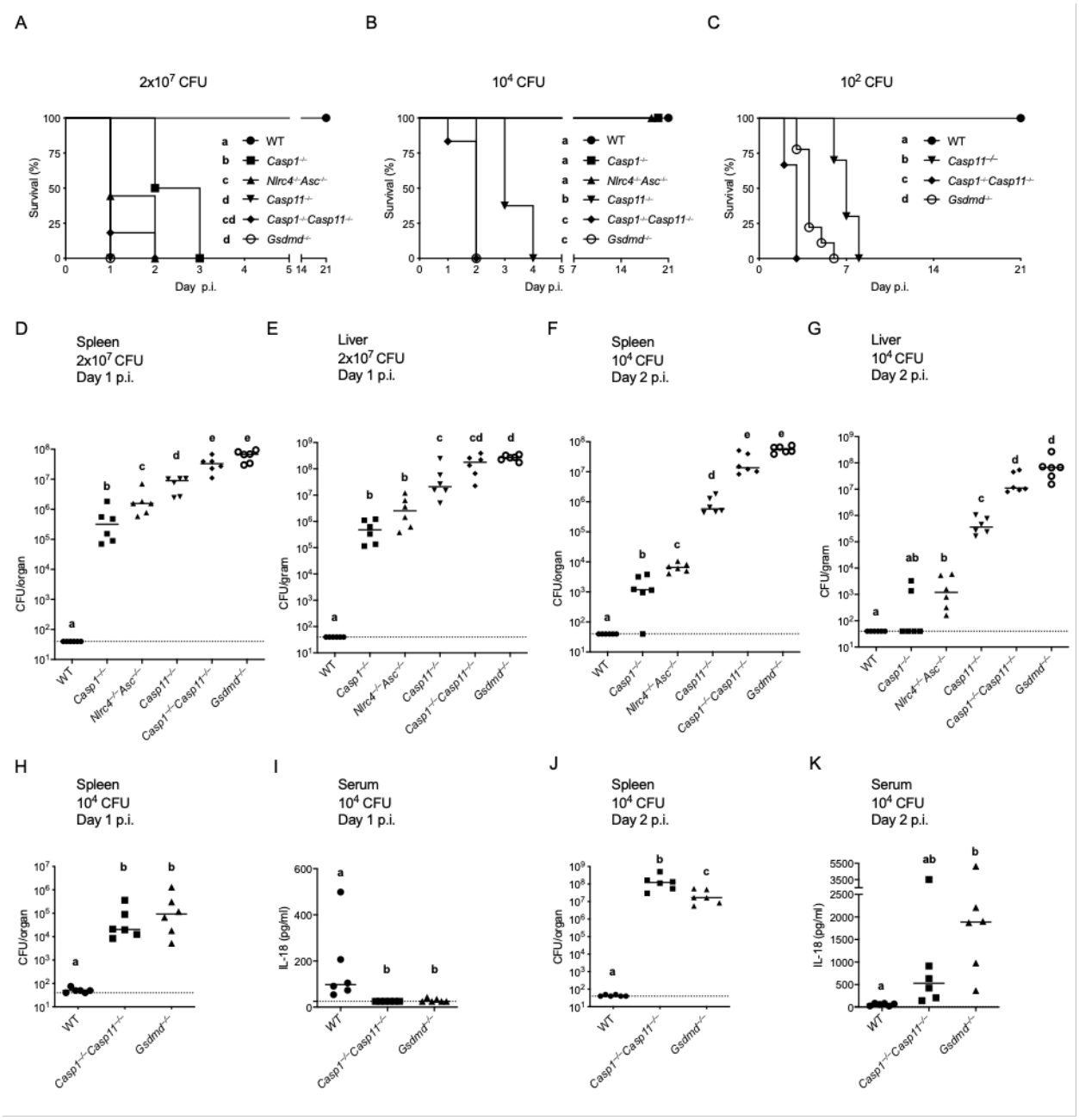

Figure 12. Gasdermin D is essential for defense against *B. thailandensis* in vivo.

(A-C) Mice were infected i.p. with *B. thailandensis* at the indicated dose and survival was monitored.

(D-G) Mice were infected i.p. with *B. thailandensis* at the indicated dose and bacterial burdens were determined in spleen or liver at the indicated time post-infection (p.i.).

(H-K) Mice were infected i.p. with 10^4 CFU *B. thailandensis* and bacterial burdens in the spleen were determined on the indicated days p.i (H, J). Serum IL-18 levels were determined by ELISA (I, K).

All data for survival are pooled from three experiments and pooled from two experiments for bacterial burden analysis. Bar represents median. Dashed line indicates limit of detection. For number of mice in survival panel see Table 7. Survival curves were compared using Log-rank tests. Bonferroni-corrected thresholds for statistical significance were used ($p \leq 0.003$ for A and B, $p \leq 0.017$ for C). Bacterial burden and IL-18 levels were analyzed using one-way ANOVA followed by Tukey's multiple comparisons test. Groups that do not share a letter are statistically different from each other with $p \leq 0.05$.

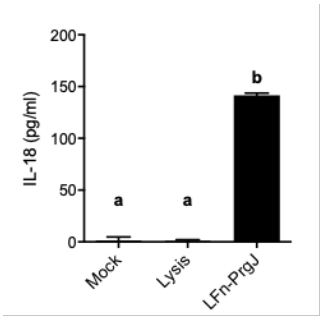

Figure 13. MBL IL-18 ELISA kit is specific for cleaved IL-18.

Pam3CSK4 primed BMMs were treated with NLRC4 agonist PrgJ-Tox (2 μg/well) for 4hours. IL- 18 was determined by ELISA using MBL IL-18 ELISA kit. Bar represents mean ± SEM.

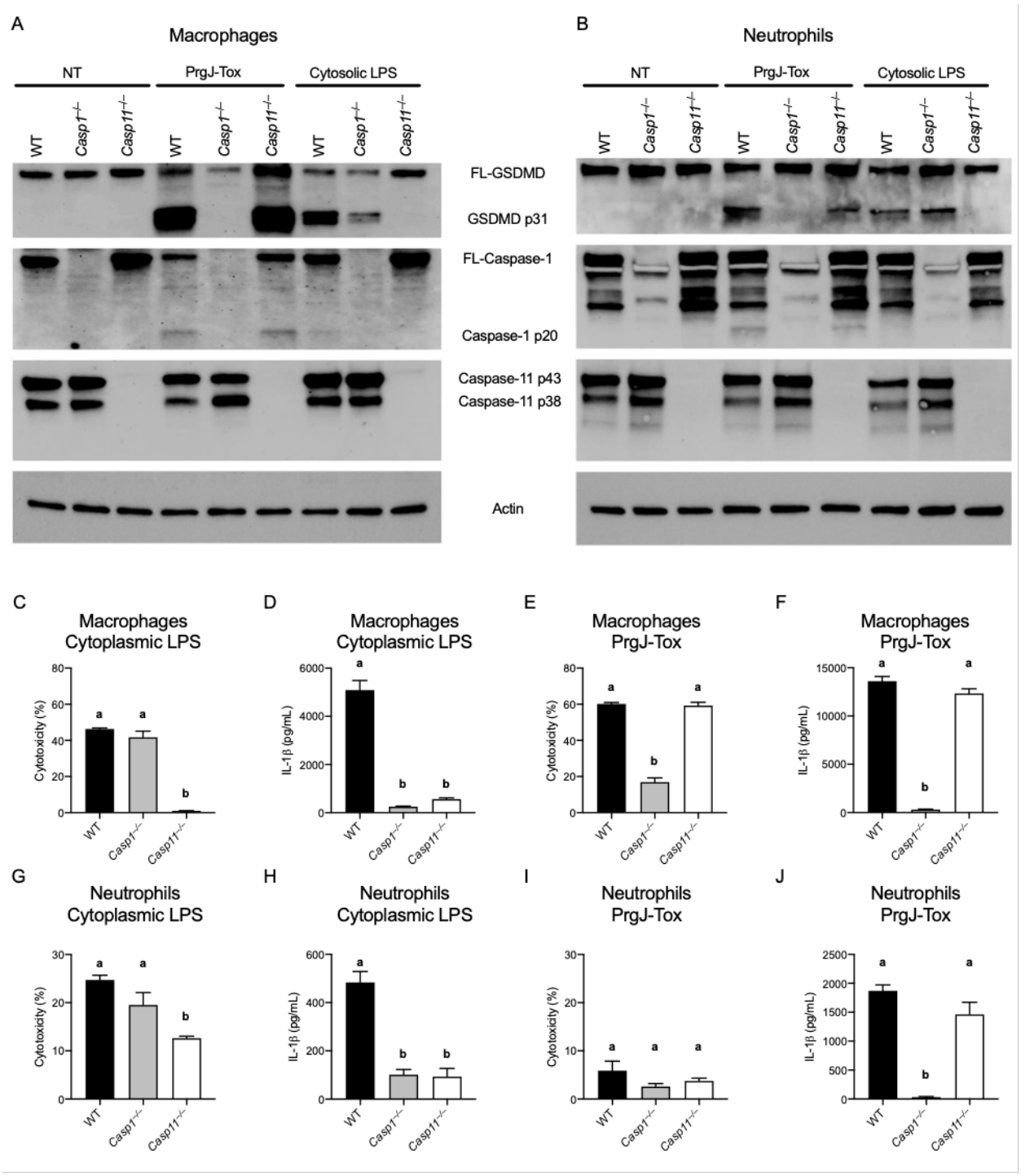

Figure 14. Neutrophils undergo pyroptosis in response to caspase-11 agonists but not NLRC4 agonists.

(A-E) IFN-γ/LPS-primed macrophages or neutrophils were treated with NLRC4 agonist PrgJ-Tox (2 μg/well) or transfected by LPS (10 μg/ml) for 5 hours. Gasdermin D, caspase-1, and caspase-11 cleavage were determined by western blot in macrophages (A) and neutrophils (B). Cytotoxicity was determined by LDH release assay (C, E, G, I), and IL-1β release was determined by ELISA (D, F, H, J). Dashed line indicates limit of detection. Bar represents mean ± SEM. Data are representative of three independent experiments. Cytotoxicity and IL-1β levels were analyzed using one-way ANOVA followed by Tukey's multiple comparisons test. Groups that do not share a letter are statistically different from each other with $p \leq 0.05$. NT: No treatment. FL-GSDMD: Full length gasdermin D. *Bt* background band: background band of *B. thailandensis* components.

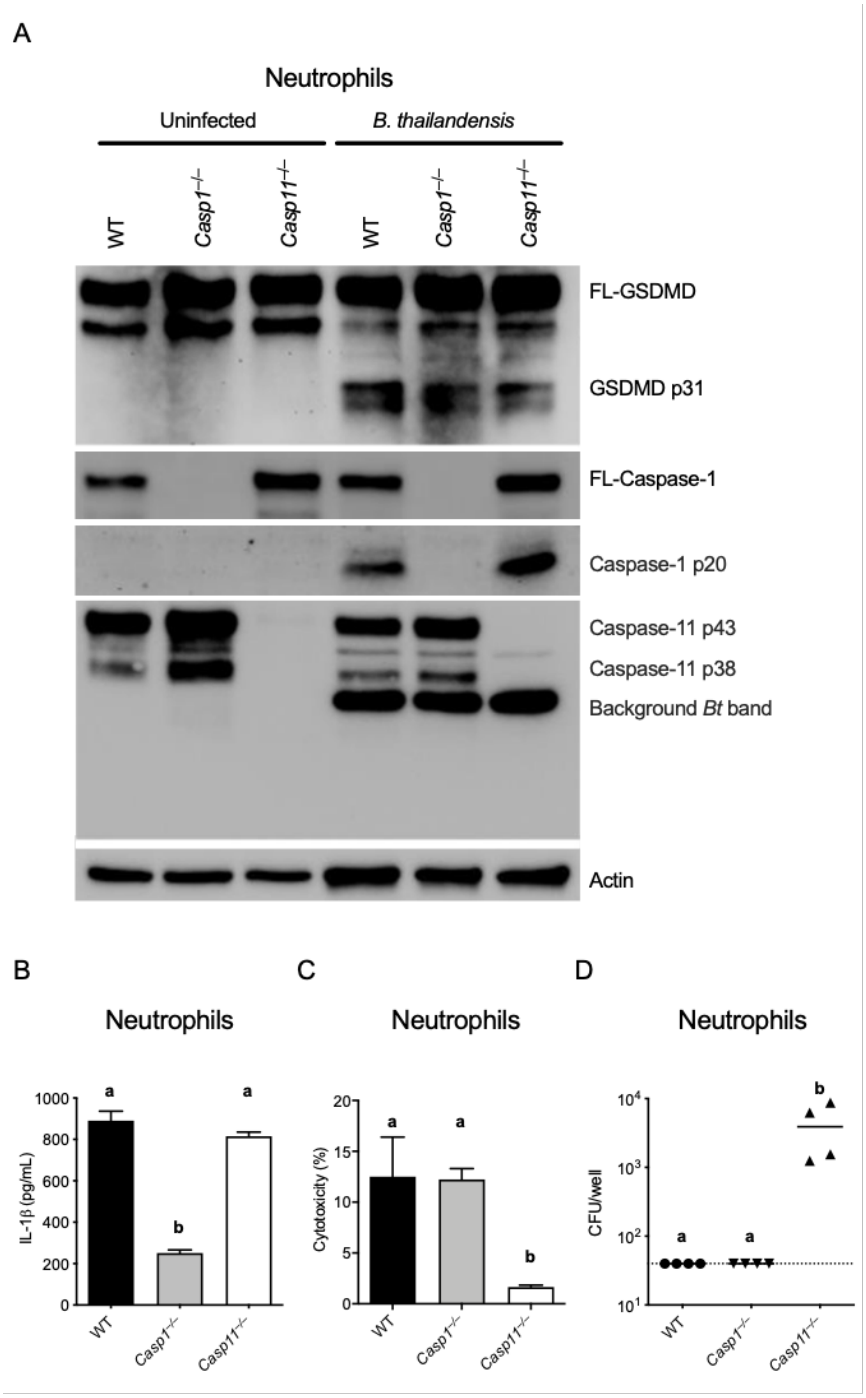

Figure 15. Neutrophils require caspase-11 to trigger pyroptosis and clear *B. thailandensis* infection in vitro. Pam_3CSK_4 primed Neutrophils were infected with *B. thailandensis* (Bt) at MOI 100 for 5 hours. Gasdermin D, caspase-1, and caspase-11 cleavage were determined by

western blot (A), IL-1β release was determined by ELISA (B), and cytotoxicity was determined by LDH release assay (C).

(D). Neutrophils were infected at MOI 100 for 4 hours. After 1 hour, extracellular bacterial growth was stopped by addition of 500 μg/ml kanamycin and CFU was determined at 4 hours. Data are representative of three independent experiments. Bar represents mean ± SEM for (B-C), median for (D). IL-1β, cytotoxicity, and recovered CFUs were analyzed using one-way ANOVA followed by Tukey's multiple comparisons test. Groups that do not share a letter are statistically different from each other with $p \leq 0.05$.

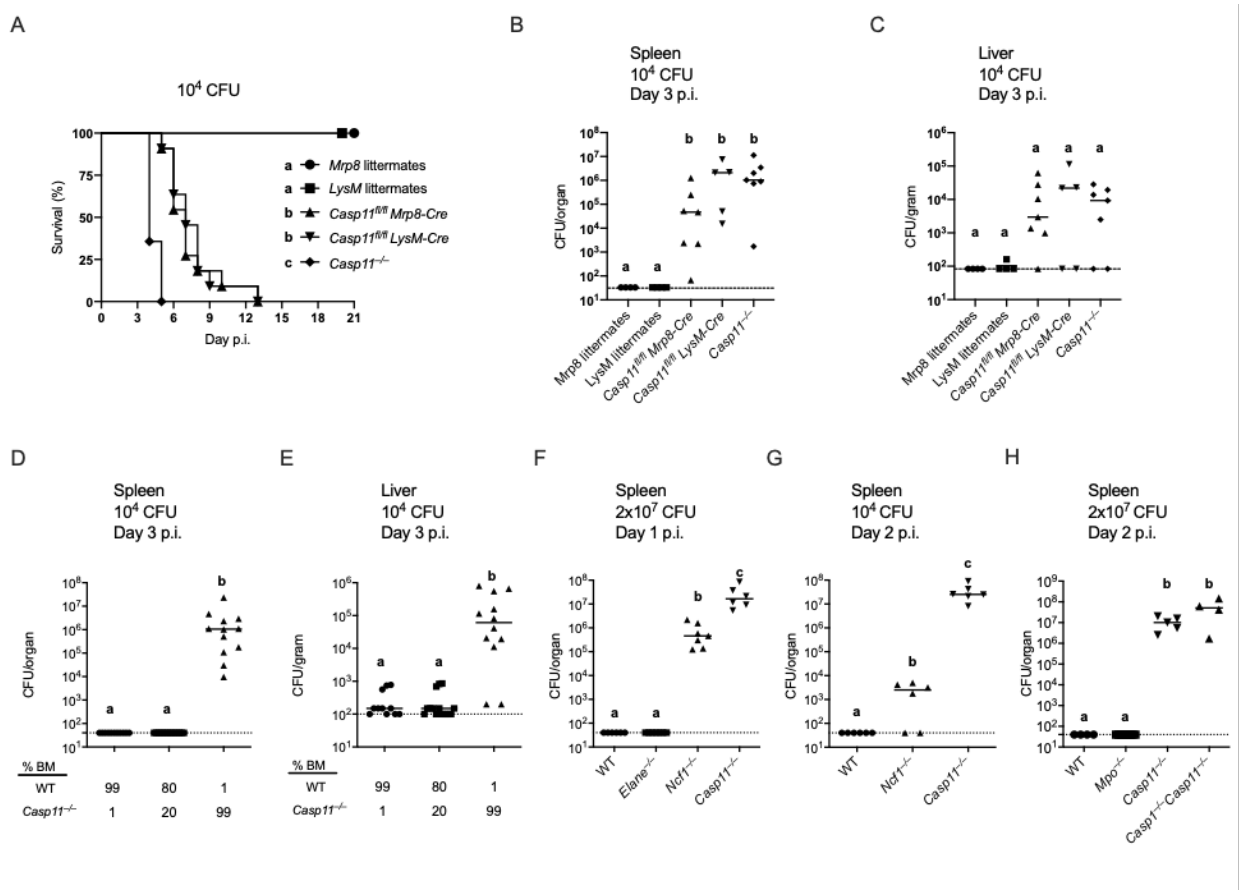

Figure 16. Caspase-11 in neutrophils is essential to clear *B. thailandensis* infection in vivo.

Mice were infected i.p. with 10^4 CFU *B. thailandensis* and survival was monitored (A). Bacterial burdens at three days post-infection (p.i.) were determined in spleen (B) and liver (C). *Mrp8* littermate controls and *LysM* littermate controls consisted of *Casp11*$^{+/fl}$ *Mrp8-cre* and *Casp11*$^{+/+}$ *Mrp8-cre*, and *Casp11*$^{+/fl}$ *LysM-cre* and *Casp11*$^{+/+}$ *LysM-cre*, respectively. (D-E) Lethally irradiated mice were transferred CD45.1$^+$ wild type and CD45.2$^+$ *Casp11*$^{-/-}$ at the ratios indicated and allowed to engraft for 6 weeks. Mice were then infected i.p. with 10^4 CFU *B. thailandensis*, and splenic (D) and liver (E) bacterial burdens were determined three days p.i. (F-H) Mice were infected i.p. with *B. thailandensis* at the indicated doses, and splenic burdens were determined at the times p.i. indicated.

All data are pooled from two experiments. Bar represents median. Dashed line indicates limit of detection. For number of mice in survival panel see Table 7. Survival curves were compared using Log-rank tests using Bonferroni-corrected threshold for statistical significance of $p \leq 0.005$. Bacterial burdens were analyzed using one-way ANOVA followed by Tukey's multiple comparisons test with a statistical threshold of $p \leq 0.05$. Groups that do not share a letter are statistically different from each other.

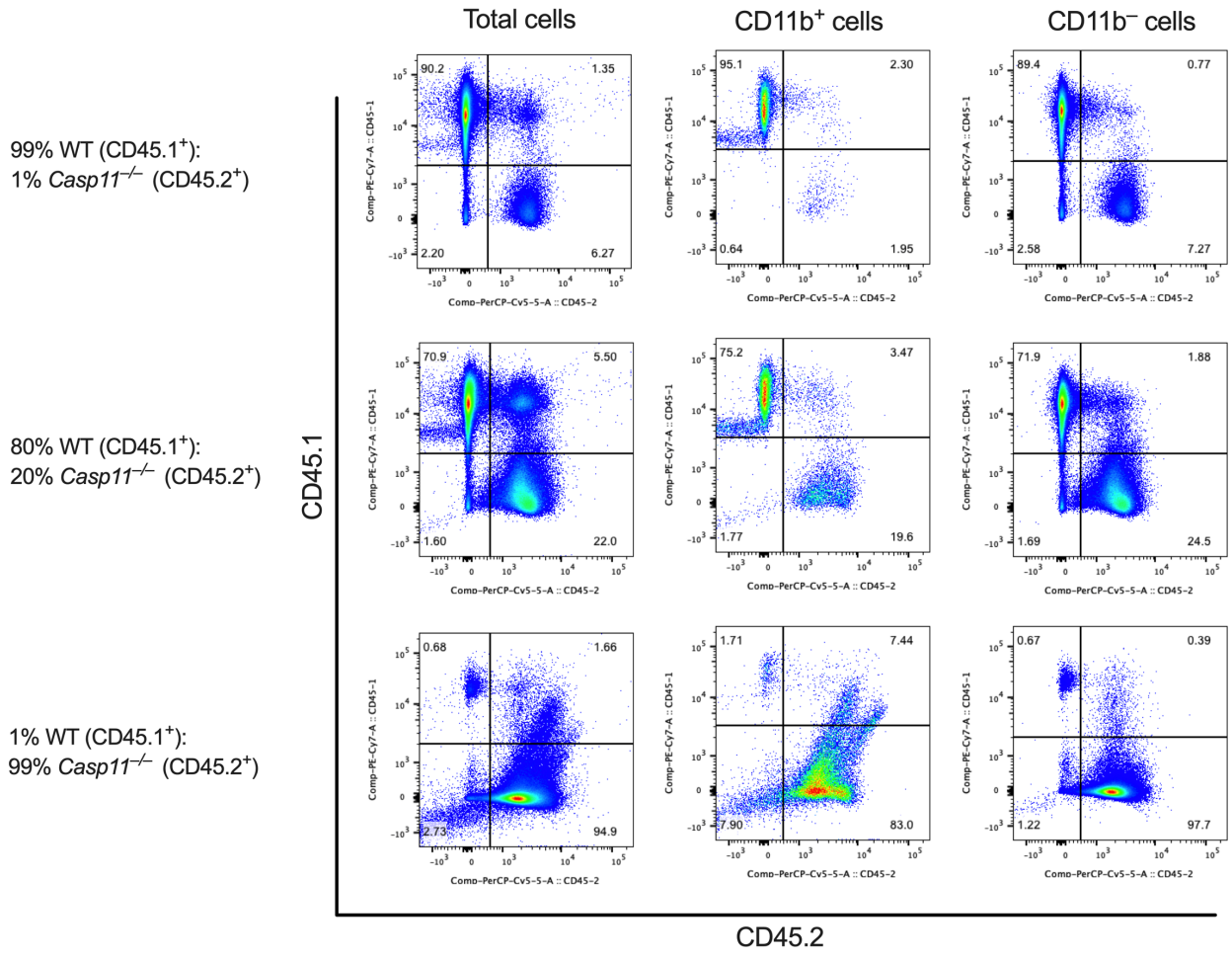

Figure 17. Ratios of bone marrow transplant was maintained after engraftment.

(A) WT mice were lethally irradiated and transplanted with bone marrow from CD45.1^{+} WT mice and CD45.2^{+} Casp11$^{-/-}$ mice. After 6 weeks of engraftment, mice were infected i.p. with 10^{4} CFU *B. thailandensis* and harvested 3 days post-infection. Representative flow cytometry of splenocytes from these mice are shown.

Figure	Mice Genotype	n
Fig.9A	C57Bl/6	11
	Ifng$^{-/-}$	6
	Rag1$^{-/-}$	6
	Rag2$^{-/-}$*Il2rg*$^{-/-}$	12
Fig.9E	C57Bl/6	9
	Ifng$^{-/-}$	6
	Rag1$^{-/-}$	6
	Rag2$^{-/-}$*Il2rg*$^{-/-}$	11
Fig.12A	C57Bl/6	13
	Nlrc4$^{-/-}$*Asc*$^{-/-}$	9
	Casp1$^{-/-}$	8
	Casp11$^{-/-}$	8
	Casp1$^{-/-}$*Casp11*$^{-/-}$	6
	GsdmD$^{-/-}$	12
Fig.12B	C57Bl/6	13
	Nlrc4$^{-/-}$*Asc*$^{-/-}$	8
	Casp1$^{-/-}$	7
	Casp11$^{-/-}$	8
	Casp1$^{-/-}$*Casp11*$^{-/-}$	10
	GsdmD$^{-/-}$	9
Fig.12C	C57Bl/6	7
	Casp1$^{-/-}$*Casp11*$^{-/-}$	9

	Casp11$^{-/-}$	10
	GsdmD$^{-/-}$	9
Fig. 16A	*Casp11*$^{+/+ \text{ or } fl/+}$ *Mrp8-cre*	13
	Casp11$^{-/-}$	14
	Casp11$^{fl/fl}$ *Mrp8-cre*	11
	Casp11$^{+/+ \text{ or } fl/+}$ *LysM-cre*	8
	Casp11$^{fl/fl}$ *LysM-cre*	11

Table 7. Numbers of mice used in survival experiments.

CHAPTER 4: DEVELOPING A MOUSE MODEL TO EXPLORE CELL AND TISSUE-SPECIFIC ROLES OF GASDERMIN D[4]

Introduction

Originally, inflammasomes were thought to be primary restricted to traditional immune cell types, most notably macrophages. Most experiments characterizing the function and activity of inflammasomes were performed using primary macrophages or monocyte/macrophage cell lines. However, recent studies have demonstrated the fallacy of restricting our understanding of inflammasomes to macrophages. Indeed, our studies using *Burkholderia thailandensis* described in Chapter 3 demonstrate that even within the immune compartment, inflammasomes and gasdermin D behave differently in neutrophils compared to macrophages[8]. In addition, others have demonstrated that inflammasome pathways can trigger pyroptosis of non-immune cells. For example, Rauch et al. demonstrated that caspase-1 and gasdermin D can trigger pyroptosis of intestinal epithelial cells[28] while Mitchell et al. demonstrated that inflammasome activation within intestinal epithelial cells is sufficient to clear infection with *Shigella* in mice[126]. Similarly, inflammasome activation and gasdermin D-triggered pyroptosis in respiratory epithelial cells has been implicated in both infection and asthma[127,128].

Given these diverse cell types and cell type-dependent responses to inflammasome activation, it becomes essential to have tools available to properly differentiate the contributions of inflammasomes within various cell compartments in vivo using mouse disease models.

[4]Stephen Kovacs performed everything described once the mouse line was generated by UNC animal core. This data may be included in an eventual publication in which the final correct mice are generated and used in a disease model.

Therefore, the development of cell-specific knockout lines for components of these pathways and gasdermin D specifically is of high priority.

The modern method to generate cell-specific knockout-ready mice is to use CRISPR to insert loxP sites surrounding genes or exons in the gene of interest. When these mice are then crossed with mice expressing Cre recombinase, the gene is either completely removed from Cre-expressing cells or truncated to the point that the resulting transcript is nonfunctional and quickly degraded. Cre can be expressed under promotors functional only within the desired cell population, thereby giving cell specificity to the knockout.

The utility of Cre-lox-based, cell-specific knockout models has been clearly demonstrated with our Mrp8-specific knockouts of caspase-11 used to evaluate the role of neutrophil caspase-11 during *B. thailandensis* infection as described in Chapter 3. To date, cell-specific deletions of caspase-11and IL-1β have been published[124,129]. Cell-specific inducible expression of NLRC4 on a *Nlrc4*$^{-/-}$ background have also been published[28]. We sought to develop a mouse model for cell-specific deletions of gasdermin D to allow further characterization of this important protein in various infectious and inflammatory models.

Generation of "knockout first" gasdermin D mouse line

We purchased from European Mutant Mouse Repository (EuMMCR) C57BL/6 embryonic stem cells in which the construct shown in Figure 18A replaced the wild type gasdermin D gene. The insertion of lacZ followed by a stop codon after exon 2 of gasdermin D leads to expression of a truncated gasdermin D with β-galactosidase (encoded by lacZ) attached at the end, resulting in a non-functional protein. Since this nonfunctional gasdermin D is not cell type-restricted, this genotype is considered "knockout first". The UNC animal model core

verified the presence of the construct in the genome using Southern blotting (not shown), and then injected these embryonic stem cells into developing wild type embryos, which were then implanted into female mice. The resulting offspring were chimeras in which some cells were wild type and some contained our desired construct. F1 offspring with the desired construct were then bred to homozygosity.

We verified the presence of the construct by performing PCR for the presence of the neo cassette. Similarly, primary macrophages obtained from mice homozygous for this construct resisted pyroptosis in response to nigericin (mouse 1 in Figure 18B), demonstrating that the resulting mice were "knockout first" as expected. However, we also attempted to validate the location of this insert using primers that spanned the wild type region of the genome and the construct insert; however, these attempts failed, suggesting that the chromosomal construct as predicted by EuMMCR may not have been precisely correct. More alarming, when we sequenced the region of the genome where the distal-most loxP site should have been, we could not identify a loxP sequence, instead our sequencing showed the normal chromosomal region where the loxP site should be located. Since the construct is introduced by two homologous recombination events, it was possible that only the main part of the construct (containing the neo cassette and *lacZ* followed by a stop codon, resulting in a nonfunctional, truncated gasdermin D) was successfully inserted into the genome, but this distal lox site was not. For this to occur, we think that it is possible that the first recombination event occurred upstream of the construct as intended, but that the second recombination event could have occurred within exon 3, thus omitting the introduction of the distal loxP site. This is an error that would not have been detected by the animal core's southern blotting due to the small size of the distal loxP insert. If this was indeed the case, then it would be impossible to generate the cell-specific knockout lines

desired with our current mice. However, it remained possible that the location of the distal lox site was merely incorrectly annotated, and that it was actually present somewhere else in the gene. If this were the case, we would be able to successfully generate the cell-specific knockouts by crossing with Cre mice.

Attempt to generate the cell-specific knockout mouse for gasdermin D

To assess if the distal lox site was present but its precise location was misannotated, we decided to try to generate the cell-specific knockouts and phenotype our mice. First, we crossed the knockout first mice with mice constitutively expressing the recombinase flippase, which removes all the sequences between the two Frt sites (Figure 1A. Since the *lacZ* and *neo* cassettes, alongside their premature stop locations, are both removed, the full length gasdermin D can now be produced in all tissues regardless if the distal lox was present.

Since the flippase should have removed the lacZ and neo cassettes in all cells including germline cells, we next bred flippase out of the line. Then, we wanted to definitively identify if the distal lox site was present and the mice were indeed cell-specific knockout-ready as would be expected if the construct was correct. Therefore, we crossed these mice with *Mrp8*-cre and bred to homozygosity for the construct. The first round of breeding yielded one mouse that was homozygous for the *Gsdmd* construct and contained *Mrp8*-cre. We infected this resulting mouse with $5x10^4$ CFU *Burkholderia thailandensis* and assessed bacterial burdens three days post-infection. Given that Mrp8-specific deletion of caspase-11 resulted in susceptibility to *B. thailandensis* infection as shown in Chapter 3, a *MRP8*-specific deletion of gasdermin D would almost certainly also be susceptible to *B. thailandensis* infection; however, the tested mouse had completely cleared the infection, suggesting that these mice behaved like wild type mice and did

not have *Mrp8*-specific deletions of gasdermin D (not shown). Only a single mouse was tested, so this experiment should be repeated to validate these results. Nevertheless, this result supports our sequencing data suggesting that the distal lox site was missing from the construct (Figure 1C).

Discussion

Generating a mouse model for cell-specific deletions of gasdermin D would be an important step for discriminating the cell-specific roles of gasdermin D in various disease models. Our results here suggest that we have successfully generated a mouse line with a lox site proximal to exon 3 of *Gsdmd*, but that the distal lox site required for making this line cell-specific knockout-ready is missing. The next step should be correcting this error by performing CRISPR to restore the missing lox site through the mouse core. Since this would require only a single CRISPR recombination of a short sequence, correcting the construct in these mice would still be easier than starting from scratch and attempting to insert both proximal and distal lox sites.

Methods

Cytotoxicity assay: Bone marrow–derived macrophages (BMM) were prepared from the femur and tibia of mice by culturing with L929 cell supernatant for 7 day at 37^{o}C, 5% CO_2. 5x10^4 macrophages were plated into a 96 well plate. Macrophages were primed overnight with 50 ng/mL of *S. typhimurium* LPS. Macrophages were then treated with 10 μM for 1 hour. Cytotoxicity was defined as the percentage of total lactate dehydrogenase released into the supernatant and was determined as described[125].

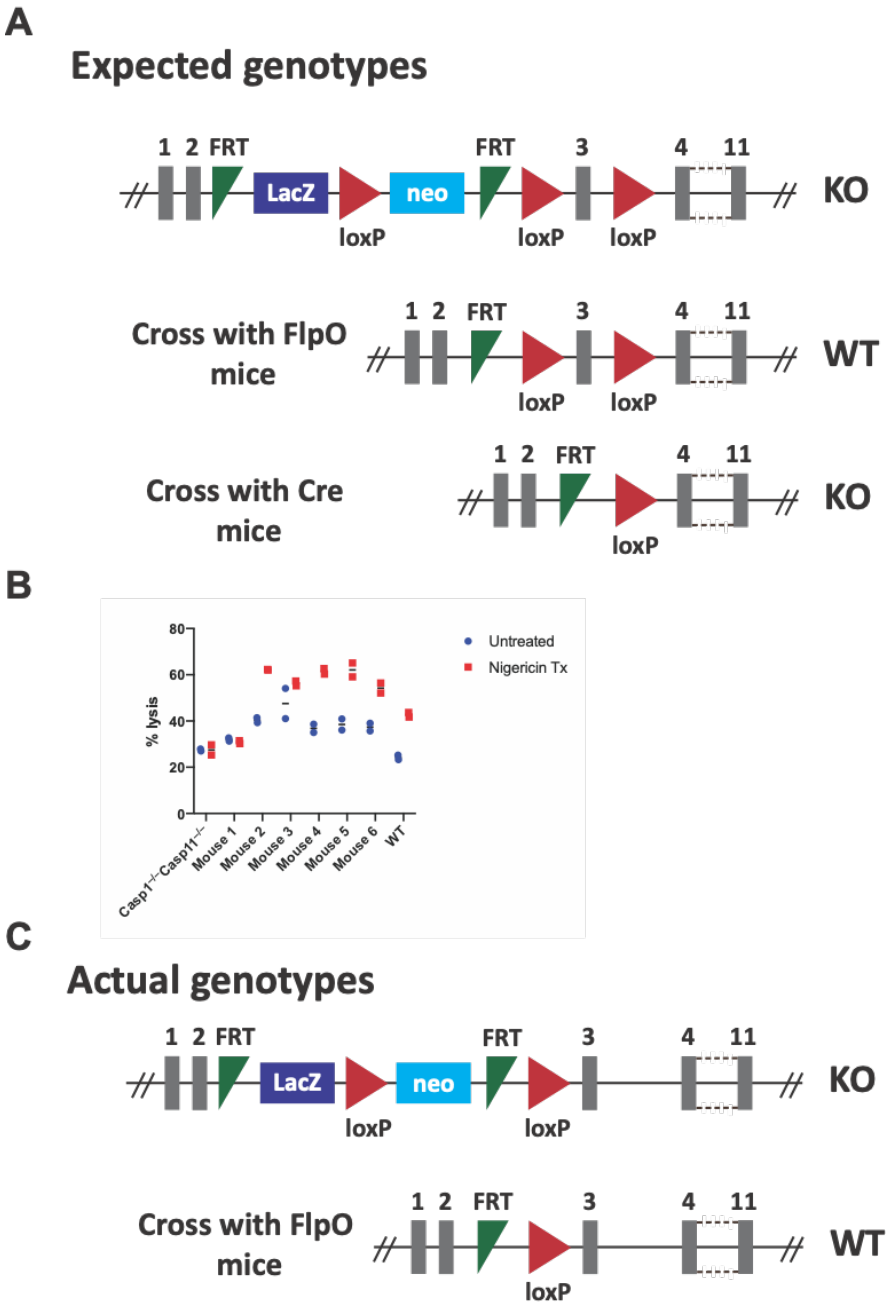

Figure 18. Creating a conditional KO mouse line for Gsdmd.

(A) Expected *Gsdmd*$^{-/-}$ genotypes in the generated EuMMCR mouse line.

(B) Percent lysis of LPS-primed primary macrophages from EuMMCR mice (mice 1-6) of unclear genotype and *Casp1*$^{-/-}$*Casp11*$^{-/-}$ and WT controls, as measured by LDH assay.

(C) What we suspect the actual genotype of the EuMMCR mice to be.

CHAPTER 5: EXPLORATIONS INTO FUNCTION AND ACTIVATION MECHANISM OF GASDERMIN A[5]

Introduction

Gasdermin A is a member of the pore-forming gasdermin family whose expression is restricted to the epidermis of the skin and epithelial cells of the upper gastrointestinal tract[40,42,43]. Whereas humans only express a single form of gasdermin A, mice have triplicated the gene such that gasdermin A1 most closely resembles human gasdermin A by sequence and is expressed in both the skin and the stomach[14,43-45], gasdermin A2 is restricted to the stomach[40], and gasdermin A3 is restricted to the skin[14,43,44,46,47]. Similar to gasdermin D and gasdermin E, the N-terminal domains of both human and mouse gasdermin A can oligomerize, form pores, and trigger pyroptosis of cells[15].

Unlike for gasdermin D, neither the physiologic function nor activation mechanism of gasdermin A have been well characterized. However, several mutations within the C-terminal inhibitory domain of gasdermin A3 have been observed to cause autoactivation of the protein and lead to an inflammatory form of alopecia in mice that resembles the human disorder alopecia areata[44,46-50]. Thus, activation of gasdermin A likely promotes inflammation in the skin, though

[5]Stephen Kovacs was involved in deciding all models tested. He performed the candidiasis and bullous pemphigoid mouse model experiments and all in vitro experiments exploring gasdermin A activation mechanisms. Dr. Ine Jorgenson bred *Gsdma*$^{-/-}$ mice to homozygosity. Dr. Helen Lazear performed the HSV model. Dr. Sanajay Sarkar from the lab of Dr. Mark Heise performed the CHIKV model. Susan Burette from the lab of Dr. Zhi Liu performed psoriasis and contact hypersensitivity models. Elena Mulligan and Susan Burette from the lab of Dr. Zhi Liu performed the atopic dermatitis model. Given the negative nature of most of the included data, it will likely be published as supplemental data to any publication from the Miao lab in which a phenotype for the *Gsdma*$^{-/-}$ is discovered.

what normally triggers activation of wild type gasdermin A nor the precise biochemical mechanism by which it is activated is known. SNPs within gasdermin A have also been associated with asthma in humans[53], though the mechanism by which a protein with expression restricted to skin and the upper gastrointestinal tract could promote lung pathology remains unknown.

We hypothesized that gasdermin A functions analogous to gasdermin D to trigger pyroptosis of epithelial cells and inflammation in the skin and upper gastrointestinal tract in defense against infections. We aimed to further characterize models in which wild type gasdermin A promotes inflammation either in defense against microbes or contributing pathology during autoimmune/autoinflammatory disorders using various mouse models. We then hoped to leverage such a model to complement in vitro experiments and ultimately characterize physiologic cleavers of gasdermin A in mice and humans.

Generation of a gasdermin A triple knockout mouse

To study the function of gasdermin A in various infectious and disease models, we developed C57BL/6 mice deficient in gasdermin A (*Gsdma*$^{-/-}$ mice) through the UNC Animal Models Core using CRISPR. Mice have triplicated gasdermin A compared to humans, so it is possible that these various gasdermin A proteins have some redundancy with each other or that the mouse gasdermin A proteins each have specialized to perform some of the functions performed by the single human gasdermin A. Therefore, we generated a triple knockout mouse line deficient in all forms of gasdermin A. However, it is possible that as the gasdermin A protein triplicated, the functions of each of these gasdermins diversified. In this case, gasdermin A1, the mouse gasdermin with most sequence homology with human gasdermin A, may be the

functional equivalent to human gasdermin A, and gasdermin A2 and A3, whose sequences have diverged more from human gasdermin A, may fulfill unique functions. As a result, using the triple knockout in disease models may risk identifying these potential "unique functions" of gasdermin A2 or A3 that may not be translatable to humans.

Generating this triple knockout was facilitated by the fact that all three gasdermin A genes are adjacent to each other; therefore, only a single CRISPR deletion was required (Figure 19A). Deficiency of gasdermin A expression was verified by western blot (Figure 19B). Interestingly, when performing these western blots, we observed three smaller bands in wild type mice in the range of 25-30 kDa. The commercial antibody used is raised against a peptide from the amino-terminal domain, thus this size range is approximately the expected size for the cleaved, active gasdermin A N-terminus. Two bands were predominantly within the PBS extract, which signifies the protein is mostly found in the cytosol. The third band was predominantly within the RIPA buffer extracts, which signifies the protein is mostly found in hydrophobic membrane compartments. These bands disappeared in the *Gsdma*$^{-/-}$ mice, suggesting that these bands are in fact derived from full length gasdermin A. However, if these bands in fact are gasdermin A, it is hard to determine if this cleavage signifies a basal level of cleavage of gasdermin A that occurs in normal skin, or if the creation of these fragments is an artifact resulting from the procedures used to process the tissue and extract proteins.

We bred the *Gsdma*$^{-/-}$ mice in a specific pathogen free facility. The *Gsdma*$^{-/-}$ mice appeared grossly normal, displaying no sign of alopecia or developmental defects. Similarly, histology of ears from these mice demonstrated normal skin structure with no signs of inflammation (Figure 19C). These observations support the conclusion made by others that the *Gsdma3* mutations that promote inflammation and alopecia are in fact auto-activating[130,131].

Importantly, the lack of inflammation and the absence of spontaneous infections while in our breeding colony suggest that loss of gasdermin A does not inherently make mice extremely susceptible to infection from commensals or other potential pathogens commonly found in specific pathogen free mouse facilities. Thus, if gasdermin A plays an active immunologic role, then either gasdermin A is primarily involved in the defense against particular pathogens or under specific conditions (e.g. scratches that damage the cornified layer of the skin), or redundant immunologic mechanisms protect mice from the low inoculum of various bacteria that the mice encounter every day in our facilities.

Evaluating the role of gasdermin A in infectious models

To assess the role of gasdermin A in promoting defense against infection in skin akin to gasdermin D, we utilized several models of infections of the skin and upper gastrointestinal tract:

Herpes Simplex Virus (HSV)

HSV is a DNA virus that initially infects the keratinocytes at the inoculation site, causing the formation of a characteristic lesion. It then travels retrograde through neurons until it reaches a sensory ganglion[132]. In humans, HSV can persist in the ganglion for a person's life, occasionally traveling anterograde through the neurons' axons to cause skin outbreaks[132]. In mice, this anterograde movement happens soon after infection, causing the formation of a lesion that can in its most severe form encompass the entire dermatome innervated by the infected neurons[132,133]. Since HSV is a prominent skin infection in both mice and humans that directly infects keratinocytes, the cell type expressing gasdermin A, we assessed the contribution of

gasdermin A to the defense in a mouse model of HSV in collaboration with the lab of Dr. Helen Lazear.

Dr. Lazear infected mice with HSV-1 strain NS (a low passage clinical variant) on depilated and scratched skin, and monitored these mice for 10 days for development and extent of skin lesions. *Gsdma*$^{-/-}$ mice failed to develop lesions, whereas WT mice transiently developed mild lesions and positive control *Ifnlr1*$^{-/-}$ developed severe lesions (Figure 20A). This data suggests that deficiency of gasdermin A does not lead to high susceptibility to HSV, unlike deficiency in interferon-lambda signaling; however, the strain of HSV used in this experiment tends to not to be highly virulent in C57BL/6 mice, and is more typically used in mouse models involving BALB/c mice. Indeed, few WT mice developed substantial lesions in this experiment, whereas WT BALB/c mice would typically develop more significant lesions. Thus, this experiment should be repeated using a strain of HSV that is better at infecting C57BL/6 mice, or a higher dose of viral inoculum, to explore the possibility that gasdermin A deficiency leads to a mild susceptibility.

Chikungunya virus (CHIKV)

CHIKV is a positive sense RNA virus transmitted by mosquitos that causes flu-like symptoms and arthralgias[134]. After a mosquito bite, CHIKV is deposited within the skin, where it replicates within fibroblasts in the dermis, and then spreads systemically[134]. Since the skin is the initial replicative niche of CHIKV, we hypothesized that gasdermin A could induce inflammation to prevent systemic spread of CHIKV and thereby promote clearance.

To test this, we collaborated with the lab of Dr. Mark Heise to test the role of gasdermin A in a mouse model of CHIKV. These experiments were performed by Dr. Sanjay Sarkar, a

post-doc within Dr. Heise's lab, using a protocol previously described[135,136]. *Gsdma*$^{-/-}$ mice phenocopied WT mice with similar kinetics of joint swelling, suggesting that gasdermin A does not play a significant role during CHIKV infection (Figure 20B). This result was perhaps not completely unexpected as the primary cell type within the skin infected by CHIKV is the dermal fibroblast whereas gasdermin A expression is restricted to the keratinocytes in the epidermis. Thus, any activation of gasdermin A would have necessitated an external signal to keratinocytes, whereas the paradigm established by other gasdermins is that gasdermins trigger pyroptosis within the cells that are infected.

Candida albicans

C. albicans is a fungal yeast that causes multiple types of infections at the interface between oral thrush in immunocompromised patients or patients with recent antibiotic treatment, vaginal candidiasis, and dermatitis in infants. Others have previously implicated inflammasomes in the defense and pathology of infection by *C. albicans*[137]. Importantly, Hise et al. observed that IL-1R (the receptor for IL-1β, a cytokine released as a consequence of pyroptosis) promoted defense both locally in the oral cavity as well as systemically[137]. In contrast, caspase-1 promoted defense against systemic infection without significantly affected local oral burdens. We therefore hypothesized that while caspase-1 and gasdermin D primarily contribute to systemic defense, gasdermin A could fulfill a similar function at the local level by activating pyroptosis and mediating cytokine release at the initial site of infection.

To test our hypotheses, we utilized a mouse model of *C. albicans* previously described using both untreated and cortisone-treated mice[138]. Cortisone treatment makes wild type mice mildly immunocompromised and susceptible to thrush. This model is clinically relevant because

steroid treatment is a common predisposing factor to development of thrush in otherwise immunocompetent individuals.

Contrary to our hypothesis, gasdermin A did not significantly affect local oral burdens of *Candida.* In the groups that did not receive cortisone treatment, *Gsdma*$^{-/-}$ mice completely cleared infection by day 5, while a couple of WT mice had mild burdens (Figure 20C). In cortisone-treated mice, WT and *Gsdma*$^{-/-}$ mice had similarly elevated burdens of *C. albicans* on the tongue (Figure 20C). Together, these data suggest that gasdermin A does not lead to an overt increase in local susceptibility to thrush. However, these results do not completely exclude the possibility that gasdermin A restricts local infection. Indeed, the burdens of *C. albicans* accumulating on the surface of the tongue (giving the white tongue appearance characteristic of thrush) likely overwhelm the number of yeasts that have locally invaded the tissue of the tongue. It remains possible that gasdermin A could reduce the local invasion without affecting surface yeast burdens. Future experiments could incorporate histology with staining for *C. albicans* to definitively explore this possibility.

Intriguingly, when looking for systemic spread, both *Gsdma*$^{-/-}$ mice treated with cortisone had about a log elevated number of *C. albicans* in the liver compared with cortisone-treated WT mice that trended toward significance ($p=0.08$), despite having comparable levels of burden on the tongue (Figure 20C). These results suggest the possibility that gasdermin A could actually contribute to the prevention of systemic spread of the yeast, and increasing the sample size may allow a significant difference to be observed. While the relatively low burdens in the liver and the fact that elevated burdens within the kidney make this possibility less likely, a barrier defect caused by loss of gasdermin A in the presence of an otherwise intact systemic immune system could mean that kinetics of infection may be slow, at least initially. Thus, it may

be worth repeating this experiment with a larger sample size, as well as extending the timepoints being observed beyond the five days used here.

Evaluating the role of gasdermin A in skin autoinflammation models

While our primary hypothesis was that gasdermin A promoted inflammation in the skin to defend against infections, this inflammation could also have the potential of damaging host tissue. Indeed, this potential is most clearly demonstrated by the autoactivating mutations of gasdermin A3 that cause inflammatory alopecia in mice[44,46-50]. Thus, we hypothesized that aberrant activation of gasdermin A could contribute to common skin inflammatory conditions. Identification of such a condition involving wild type gasdermin A could provide an alternative avenue from infection models to better study the function and activation mechanism of gasdermin A.

Bullous pemphigoid

Bullous pemphigoid (BP) is an autoimmune disorder characterized by the formation of tense, fluid-filled blisters on the skin of patients. BP typically develops in elderly patients, and is the most common autoimmune blistering disorder[139]. BP is driven by autoantibodies targeting BP180, a component of the hemidesmosomes that attach basal keratinocytes to the basement membrane and anchor the epidermis to the dermis[140]. Accumulation of antibodies on the basement membranes leads to complement fixation, ultimately recruiting neutrophils that release proteases that directly cleave BP180 as well as other components of the hemidesmosome[141-144]. The destruction of hemidesmosomes leads to separation of the epidermis from the dermis and the formation of blisters. One of the primary functions of gasdermin D is to promote neutrophil

recruitment through the release of IL-1β and DAMPs. Therefore, if gasdermin A functioned analogous to gasdermin D within keratinocytes, the target cell of the BP antibodies, then we hypothesized that gasdermin A may promote neutrophil recruitment and ultimately contribute to BP pathology.

To test this hypothesis, we utilized a mouse model for BP developed by Dr. Zhi Liu[145,146]. In this model, we intradermally inject polyclonal pathogenic anti-mouse BP180 antibody into the ears of adult mice, and 24 hours later assess inflammation and blister formation by histology. This model likely represents the pathogenesis of an acute outbreak of BP. Initial experiments using our *Gsdma*$^{-/-}$ mice in the BP model were promising: *Gsdma*$^{-/-}$ mice lacked disease pathology and had lower levels of IL-1β in the ears compared to wild type mice, consistent with gasdermin A promoting inflammation and pathology in the BP model (Figure 21A, B, D). Furthermore, pathology could be restored by intradermally injecting IL-1β alongside the pathogenic antibody (Figure 21C). However, attempts to use pathogenic antibodies generated in different rabbits as well as more recent attempts to replicate the phenotype using the original batch of antibodies failed (Figure 21E, F). We did not repeat assessments of IL-1β levels given the lack of significant difference in pathology and low supplies of pathogenic antibody.

Why we previously observed a significant phenotype using the *Gsdma*$^{-/-}$ mice but no longer observed one remains an unanswered question. Furthermore, inflammation appeared more severe in all samples (both WT and *Gsdma*$^{-/-}$) in 2020 compared to 2016, with markedly increased neutrophil infiltrate visible on H&E (Figure 21E, F). The reason for this change between the experiments performed several years apart remains unclear. Regardless, this data suggests that if gasdermin A does in fact play a role in BP pathology, its role is likely mild, and that alternative mechanisms may compensate for any role gasdermin A plays.

Atopic dermatitis

Atopic dermatitis is a common Th2-mediated skin disorder in which the skin becomes itchy and a characteristic rash forms. We next tested the role of gasdermin A as well as gasdermin D in atopic dermatitis using a previously characterized mouse model of atopic dermatitis in which mice are treated with the vitamin D-derivative MC903[147]. However, we observed no significant differences in either *Gsdma*$^{-/-}$ or *Gsdmd*$^{-/-}$ mice compared to wild type mice (22A-C).

Psoriasis

Psoriasis is a Th17-mediated skin disorder characterized by the development of skin rashes. We tested the potential role of gasdermin A in psoriasis using a well characterized model of psoriasis in which we treat the backs and ears of mice with the TLR7 agonist imiquimod. While we potentially observed a small decrease in redness in *Gsdma*$^{-/-}$ mice compared to WT mice, the fact that this difference was small and that there were no significant differences in either scaliness or ear thickness suggests that any contribution by gasdermin A to psoriasis pathology is likely minimal (Figure 22D-F).

Contact hypersensitivity

The final skin disorder we tested was contact hypersensitivity, a skin allergy response to a sensitized allergen. To test the contribution of gasdermin A to contact hypersensitivity, we first sensitized mice to oxazolone by treatment on their backs, and then we challenged these mice five days later with oxazolone on their ears. However, we observed no significant difference in either

ear thickness or weight between *Gsdma*$^{-/-}$ and WT mice, suggesting that gasdermin A does not significantly contribute to contact hypersensitivity (Figure 22G-H).

The search for the activation mechanism of gasdermin A

Since all other known activation mechanisms of gasdermin family members involve cleavage of the linker by a protease, we reasoned that gasdermin A would similarly be activated by cleavage with a protease. Since mouse gasdermin A1 is most closely similar to human gasdermin A and therefore likely functions as its most direct ortholog, we focused on using mouse gasdermin A1 and human gasdermin A for screening for potential cleavers.

Caspases

Given that gasdermin D and gasdermin E are both activated by caspases (caspase-1 and -3, respectively), we first focused on the potential ability for caspases to cleave gasdermin A. Indeed, as I discuss further in Chapter 6, Human gasdermin A and mouse gasdermin A1 have a conserved QASD motif that could serve as a caspase cleavage site within its linker region (Figure 23A red box). However, consistent with what others have observed, neither recombinant caspase-1 nor caspase-3 could cleave gasdermin A despite cleavage of other substrates (Figure 23B).

Since expression of caspase-14 is restricted to the skin in a similar manner as gasdermin A, caspase-14 is an intriguing candidate as a potential cleaver of gasdermin A[148]. However, the mechanism by which caspase-14 becomes activated remains unclear, and obtaining active caspase-14 is significantly more difficult than for other caspases. Indeed, while previous publications said that granzyme B cleaved caspase-14 into its active form, granzyme B did not

cleave mouse caspase-14 in my hands (data not shown) [148,149]. To bypass this issue of how to obtain active caspase-14, we generated a caspase-14 construct with an artificial cleavage site for PreScission protease within the protein's linker region (Figure 23C). The second obstacle to obtaining active caspase-14 is that under typical caspase activity assay conditions, cleaved caspase-14 has low activity. Instead, others have shown that high concentrations of salts (1.1-1.3M sodium citrate) were required to see significant levels of caspase-14 activity[149]. Why such high salt concentration is required in vitro remains unknown, as no other caspase has this requirement for activity. Regardless, this high salt concentration also makes several of the more typical assays for assessing caspase-14 activity and cleavage capabilities more difficult (for example, the high salt concentration makes western blots difficult to run without dialysis of samples). Thus, further optimization needs to be completed in order to properly assess if caspase-14 can cleave gasdermin A.

Granzymes

Granzymes are serine proteases produced primarily by NK cells and $CD8^+$ T cells[150]. While the function of granzyme B as a trigger for apoptosis is well known, the function of other granzymes are not as well understood[150]. With the recent discovery that granzyme A cleaves human gasdermin B to trigger pyroptosis[68], we became intrigued by the possibility that granzyme A or another granzyme could cleave gasdermin A. However, while granzyme A did successfully cleave gasdermin A, the resulting small fragment indicates that granzyme A cleaves gasdermin A within the N-terminal domain, which would likely be deactivating (Figure 23D). Granzymes B and K failed to cleave gasdermin A despite cleaving other known control substrates (caspase-7 for granzyme B, SET for granzyme K; Figure 23D-E).

Trypsin-like proteases

Trypsin-like proteases are serine proteases that cleave after positively charged residues, and gasdermin A has several conserved lysines within its linker region (Figure 23 A blue boxes) [150]. To test for cleavage of gasdermin A by trypsin-like proteases, we used human recombinant mast cell tryptase as a representative protease for this family. However, while tryptase successfully cleaved its fluorogenic substrate N-benzoyl-Phe-Val-Arg-p-nitroanilide (assessed by increased absorption at 405 nm; not shown), it could not cleave gasdermin A (Figure 23F).

Chymotrypsin-like proteases

Chymotrypsin-like proteases are serine proteases that tend to cleave after large aromatic residues (tryptophan, phenylalanine) or leucine[150], of which there are several in the linker region of gasdermin A (Figure 23A yellow boxes). Mast cells and the mast cell protease MCPT4 have been implicated in the pathology of the murine BP model by Dr. Liu's lab[151]. To test the cleavage potential by this family, we used recombinant human mast cell chymase (which is considered the functional homolog of murine MCPT4) as a representative protease for this family. Intriguingly, we observed significant cleavage of all gasdermin A proteins from mouse and humans yielding fragments approximately the expected size of active N-terminal domains (perhaps a kDa or two smaller than expected, but within the margin of error of reading a western blot and which may yield an active N-terminal domain even if it is a little short; Figure 24A-D). In contrast, chymase cleaves gasdermins B and D within their N-terminal domain, which is likely inactivating and suggests specificity for cleaving gasdermin A (Figure 24E-F).

However, when performing protein transfections of chymase into HEK293T cells that express the various gasdermin A proteins, we could not trigger gasdermin A-specific cytotoxicity

prior to achieving levels of chymase that were cytotoxic to cells. This result suggests that even if the cleaved fragment is capable of forming pores, it may require concentrations of chymase that are in themselves cytotoxic, which would appear to defeat the purpose of activating gasdermin A. Chymase and MCPT4 have been published to cause significant skin edema when intradermally injected into the ear of BALB/c mice[152,153]. In contrast, when we performed this injection into the ears of C57BL/6 wild type mice, we did not observe significant edema (as determined by weight of standardized area of ear) or gross inflammation, which suggests that extracellular chymase may have difficulty in entering the cells in sufficient enough concentration to trigger gasdermin A activation (data not shown). Finally, this proposed mechanism lacks specificity to target only the subset of cells that would need to undergo pyroptosis, which is contrary to the paradigm established by activation mechanisms of other gasdermins. This specificity is currently a hallmark of gasdermin activation, and is important since aberrant activation can lead to significant tissue damage. Thus, while our in vitro data suggests that chymase can cleave gasdermin A to perhaps produce pore-forming fragments (though their pore-forming capabilities were never assessed), we do not believe that chymase is the physiological cleaver of gasdermin A. It remains possible that during BP, human chymase or murine MCP-4 might enter keratinocytes by unknown mechanisms and thereby activate gasdermin A, resulting in skin pathology. Note that this pathway would represent pathologic activation of gasdermin A, which may be different from the evolved mechanism to activate gasdermin A to defend against keratinocyte infection. However, since the in vivo BP model in *Gsdma*$^{-/-}$ mice was not reproducible, this line of investigation was not continued in this thesis research.

Our results do suggest the possibility that another chymotrypsin-like protease may be the cleaver. However, at least one other chymotrypsin-like protease found in the skin, KLK7[154],

could not cleave gasdermin A despite being capable of cleaving gasdermin D to a size that could be an active fragment (Figure 24G-H). Thus, the search for the identity of a chymotrypsin-like protease that may be the physiological activator of gasdermin A remains a potential route for further exploration.

Discussion

The immune system plays several indispensable roles in the skin. First, it prevents local infection. Second, since the skin forms one of the primary interfaces between the body and the external environment and therefore can serve as the entryway for microbes, immune responses in the skin prevents the systemic spread of many potential pathogens. Finally, since the skin houses many commensals that can actually be beneficial to the host, immunity of the skin must discriminate between these commensals and potentially pathogenic and invasive microbes. Historically, keratinocytes were considered to play a relatively passive role in immunity, providing the structural barrier via epithelial layer and the overlying cornified layer of dead keratinocytes. However, more recently, their active roles in immunology have been appreciated via the release of cytokines, chemokines, DAMPs, and anti-microbial peptides.

Gasdermin A likely fits in this same paradigm as another mechanism by which keratinocytes can actively promote inflammation, as auto-activating mutations in *Gsdma3* that lead to massive alopecia demonstrate the profound potential for gasdermin A to trigger inflammation and pathology of the skin. How might gasdermin A promote immunity and inflammation? Just as gasdermin D and E trigger pyroptosis in the cells they are expressed in, Gasdermin A may trigger pyroptosis of keratinocytes. Furthermore, regardless of whether or not gasdermin A triggers keratinocyte pyroptosis, gasdermin A could mediate release of DAMPs as

well as IL-1 family cytokines within the cytosol of keratinocytes simply by forming pores. Notably, keratinocytes constitutively produce IL-1α, which promotes Th1/17 type inflammation, IL-18, which promotes Th1 type inflammation, and IL-33, which promotes Th2 type inflammation, all of which require pore formation or cell damage for release[110,155]. These IL-1 family cytokines could be released by non-programmed cellular lysis, or might be released by programmed opening of the gasdermin A pore.

Despite gasdermin A's clear potential for causing inflammation, our studies did not identify a mouse model in which gasdermin A played a prominent role. Future studies could continue our targeted screening using potential pathogens. Since we know that gasdermins and pyroptosis generally defend against intracellular infection, of most interest would be assessing the role of gasdermin A during skin infection with *Staphylococcus aureus*, one of the most prominent bacterial skin pathogens and one of the few bacteria documented to potentially enter keratinocytes and for which epicutaneous infection models have been described[156-158], and viral pathogens. Viral pathogens of note to test include using an optimized protocol for HSV (e.g. a strain of HSV that is more virulent in C57BL/6 mice), human papillomavirus (a prominent skin pathogen that causes warts for which model viruses that infect mice are available)[159], and vaccinia (a well-established model for poxvirus family of viruses that cause prominent skin infections such as smallpox or molluscum contagiosum)[160]. Other pathogens to consider are *Pseudomonas aeruginosa* (another prominent bacterial cause of skin infections), fungal pathogens (e.g. ring worms), and flaviviruses (which include arboviruses such as West Nile virus or Zika virus, and which usually locally infect keratinocytes at the site of the inoculating mosquito bite before spreading systemically)[161,162].

All of our negative data do raise an important question: if the inflammation potential for gasdermin A is high, why is it so difficult to find an adequate model in which wild-type gasdermin A plays a prominent role?

One obvious possibility is that we merely chose the wrong type of models to test. Indeed, infections chosen were "true" pathogens. If gasdermin A is in fact important for skin immunity, then true pathogens may have developed mechanisms of avoiding gasdermin A activation or its effects. Thus, may need to find an environmental pathogen that would not have developed these avoidance mechanisms similar to how we used *Burkholderia thailandensis* to study inflammasomes. Furthermore, none of the infection models we performed involved bacteria. The skin models chosen have well established mechanisms for inducing inflammation, be it complement in the BP model or toll-like receptor activation in the psoriasis model, and with the exception of the BP model reflect more subacute or chronic pathologies (1-2 weeks+). Gasdermin A may play more of a role in acute pathologies similar to how other gasdermins primarily play prominent roles in the innate phase of immunity.

It also cannot be discounted that our lack of identification of a significant role for gasdermin A in any of our tested models could also reflect true characteristics of gasdermin A's place in skin immunity. The skin is constantly in contact with microbes and microbial products, many of which have no significant pathogenic potential, as well as allergens. As the auto-activating *Gsdma3* mutations demonstrate, the potential for devastating consequences of errant gasdermin A activation is high. Therefore, the barrier for activation of gasdermin A may be particularly high, requiring specific signals to signify that gasdermin A could be detecting a true pathogen and to reduce the potential for false positives. As a consequence, the circumstances that activate gasdermin A may be more limited. Second, since the skin is such an important location

for stopping potential pathogens before they spread systemically, multiple redundant mechanisms may promote skin inflammation with similar kinetics. Indeed, damage to keratinocytes caused by the pathogens themselves could lead to the release of DAMPs, including IL-1α, which may reduce the need for a pore. Similarly, multiple cell types act as sentinels in the skin, including Langerhans cells, mast cells, and dendritic epithelial T cells[163]. Thus, knocking out gasdermin A may not have a significant impact on phenotypes or may result in milder phenotypes so long as the other redundant or compensatory mechanisms persist. The counterpoint to redundancy is the observation that the presence of a gasdermin A gene is highly conserved among mammals. Whereas other gasdermins may be lost, gasdermin A is not, suggesting that it is important and not merely redundant.

Our studies did not identify the physiological activator for gasdermin A. However, the identification of chymase as capable of cleaving gasdermin A suggests that testing other chymotrypsin-like proteases presents a potentially promising avenue for further exploration. Given the similar expression pattern of gasdermin A and caspase-14 and the precedence of gasdermins being activated by caspases, the potential for caspase-14 to cleave and activate gasdermin A should also be continued to be explored. Notably, human gasdermin A and mouse gasdermin A1 contain a conserved QASD within their linkers that could serve as potential caspase cleavage sites. In contrast, mouse gasdermins A2 and A3 do not contain this sequence or any other obvious potential caspase cleavage site, so their activation mechanisms likely do not involve caspases.

Methods

Assessing gasdermin A in mouse skin: For each mouse, two ears were treated with liquid nitrogen and crushed using mortar/pestle. 200 uL of PBS with 1X protease inhibitor (Sigma; Cat#11836153001) was added to the powder, spun at 13,800 RPM for 10 minutes at 4^{o}C. The supernatant was taken for western blot, and the powder was washed twice with 500 uL of PBS with protease inhibitor. Finally, 200 uL of RIPA buffer with protease inhibitor was added to the powder, spun at 13,800 RPM for 10 minutes at 4^{o}C. The supernatant was taken for western blot. Western blot was performed using anti-gasdermin A antibody (Santa Cruz; customized carrier-free version of Cat#sc-376318) that was biotinylated using an antibody biotinylation kit (ThermoFisher; Cat#90407).

Infection models:

HSV: Mice were infected with HSV-1 strain NS (a low passage clinical variant) using a model previously described by others[133]. Briefly, mouse flanks were shaved and treated with Nair to remove overlying hair at the inoculation sites. The next day, 5x10^{5} PFU of HSV in 10 uL of PBS was placed on the bare skin of the mice, and the inoculation sites were scratched 40 times with a 27G needle through the drop. The mice were then monitored and graded for 10 days for development and extent of the characteristic rash.

CHIKV: CHIKV infections were performed as previously described[135,136]. Mice were injected with 100 PFU of CHIKV isolate SL15649 (a clinical isolate) in 10 uL of sterile PBS into the left rear footpad. Control mice were injected with 10 uL of sterile PBS without virus. Mice were monitored for 10 days post infection. Inflammation was measured by using calipers to

measure swelling of the ipsilateral footpad, normalized to initial caliper measurements on the day of infection.

C. albicans: Oral infections with *C.* albicans were performed using a previously published protocol[138]. Briefly, for each genotype tested, we had two experimental groups: a cortisone-treated group and an untreated mice. Cortisone treatment makes the mice mildly immunocompromised and is required for the reliable development of thrush in wild type mice. Cortisone-treated mice were injected subcutaneously with 225 mg/kg of cortisone acetate starting one day prior to infection, and were given repeated doses every two days for the duration of the experiment. The inoculum was created by growing *C. albicans* strain SC5134 (wild type strain) in yeast extract-peptone-dextrose (YPD) media at 30^{o}C overnight, and soaking a calcium alginate swab in an HBSS solution containing 1x10^{6} *C. albicans*/ml for 5 minutes. Mice were anesthetized with ketamine and xylazine, and the inoculation swabs were then placed under the tongues of the anesthetized mice for 90 minutes. Five days after infection, mice were euthanized. Tongue, esophagus, liver, and kidney were harvested and evaluated for CFUs by spot dilution plating.

Skin inflammation models:

Bullous pemphigoid: The BP model was performed using pathogenic antibodies against mouse NC16A component of BP180, as previously characterized. 20 uL of titrated pathogenic antibody were injected intradermally into the ears of 8-12 week old mice. After 24 hours, mice were euthanized. For histology, ears were frozen in OCT, and sectioned and stained for H&E by the UNC dermatology pathology core. In parallel experiments, to assess IL-1β levels within the ear, we injected 100 uL of PBS into the ears and then removed this volume after one minute to

generate a “PBS wash” of the ear’s interstitium. We then assessed IL-1β levels in the PBS wash by ELISA.

Atopic dermatitis: The MC903 model of atopic dermatitis was performed as previously described[147]. Briefly, the ears of mice were treated with 90 uM of MC903 in ethanol every day for 16 days. Clinical scores for redness and scaliness were assessed daily, and ear thickness was measured using a caliper on days 5, 12, and 16.

Psoriasis: Mice 6-8 weeks of age receive daily topical dose of 62.5 mg (2.125 mg each day) of either imiquimod cream (Aldara) or control vehicle cream on shaved back and right ear for 6-10 consecutive days. Erythema and scaling at treated sites were observed pre-treatment and every other day after treatment. Additionally, ear thickness was measured every other day using a caliper. On day 10, mice were euthanized. Ears were frozen in OCT, and sectioned and stained for H&E by the UNC dermatology pathology core.

Contact hypersensitivity: On day one, backs of mice were dilapidated using Nair. Mouse backs were treated with 100 uL of 3% oxazolone in ethanol. On day five, base ear thicknesses were measured using a caliper. Then, 100 uL of 3% oxazolone in ethanol was applied to the mouse ears. On day 6, ear thickness was measured using a caliper. In addition, mice were euthanized, and punch biopsies of uniform size of the ears were taken and weighed.

Source of caspase-14 or gasdermin proteins: HEK293T cells transfected with plasmids expressing the various proteins were grown to confluence in 6 well plates and lysed with 200 uL of 1% IGEPAL. Lysates were spun 15,000 RPM on a tabletop minicentrifuge at 4^{o}C for 10 minutes to remove cell debris and nuclei. The resulting supernatants were used as sources of protein.

Cleavage assays:

Caspase-1 and 3: HEK293T lysates containing myc-tagged bird or human gasdermin A, bird gasdermin E, or human gasdermin D were treated with 2 U of either recombinant active human caspase-1 (Sigma; Cat#CC126) or caspase-3 (Sigma; Cat#CC119) for 90 min at 37oC in buffer containing 50 mM HEPES, 3 mM EDTA, 150 mM NaCl, 0.005% Tween20, 5 mM DTT, pH7.44. Cleavage was evaluated by western blot.

Caspase-14 cleavage by PreScission protease: Caspase-14 cloned with a PreScission protease cleavage site (LEVLFQGP) inserted into the linker region of caspase-14. HEK293T lysate containing this construct was treated with 4 U of PreScission protease (Sigma; Cat#GE27-0843-01) for up to 20 minutes at 37ºC in buffer containing 50 mM Tris•HCl, 150 mM NaCl, 1 mM EDTA, pH 7.0. Cleavage was evaluated by western blot using anti-caspase-14 (CST; Cat#8519S).

Granzyme A: Recombinant human granzyme A was first activated by treating 1.5 ug of granzyme A with 0.1 ug/mL of lysyl-endopeptidase in 0.05 M Tris, pH 9 buffer for 1 hour at 37ºC. 4 uL of 293T lysate containing the protein substrate of interest was then treated with 16 ng/uL of granzyme A in 25 mM Tris, pH 8 buffer for a total reaction volume of 20 uL for 2 hours at 37ºC. 2 ug of recombinant SET protein was added in parallel reactions to serve as a positive control.

Granzyme B: 4 uL of 293T lysate containing the protein substrates of interest were treated with 16 ng/uL of recombinant human granzyme B in PBS for a total reaction volume of 20 uL for 2 hours at 37ºC. Cleavage of caspase-7 endogenous to 293T lysate was used as a positive control.

Granzyme K: 4 uL of 293T lysate containing the protein substrates of interest were treated with 16 ng/uL of recombinant human granzyme K in buffer containing 20 mM Tris, 150 mM NaCl, pH 8, for a total reaction volume of 20 uL for 2 hours at 37ºC. 2 ug of recombinant SET protein was added in parallel reactions to serve as a positive control.

Tryptase: 10 uL of 293T lysate containing the protein substrates of interest were treated with either 50 ng/uL or 0.5 ng/uL recombinant human tryptase (Millipore; Cat#650366) in buffer containing 12.5 mM Tris•HCl, 10 mM EDTA, pH 8 for a total reaction volume of 100 uL for 30 or 90 minutes at RT.

Chymase: 10 uL of 293T lysate containing the protein substrates of interest were treated with 1:10 serial concentrations of recombinant human chymase (highest concentration was 16 ng/uL) in buffer containing 50 mM NaCl, 25 mM Tris, pH 7.4 for a total reaction volume of 100 uL for 90 minutes at 37ºC.

KLK7: Recombinant human KLK7 was first activated by treating 2 ug of KLK7 with 20 ug/ml of thermolysin in buffer containing 50 mM Tris, 10 mM $CaCl_2$, 150 mM NaCl, 0.5% (v/v) Brij-35, pH 7.5 for 2 hours at 37ºC. 10 uL of 293T lysate containing the protein substrates of interest were then treated with 1:10 serial dilutions of activated KLK7 (highest concentration was 8 ng/uL) for 90 minutes at 37ºC.

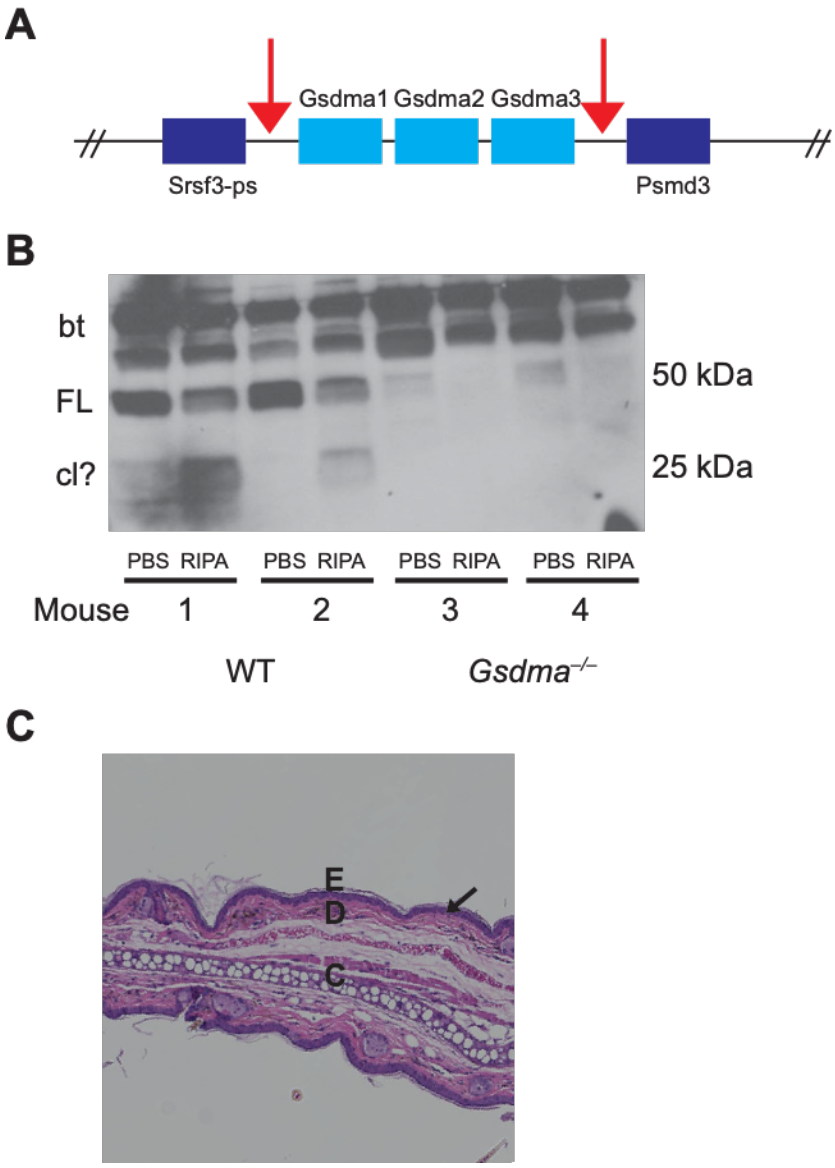

Figure 19: Generation of *Gsdma*$^{-/-}$ mice.
(A) *Gsdma*$^{-/-}$ mice deficient in all three gasdermin A genes was generated by CRISPR deletion at the arrows.

(B) Western blot for gasdermin A of protein extracts of ears in PBS or RIPA buffer. FL is full length gasdermin A, cl? is potential cleaved bands of gasdermin A, and bt are background staining of endogenous biotinylated proteins.

(C) H&E staining of section from ear of *Gsdma*$^{-/-}$ mouse. E = epidermis. D = dermis. C = cartilage. Arrow points to epidermal-dermal junction.

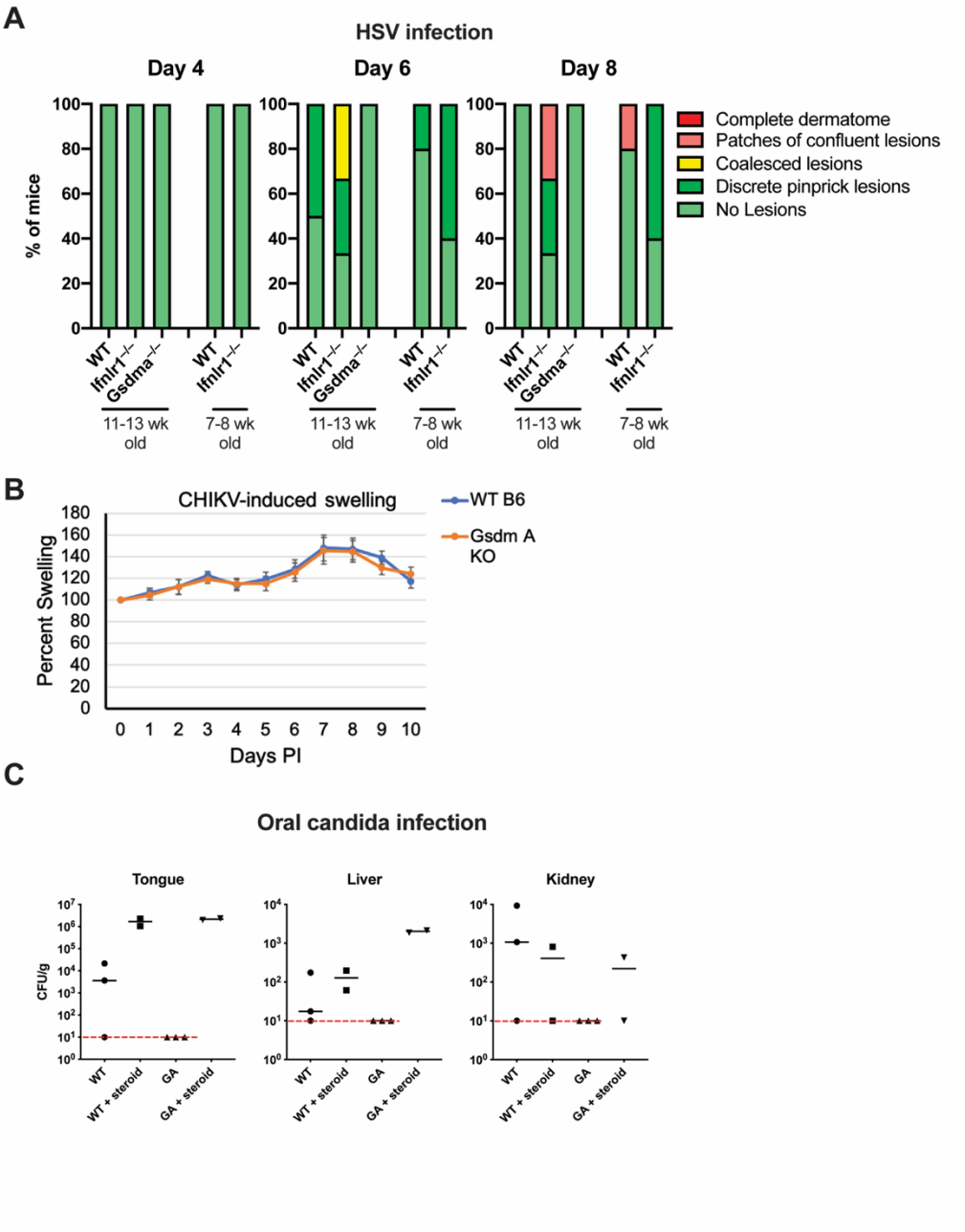

Figure 20: Gasdermin A does not significantly contribute to defense in several infectious models.

(A) Mice were infected with $5x10^5$ PFU of HSV-1 strain NS on skin that was disrupted by needle abrasion, and evaluated for skin lesion formation on the indicated days post-infection.

(B) Mice were infected with 100 PFU of CHIKV isolate SL15649 by injection into left rear footpad. Swelling of ipsilateral footpad was measured daily and normalized to baseline measurements.

(C) Mice were orally infected with $1x10^6$ CFU of *C. albicans* strain SC5134, and burdens in the indicated tissues were evaluated 5 days post-infection.

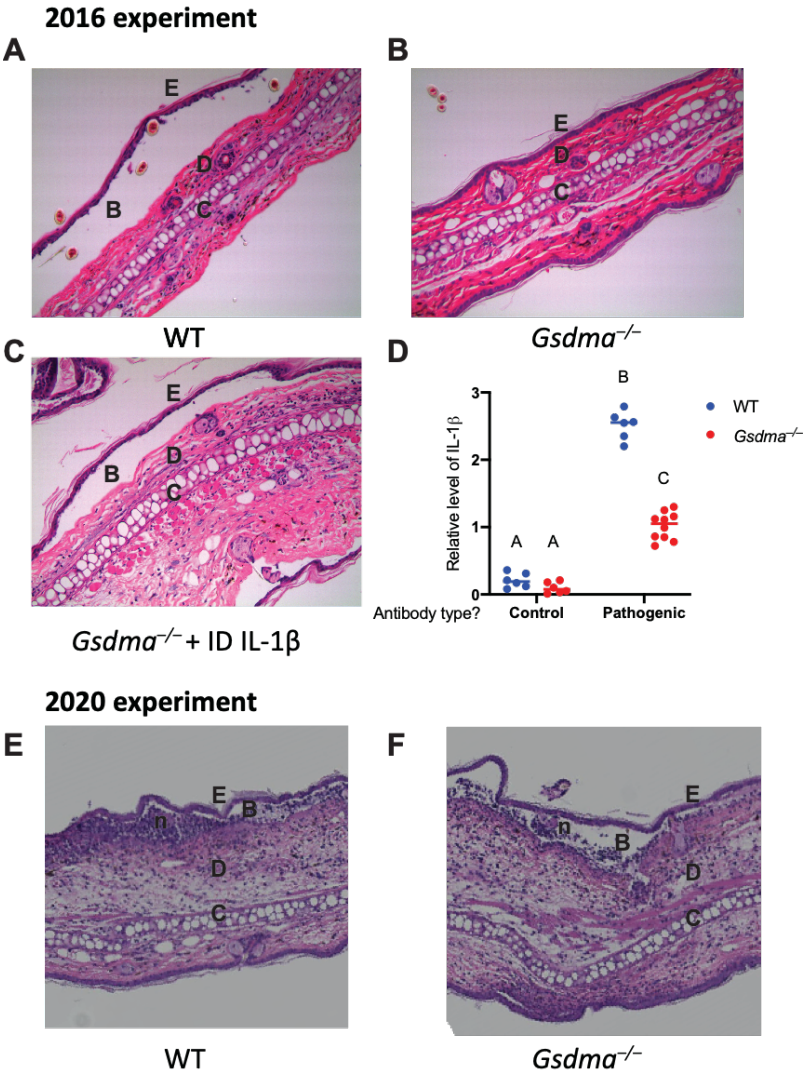

Figure 21: Gasdermin A likely does not significantly contribute to bullous pemphigoid pathology.

Mice were injected intradermally in the ears with control or pathogenic antibody and evaluated 24 hours post-treatment. (A-D) Initial experiments performed in 2016. H&E in WT (A), *Gsdma*$^{-/-}$ (B), or *Gsdma*$^{-/-}$ mice treated with intradermal IL-1β alongside pathogenic antibody. IL-1β levels in PBS washout of ears were measured by ELISA and expressed as relative level to the average level in *Gsdma*$^{-/-}$ mice treated with pathogenic antibody. (E-F) Results from repeat experiment performed in 2020. E = epidermis. D = dermis. C = cartilage. B = blister. n = neutrophil infiltrate into blister fluid.

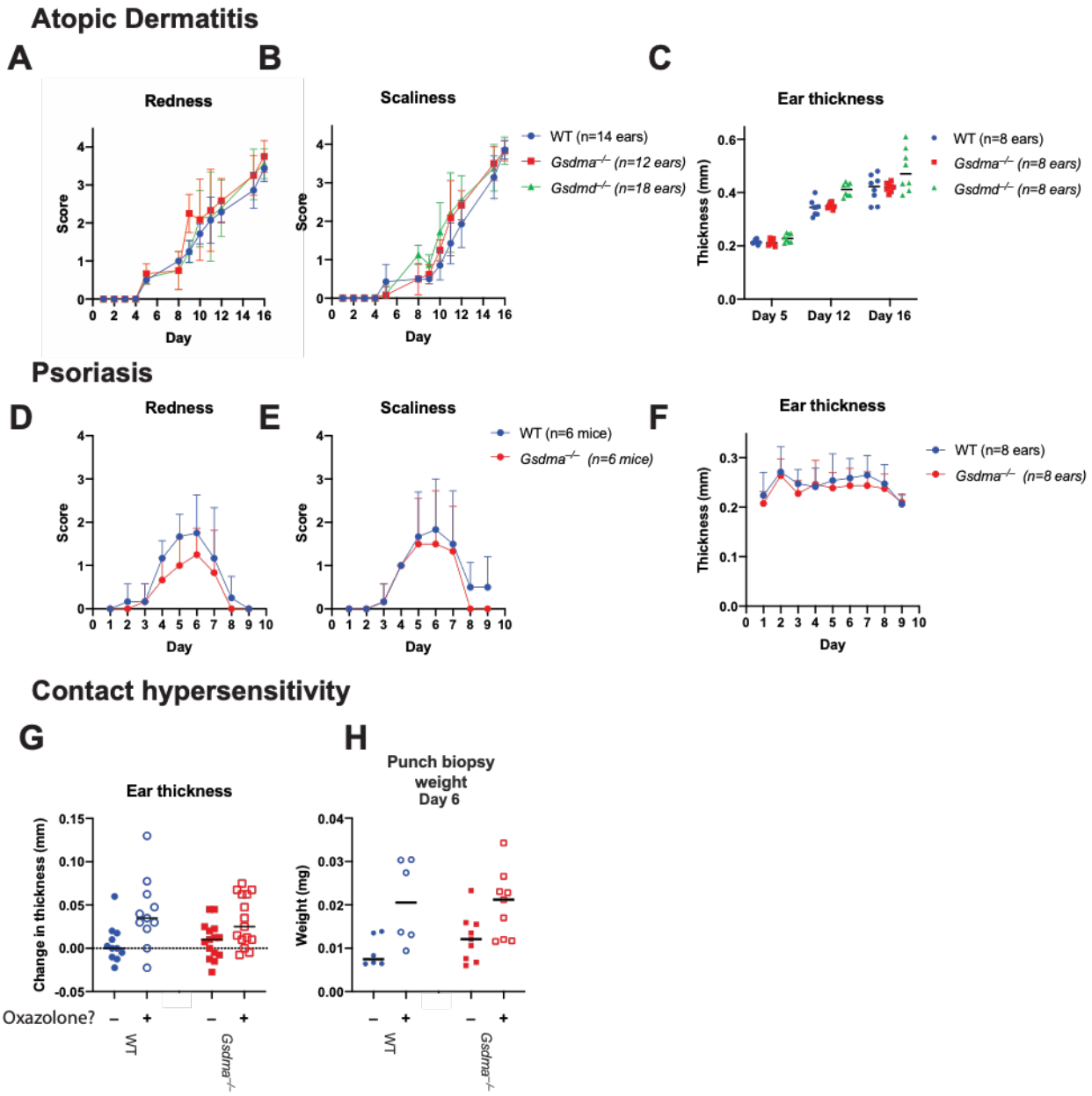

Figure 22: Gasdermin A does not significantly contribute to common skin pathology models.

(A-C) Mouse ears were treated with 90 μM of MC903 to trigger development of atopic dermatitis. Redness (A) and scaliness (B) were evaluated daily on a scale of 0 (none), 1 (mild), 2 (moderate), 3 (severe), and 4 (very severe). We measured ear thickness using a caliper on days indicated.

(D-E) Mice were treated daily with 2.125 mg of imiquimod to trigger development of psoriasis, and evaluated for redness (D), scaliness (E), and ear thickness (F).

(G-H) Mice were treated with 4% oxazolone on their backs on day 1 followed by treatment of their ears on day 5 to trigger contact hypersensitivity. Change in ear thickness from day 5 prior to treatment (baseline) and day 6 (one day post-hypersensitivity challenge) (G) and weight of ear punch biopsies on day 6 (H) were measured.

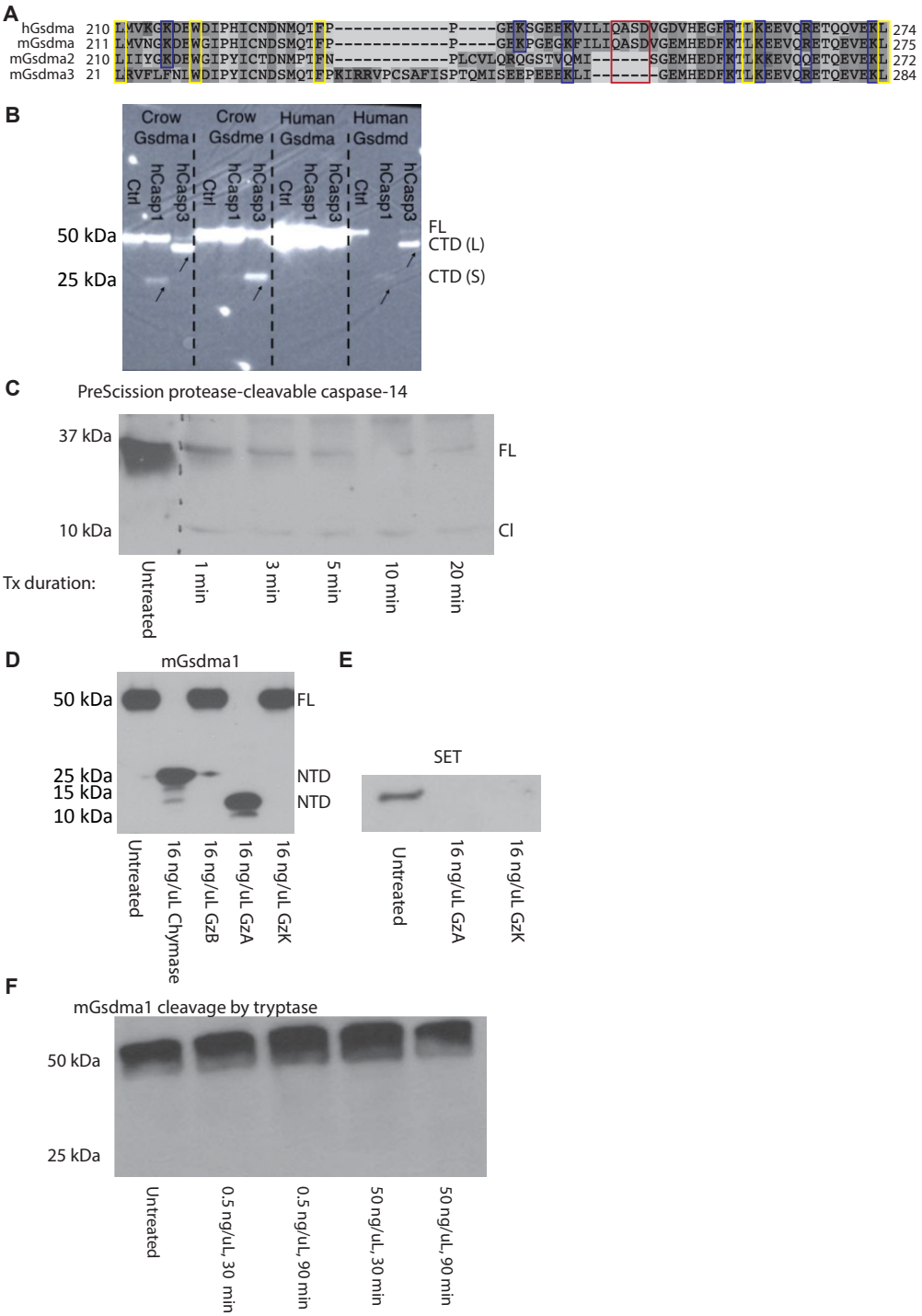

Figure 23: Assessment of various proteases abilities to cleave gasdermin A.

(A) Alignment of human and mouse gasdermin A proteins. Red box is potential caspase cleavage site. Red boxes are potential tryptase cleavage sites. Yellow boxes are potential chymase cleavage sites.

(B-F) Assessment of the indicated proteases to cleave gasdermin A (B-D, F) or SET (E). GzB = granzyme B. GzA = granzyme A. GzK = granzyme K. FL = full-length. CTD = C-terminal domain. Cl = cleaved fragment. CTD (L) = long fragment of CTD. CTD (S) = short fragment of CTD. NTD = N-terminal domain.

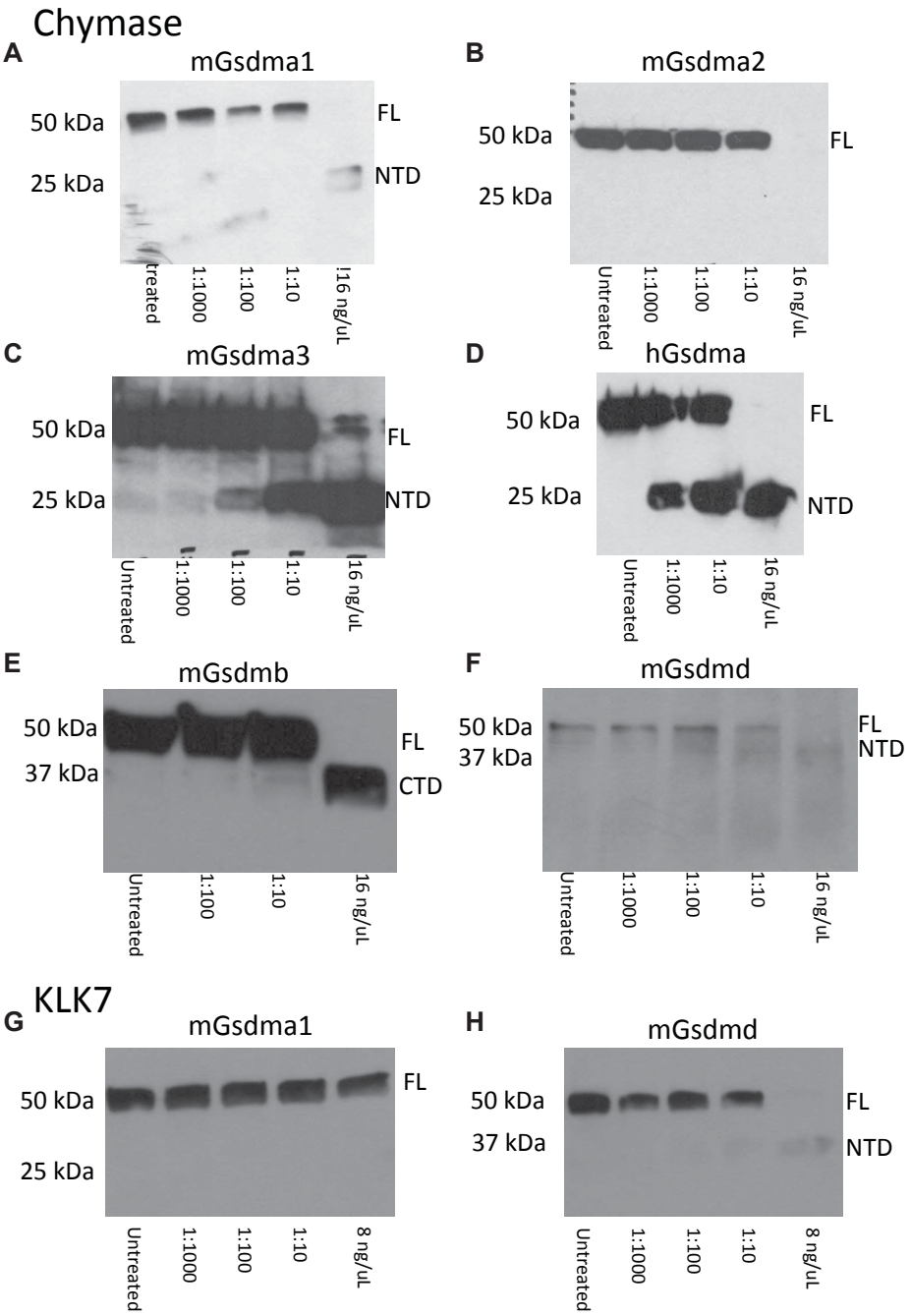

Figure 24: Chymase specifically cleaves gasdermin A to yield fragments approximating the expected sizes for an activating cleavage.

The indicated gasdermins were treated with human recombinate chymase (A-F) or KLK7 (E-F) and evaluated for cleavage by western blot. FL = full length, NTD = N-terminal domain. CTD = C-terminal domain.

CHAPTER 6: MOLECULAR EVOLUTION OF THE GASDERMIN FAMILY[6]

Introduction

The gasdermin family consists of novel pore-forming proteins. The gasdermin family includes six members: gasdermin A, B, C, D, and E, and pejvakin. Recent interest in this family has been driven by the discovery that one member of this family, gasdermin D, was identified as the substrate for caspase-1 that directly mediates pyroptosis, a significant defense mechanism in innate immunity[10-12].

Gasdermins A-E each contain an N-terminal pore-forming domain that can oligomerize and form pores in plasma membranes, a C-terminal repressor domain that inhibits this oligomerization, and a linker that holds these two domains together[15]. Cleavage of the linker region allows the pore-forming domain to dissociate from the repressor domain and trigger pyroptosis. Activating proteases have been identified for human and mouse gasdermin D (caspase-1/11) and gasdermin E (caspase-3) and human gasdermin B (granzyme A), while the activation mechanisms for gasdermins A and C remain uncertain[10-12,21,41,68].

Pejvakin contains an N-terminal domain that is homologous to that of the other gasdermin family members, but has not yet been demonstrated to oligomerize and form pores. Furthermore, the C-terminal domain is notably shorter than that of other members of this family.

[6]Stephen Kovacs performed all analyses discussed in this chapter. This data will form the basis of an eventual paper as first author. Other authors will include Dr. Cisse Ousmane, our collaborator from NIH who mentored Stephen on molecular evolution and performed some of the more advanced computational analyses, Dr. Edward Miao, and other lab members of the Miao lab who finish any remaining experiments.

It is believed that cysteines within this domain detect reactive oxidative species to activate the protein and promote replication of peroxisomes in response to redox stresses[77,78].

The gasdermin family is still actively evolving in mammals. Indeed, compared to humans, mice have lost gasdermin B, triplicated gasdermin A, and quadruplicated gasdermin C. Therefore, we sought to integrate molecular evolutionary analyses with what we already know about individual members of this family in an effort to obtain new insights into the function and activation mechanisms of gasdermins. Some insights into gasdermin roles across evolutionarily diverse species have recently been published. While mammalian caspase-1 can cleave gasdermin D but not gasdermin E, it was recently shown that gasdermin E in fish (which lack gasdermin D) is activated predominantly by the fish caspase-1 ortholog and, to a lesser degree, caspase-3 and -7[10,164]. Thus, the connections between caspases and gasdermins has changed over time. To this end, we have performed molecular evolution studies examining the evolution and co-evolution of the gasdermin and caspase families. In collaboration with the molecular evolutionist Dr. Ousmane Cisse at the National Institutes of Health, more thorough analyses are currently underway.

Collection of sequences of gasdermin family for preliminary analyses

We first wanted to understand the general topography of gasdermin evolution to guide further analyses. Therefore, we sought to identify which major phylogenetic groups have gasdermin homologues by performing homology searches of the NCBI non-redundant protein database using HMMER on each member of the gasdermin family from humans.

Using this methodology, gasdermin A could be identified in amphibians (specifically caecillians), reptiles, birds, and mammals, whereas gasdermins B, C, and D could only be

identified in mammals (with gasdermin D identified in monotremes, marsupials, and placentals and gasdermins B and C identified in marsupials and placentals). This suggests that gasdermin A arose prior to gasdermins B, C, and D, which arose from gene duplication events in mammals. Pejvakin was identified as far back as fish. Gasdermin E homologues could be identified as far back as cnidarians, mollusks, brachiopods, and lancelets by both us and other labs. Notably, cnidarian proteins were recently identified to function similar to gasdermin E[165]. This suggests that pejvakin emerged from the ancestor gasdermin E after fish diverged from lancelets.

Gasdermin B interestingly had not only the fewest sequences, but also a large number designated as "low quality" or were only partial sequences. Low quality sequences are defined as those where the protein sequence was altered during annotation relative to the genome sequence in order to correct potential indels or other protein-altering mutations, accounting for the possibility that sequencing errors interrupted the coding sequence. Furthermore, the complete collection of gasdermin B genes had a relatively high frequency of gaps within their sequences. Together, these observations suggest that there may have been difficulty properly annotating gasdermin B sequences. However, gasdermin B is known to be absent in at least one species: *Mus musculus* (house mouse). Thus, it remains possible that gasdermin B's evolution remains significantly in flux, and that it remains as one of the more expendable members of this family. Thus, the genomic sequences of the "low quality" reads may be correct, and represent gasdermin B genes that have been disrupted by mutation. A more thorough examination of the genome annotations will be necessarily to further explore these possibilities.

The phylogenetically oldest species in which a possible gasdermin homologue could be identified by both us and Saeki et al. was *Trichoplax adhaerens*[166]; however, the current annotation of this hypothetical protein appears to be missing most of the gasdermin C-terminal

domain. Thus, given that gasdermin C-terminal domains function to inhibit lytic pore formation, if this gene is in fact a gasdermin ancestor, it may have a partial annotation such that the C-terminal domain is not yet annotated, or the C-terminal domain may in fact be absent, which would suggest that the *T. adhearens* protein functions significantly differently than other gasdermins.

Notably, there appears to be a phylogentic gap, where species that diverged after cnidarians but before mollusks/brachiopods lack gasdermin genes. This gap includes several well-studied and well-annotated genomes like *Drosophila melanogaster* and *Caenorhibditis elegans*. This gap could represent missed gene annotations, true losses of this gene (similar to the loss of NLRs in *D. melanogaster and C. elegans*), or significant evolution of the gasdermins that make it more difficult to identify genes by protein sequence homology[167].

Evolutionary relationship of gasdermin proteins

To allow for a more thorough evaluation of evolutionary relationships, we built a phylogenetic tree using PhyML maximum likelihood model from a pooled multiple sequence alignment of collected gasdermin sequences (performed in the software SeaView version 4.6). The sequences chosen for this preliminary tree were chosen by collected all annotated gasdermin A-E and pejvakin proteins and excluding all proteins annotated as “low quality” or “partial”. When multiple isoforms for a single gasdermin was predicted within a species, we chose the isoform that minimized insertions, deletions, and frameshifts compared to that of closely related species aligned using ClustalO. A complete list of proteins sequences used to generate this tree can be found in the Appendix. We used FigTree to visualize the generated tree (Figure 25). The tree generated correctly grouped gasdermins of a given type together, and tended to group the

same protein from similar phylogenetic groups together, suggesting that the overall tree topography was reliable.

Given that cnidaria are the phylogenetically oldest organisms with an identified gasdermin that we are confident is complete (*Trichoplax adhaerens* was not included in this tree), we rooted the tree using these cnidarian gasdermins as the outgroup. However, this leads to a tree topography implying that gasdermin E and pejvakin together evolved separately from the remaining gasdermins, yet an ancient relative to those other gasdermins does not exist in the fish as the tree suggests it should. One possibility is that this topology is in fact correct, and that fish lost the ancient ancestor for gasdermin A-D. However, another possibility is an abrupt and large genetic change could have resulted in the generation of pejvakin. Generation of phylogenetic trees relies on the assumption that the molecular clock dictating the rate of accumulations of mutations in a given gene or protein is relatively constant; as a result, if an abrupt large change occurs like domain rearrangements or large insertions or deletions occur, the algorithms could produce trees with incorrect topology. Given that pejvakin is the only gasdermin protein with a C-terminal domain that is not homologous with the other family members, such an abrupt change to generate pejvakin from the ancient common ancestor to the gasdermin family seems likely.

Consistent with the earliest phyla in which we could identify each gasdermin, gasdermin A first emerged from gasdermin E. The tree shows that gasdermin B emerged next, followed by gasdermin C and D.

In the future, we will want to perform analyses that will better assess for violations of the molecular clock to assess for this possibility, as well as generate a tree that utilizes known timings for speciation events to place constraints on the tree and hopefully generate a tree with more accurate topology.

Assessing conservation of gasdermin cleavage and activation residues

One potential utility of performing an extensive molecular evolutionary analysis is the ability to identify novel conserved residues that could play important roles in the proteins' functions, and conversely, the ability to assess the conservation of purported important residues. Perhaps the most important residues to understanding and differentiating gasdermin function are those that form the activation sites of the proteins. We used the multisequence alignments for each gasdermin to assess conservation of residues involved in activation or identify potential activation sites. A full list of proteins for each family used in the sequence can be found in the Appendix.

Gasdermin A: Gasdermin A has no known activation mechanism. We therefore aligned gasdermin A sequences with gasdermins with known cleavage sites (representative subset shown in Figure 26). Remarkably, when we aligned sequences for gasdermin A from bird species (which phylogenetically predate the emergence of gasdermin D) with other gasdermins, we observed that bird gasdermin A proteins had a sequence of YVAD (or similar) that aligned with the inferred gasdermin linker region. This is notable because YVAD is the prototypical caspase-1 cleavage sequence, even used for the generation of caspase-1-specific inhibitors. Birds that did not have exactly a YVAD sequence, as well as amphibians and reptiles, generally contained variations of this tetrapeptide sequence with a bulky P4 and aspartate or (less commonly, glutamate) P1, consistent with common caspase-1 cleavage sites[168]. In contrast, mammals did not have this conserved sequence but instead had a nearby conserved QASD, which we and others have observed cannot be cleaved by either pyroptotic (caspase-1,4,11) and the primary apoptotic effector caspase, caspase-3 in humans and mice (Figure 23B) [15]. These results suggest that caspase-1 may be the activator for gasdermin A in branches of the phylogeny that predate the

emergence of gasdermin D, including birds. If this is true, then caspase-1 has long been able to cleave some gasdermin, but which gasdermin family member is cleaved has changed over time. Indeed, consistent with this difference in activation mechanism of gasdermin A in amphibians/reptiles/birds versus that in mammals, these two types of gasdermin A proteins grouped separately on our phylogenetic tree, with mammalian gasdermins being significantly more conserved than in amphibians/reptiles/birds.

Gasdermin B: Zhou et al. showed that granzyme A can cleave gasdermin B in the linker region after lysine (K) residues[68]. There are four lysines of note in the human gasdermin B linker region: K227, K229, K235, and K244. Among these, Zhou et al. identified K244 as the major cleavage site for gasdermin B by granzyme A, and K229 as the minor cleavage site. They showed that mutating both K244 and K229 completely abrogated gasdermin B cleavage by granzyme A. Generally speaking, K244 was well conserved; some species have the P1 K substituted with R, another residue after which granzyme A can cleave (Figure 27). The notable exception was marsupials, for which K244 equivalent was absent, though other lysines or arginines could be identified nearby with one in proximity to the location of K229 (aligning at 228), but with different surrounding residues (Figure 27). Panganiban et al. have also proposed that caspase-1 can cleave human gasdermin B at D236 (with the tetrapeptide sequence EEKD), though others have observed that gasdermin B cannot be cleaved by caspase-1 [15,169]. This tetrapeptide residue sequence is moderately well conserved in most species except marsupials (Figure 27).

Gasdermin C: Hou et al. proposed that caspase-8 cleaves human gasdermin C at D365 (in the tetrapeptide sequence LELD) [170]. They performed a brief alignment with human sequences and several other mammals, and observed that these cleavage site is indeed conserved (albeit

several had a conserved substitution of D365E, and caspases generally cleave after D and only relatively rarely cleave after E). We too observe that this proposed cleavage site is conserved in a number of species; however, several species not included in the alignment shown by Hou et al. do not conserve this particular cleavage site (Figure 28). Notably, several rodents (including all four forms of gasdermin C in mice) do not have this cleavage site. However, a few of these species have nearby aspartates that could serve as potential cleavage sites.

Gasdermin D: Caspase-1 cleaves and activates gasdermin D at D275 (in the tetrapeptide sequence FLTD) in humans and D276 (in the tetrapeptide sequence LLSD) in mice[10-12]. This cleavage site is well conserved in all species with gasdermin D (Figure 29).

Gasdermin E: Two types of cleavage sites in gasdermin E have been identified by others, as can be visualized in Figure 30. First, caspase-3 cleaves and activates gasdermin E in humans at D270 (in the tetrapeptide sequence DMPD), which is broadly conserved in placental mammals[21,41]. This cleavage site was also more recently identified in cnidarian species[165]. Second, caspase-1/3/7 can cleave gasdermin E in fish (at D246 in the tetrapeptide FEVD in *Cynoglossus semilaevis*), with caspase-1 cleaving with the greatest efficiency[164]. Analysis of conservation of this site demonstrates that these two types of cleavage sites are conserved throughout their respective phylogenetic groups and otherwise mutually exclusive. Notably, the separation of activation mechanisms of caspase-1 and caspase-3 to different gasdermins also occurred at least once in fish, as zebrafish (*Danio rerio*) have duplicated gasdermin E to yield one that preserves the fish caspase cleavage site and can be activated by pyroptotic but not apoptotic caspases (Gsdmeb), and one with a unique cleavage site that can be activated by pyroptotic but not apoptotic caspases (Gsdmea) [41,171,172]. However, this separation was the exception, as most fish had single gasdermin E proteins with the conserved caspase-1/3/7

cleavage site identified in *Cynoglossus semilaevis*. Finally, when aligning the sequences of gasdermin E from marsupials and monotremes (the oldest mammals), amphibians, reptiles, and birds, two conserved and overlapping potential cleavage sites (FHPDDAVD in chickens) align closely with cleavage sites in placental mammalian gasdermin E (Figure 30).

Pejvakin: While pejvakin is not known to be activated by cleavage, two cysteines within its short C-terminal domain (C328 and C343 in both humans and mice) have been implicated in detecting reactive oxidative species (ROS), allowing pejvakin to activate in response to increased intracellular ROS to promote proliferation of peroxisomes and ultimately reduce ROS back to more manageable levels[78]. Consistent with their proposed importance in activation of pejvakin, both cysteines are well conserved throughout the phylogenetic tree (Figure 31). Conserved cysteines are notable in this region of pejvakin, forming a possible motif of $CX_2CX_{12}CX_2CX_{15}C$ (Figure 31), where the last two cysteines in this string are the ones implicated in ROS sensing.

Bird gasdermin A and E likely functionally mimic mammalian gasdermin D and E

The protease that can cleave and activate a gasdermin determines the pathways in which the gasdermin is involved. Given the fact that amphibian/reptile/bird gasdermin A have sequences within their linker region highly suggestive for being caspase-1 cleavage sites, we hypothesized that gasdermin A from these species may be cleaved and activated by caspase-1 to trigger cell lysis. Thus, while the primary sequence of gasdermin A from these organisms may more closely resemble mammalian gasdermin A, its function may more closely mimic that of mammalian gasdermin D. Furthermore, with the emergence of a second pyroptotic gasdermin, we hypothesized that the activation mechanisms of pyroptotic and apoptotic caspases could be separated to different gasdermins. Indeed, the fact that the gasdermin E cleavage site found in

most fish, which can be cleaved by both pyroptotic and apoptotic caspases, is not conserved beyond fish is consistent with this hypothesis.

To test these hypotheses, we purchased plasmids that express gasdermin A and gasdermin E from *Corvus brachyrhynchos* (American crow) generated using the predicted sequences based on current genome annotations. *Corvus brachyrhynchos* was chosen as the initial model organism because it was one of the birds with YVAD in the linker region (as opposed to one of the ones with conserved mutations), thereby making it more likely to be cleaved by human caspase-1.

Consistent with our hypothesis, crow gasdermin A was cleaved by caspase-1 to yield a fragment in similar size to that produced by human gasdermin D cleavage by caspase-1, suggesting caspase-1 could cleave and activate crow gasdermin A (Figure 23B). Furthermore, human recombinant caspase-3 cleaved crow gasdermin E to yield fragments consistent with a cleavage of human gasdermin D by caspase-3 previously identified to be inactivating (Figure 23B). In contrast, human gasdermin A completely resisted cleavage by either caspase-1 or -3 (Figure 23B). Thus, the cleavage pattern of crow gasdermin A more closely matches that of human gasdermin D than human gasdermin A, suggesting that crow gasdermin A is functionally more similar to human gasdermin A.

Recombinant human caspase-3 cleaved crow gasdermin E to produce the expected N-terminal fragment, whereas crow gasdermin E completely resisted cleavage by caspase-1 (Figure 23B). This cleavage pattern matches that of mammalian gasdermin E, again consistent with our hypotheses.

It is notable that the loss of cross-species efficacy of the recombinant human caspases to cleave crow gasdermins was greater for caspase-1 than for caspase-3. This likely reflects the

further divergence of caspase-1 as it specialized to cleave gasdermin D. Indeed, whereas caspase-3 is well conserved between birds and mammals (63% identity and 74% similarity between chicken and human caspase-3), caspase-1 is less well conserved (42% identity and 52% similarity between chicken and human caspase-1).

We next want to test cleavage of bird gasdermin A with bird caspase-1 to validate this observation, as well as assess lytic potential of any resulting cleaved fragments. To this end, we have obtained chicken macrophages and tissues from the lab of Dr. Luke Borst (North Carolina State University), and we have successfully cloned chicken caspase-1, caspase-3, and gasdermin E. Further, I have successfully PCR amplified chicken gasdermin A from the spleen, I have verified that the PCR product is gasdermin A by Sanger sequencing (performed by GeneWiz), and I am currently in the process of cloning this product. In addition, we want to generate gasdermin A and E with the hypothesized cleavage sites mutated to confirm cleavage locations.

Discussion and future directions

The gasdermin family contains pore-forming proteins that form an essential part of the innate immune system. While we are currently knowledgeable about a few of the gasdermins in mammals, much remains to be understood. With our initial studies here, we provide insights into this family that extend beyond mammalian gasdermins. In particular, our findings regarding bird gasdermins have potential utility for the agriculture industry as poultry is a major food source.

Our data as well as others suggests that since the emergence of this family, there has been constant connection of traditional cell death pathways to gasdermin and gasdermin-mediated cell death. Importantly, with the discovery of bird gasdermin A being integrated with caspase-1 and inflammasome pathways, we fill an evolutionary gap. Our results suggest that since emergence

of caspase-1-like proteases in fish, there has been an uninterrupted connection of caspase-1 to gasdermins, even if the specific gasdermin connected with caspase-1 shifts between different gasdermin genes. Significantly, this suggests that caspase-1 did not merely evolve as a processor of IL-1 family cytokines, but functionally was likely involved in promoting pyroptotic cell death via cleavage of gasdermins from its inception. Consistent with this hypothesis, caspase-1 cannot cleave IL-1β in at least several species of fish[173].

Gasdermin E in fish, which phylogenetically predates the emergence of gasdermin A, was recently demonstrated to be activated by caspase-1, 3, and 7, suggesting that gasdermin E originally functioned as the convergence point downstream of both pyroptotic caspase and apoptotic caspase activation[164]. Our results now suggest that in birds, the development of gasdermin A coincided with the separation of activation of gasdermins by pyroptotic caspases (e.g. caspase-1) and apoptotic caspases (e.g. caspase-3), and this is likely true in both amphibians and reptiles as well given similarities in potential cleavage sites.

The observation that there is always a gasdermin associated with inflammasome pathways also has implications for zoonotic infections. As our lab and others have demonstrated, many true intracellular pathogens require mechanisms for avoiding or inhibiting pyroptotic pathways to allow successful infection of a host. Thus, potential pathogens that evolve zoonotic hosts like birds must evolve to fight the pressures of gasdermin-mediated cell death. Even if the particulars of the gasdermins vary between species, the common origin of these pathways suggests that pathogens adapted to one host jumping to a new species is likely facilitated by the fact that these pathogens do not have to develop mechanisms for avoiding these pathways from scratch. Indeed, as our lab has demonstrated through the use of environmental pathogens like *Burkholderia thailandensis* (see Chapter 3) or *Chromobacterium violaceum*, microbes that

evolved outside of these hosts with no mechanism for avoiding gasdermin-mediated cell death, are quickly cleared by mammalian immune systems[7,8]. Of note, this has particular relevance for influenza, for which inflammasome activation has been implicated in the defense and for which a number of strains evolve in the context of birds prior to becoming infectious in humans[174].

With these preliminary molecular evolution analyses, we have demonstrated the utility of using such studies to analyze the gasdermin family. Both the large multisequence alignment of all currently identified gasdermins and the tree generation could serve as useful tools for both generating and supporting novel hypotheses, and for identifying and studying potentially important residues. Indeed, upon inspection of the multisequence alignment, we hypothesized that bird gasdermin A could be cleaved by caspase-1 and likely triggers pyroptosis in response to inflammasomes, a hypothesis that our subsequent in vitro studies now support and which has significant implications for bird immunity.

Recently, Schutter et al. also generated and published their own phylogenetic tree of the gasdermin family using a similar algorithm as the tree we generated[175]. Similar to what we observed, the tree generated by Schutter et al. suggests that gasdermin E and pejvakin evolved separately from other gasdermins. Interestingly, the broad topology of Schutter et al.'s tree differs from our tree regarding the emergence of the mammalian gasdermins. While their tree agrees with ours that gasdermin A emerged prior to gasdermins B-D, their tree suggests that mammalian gasdermin A and gasdermin B evolved separately from gasdermin C and D, whereas the topology of our tree suggests a sequential emergence of A then B, followed by the emergence of C and D. Furthermore, the identification of gasdermin A in caecillians in our analyses, which are located at the base of the amphibian evolutionary tree, pushes the emergence of gasdermin A significantly earlier compared to what Schutter et al identified.

Schutter et al. also contend that the identified gasdermin D in platypus (a monotreme and the phylogenetically oldest mammal included in both our trees) aligned more closely with gasdermin A, and therefore suggested that platypuses lacked gasdermin D but instead had two gasdermin A-like proteins. However, platypus gasdermin D grouped more closely with gasdermin D while platypus gasdermin A grouped closely with mammalian gasdermin A. Given that platypus gasdermin D is located proximal to other genes located proximal to gasdermin D in other animals (eg Mroh6) and that the linker region contains the conserved gasdermin D cleavage site (which is absent in mammalian gasdermin A), it is likely that this gasdermin is in fact truly a gasdermin D.

Finally, Schutter et al. contend that gasdermin B is completely lost in the branch that includes rabbits, rats, and mice. However, while no gasdermin B could be identified in NCBI annotations of both rabbits and most rodents, gasdermin B could be identified in at least two species of hamsters (*Mesocricetus auratus* and *Cricetulus griseus*), which would be located within this same branch, between rabbits and rats and mice (according to the mammalian tree of life[176]), suggesting that the possibility remains that gasdermin B could be present in other members of this branch. Thus, absence of the gene from current annotations, especially in lower quality annotations, should be interpreted carefully as to whether the genes are truly lost or if the genes are merely missing from current genome sequences or annotations.

Future molecular evolutionary analyses will first focus on performing more rigorous analyses of gasdermins from 38 representative organisms. Furthermore, we are reannotating genomes of non-model organisms (which tend to have less well-annotated gasdermins) from this list in which particular gasdermins are absent but present in related species, or which current annotations of the gasdermin is questionable. Using these sequences, we will assess residues for

selection and generate a new tree using BEAST, which will enable us to use known speciation times to place constraints on the tree-making algorithm and should hopefully result in a more accurate tree. Finally, we will consider performing further analyses, such as assessing conservation of sites, to provide a more granular understanding of the evolution of these proteins. In addition to these evolutionary analyses on the gasdermin family, we will perform parallel analyses on caspases and attempt to assess co-evolution of the gasdermin and caspase families.

	Cnidarians	Mollusks	Lancelets	Fish	Amphibians	Reptiles	Birds	Mammals		
								Monotremes	Marsupials	Placentals
Gsdma					X	X	X	X	X	X
Gsdmb									X	X
Gsdmc									X	X
Gsdmd								X	X	X
Gsdme	X	X	X	X	X	X	X	X	X	X
Pjvk			X	X	X	X	X	X	X	X

Table 8. Phylogenetic groups in which members of gasdermin family were identified

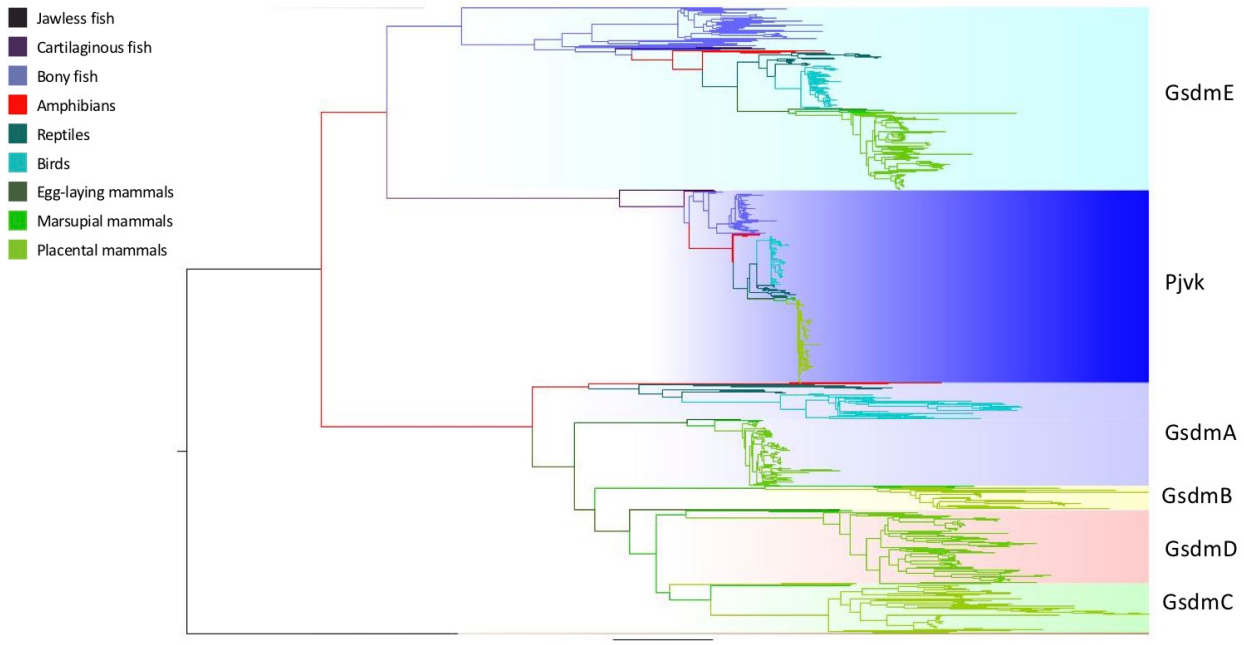

Figure 25: Phylogenetic tree of gasdermin family. Identified gasdermins were aligned by ClustalO, a tree was built using a PhyML maximum likelihood model, and the tree was visualized using FigTree. The tree was rooted using cnidarian sequences as an outgroup.

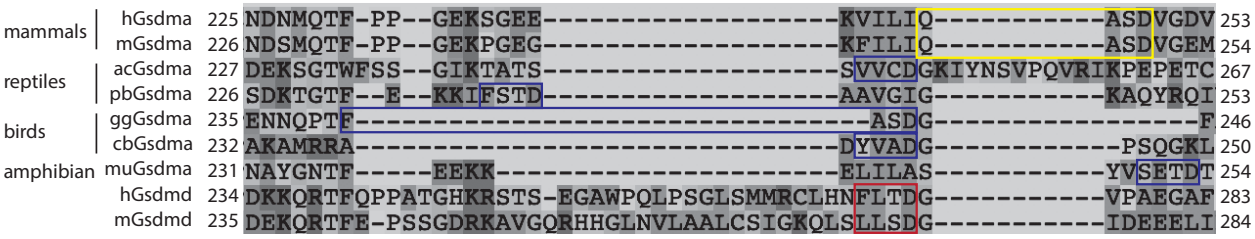

Figure 26: Sequence alignment of linker region of gasdermin A proteins.

Collected gasdermin A sequences were aligned by ClustalO, representative sequences shown here. Alignment with gasdermin D with known caspase-1/4/5/11 cleavage site (red box) was used to aid in assessing for potential cleavage sites in gasdermin A. Aligned or nearby potential cleavage sites in gasdermin A shown in blue box. Nearby potential cleavage site experimentally shown not to be cleaved by caspase-1/3 shown in yellow box.

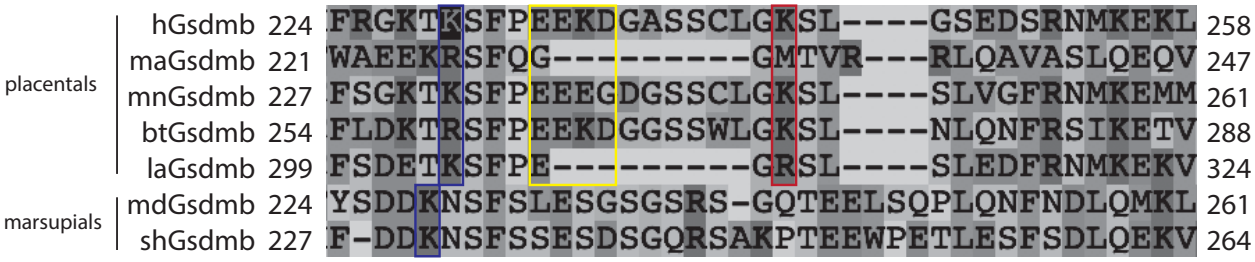

Figure 27: Sequence alignment of linker region of gasdermin B proteins.

Collected gasdermin B sequences were aligned by ClustalO, representative sequences shown here. Conserved residue aligned with lysine identified as major cleavage site for granzyme B shown in red box. Conserved residue aligned with lysine identified as minor cleavage site for granzyme B shown in red box. Site aligned with potential caspase-1 cleavage site identified in human gasdermin B shown in yellow box.

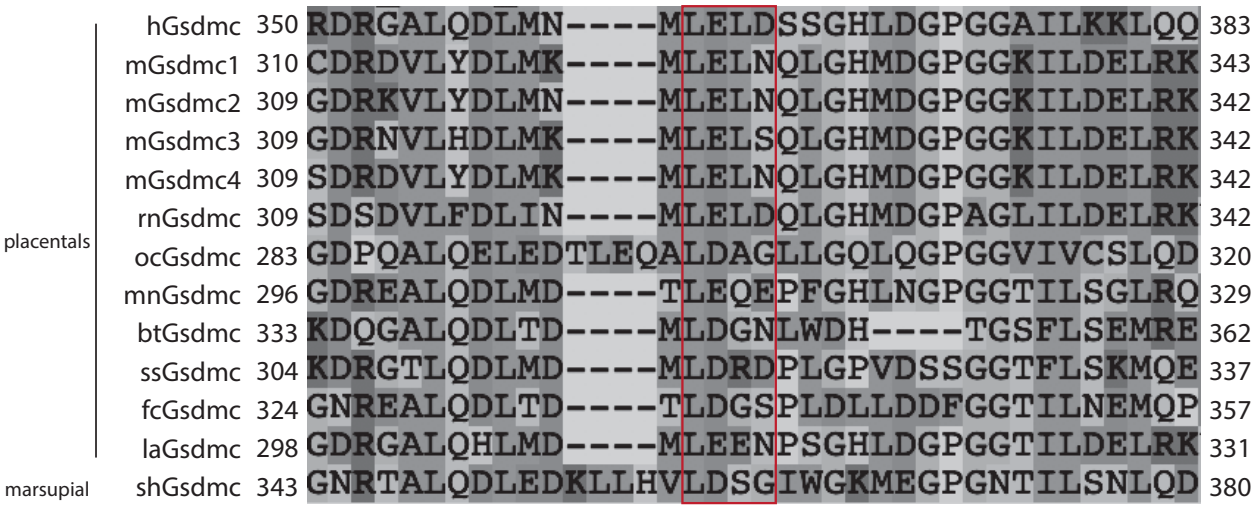

Figure 28: Sequence alignment of linker region of gasdermin C proteins.

Collected gasdermin C sequences were aligned by ClustalO, representative sequences shown here. Residues aligned with potential caspase-8 cleavage site in human gasdermin C shown in red box.

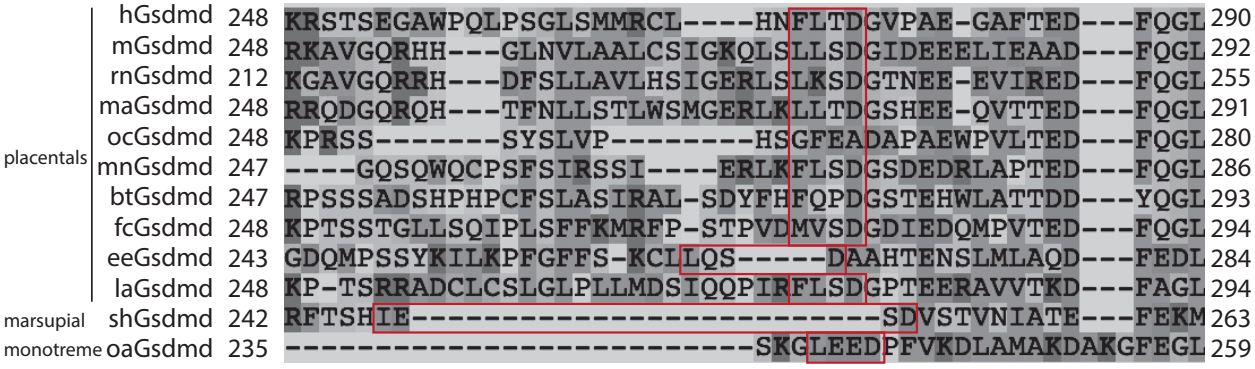

Figure 29: Sequence alignment of linker region of gasdermin D proteins.

Collected gasdermin D sequences were aligned by ClustalO, representative sequences shown here. Residues aligned with known caspase-1/4/5/11 cleavage site in human and mouse gasdermin D shown in red box.

Figure 30: Sequence alignment of linker region of gasdermin E proteins.

Collected gasdermin E sequences were aligned by ClustalO, representative sequences shown here. Residues aligned with known caspase-3 cleavage site in human and mouse gasdermin D shown in red box. Residues aligned with known caspase-1/3/7 cleavage site identified in the fish *Cynoglossus semilaevis* gasdermin E shown in green box. Likely caspase-3 cleavage site in *Danio rerio* (zebrafish) gasdermin Ea shown in blue. Potential caspase cleavage sites in marsupial/monotreme/amphibian/reptile/bird shown in yellow box, in cnidarians shown in brown boxes.

Figure 31: Sequence alignment of functional C-terminal cysteines in pejvakin proteins.

Collected pejvakin sequences were aligned by ClustalO, representative sequences shown here. Residues aligned with functionally important cysteines in human and mouse pejvakin shown in red boxes.

CHAPTER 7: CONCLUSIONS

Inflammasomes and gasdermins together form an essential part of the innate immune system. When functioning correctly, they detect intracellular pathogens and promote pyroptosis and inflammation. For my dissertation, I have first undertaken granular studies to elucidate cell-specific characteristics of inflammasome and gasdermins by studying their functions within neutrophils during *Burkholderia thailandensis* infection and by completing the initial steps for generating a cell-specific knockout mouse line for *Gsdmd*. I then attempted to expand our global understanding of the entire gasdermin family through my studies of gasdermin A and molecular evolution analyses of this essential family.

As we studied the role of inflammasomes and gasdermins in neutrophils, we observed that gasdermin D was cleaved and activated downstream of both caspase-1 and caspase-11 pathways, but only gasdermin D cleaved by caspase-11 lead to pyroptosis, a stark contrast with macrophages in which gasdermin D cleaved by either caspase-1 and caspase-11 leads to pyroptosis. The fact that both caspase-1 and caspase-11 cleave gasdermin D at the same residues suggests the possibility that differences in the cellular characteristics contributing to differences in responses to inflammasome and gasdermin activation, such as the presence of granules or other organelles serving as gasdermin sinks.

Ultimately, when the behavior of a single gasdermin can vary based on the cell type in which it is being expressed, similar considerations must be made when studying other members of the gasdermin family. Indeed, each gasdermin has a specific expression pattern, meaning that

each must deal with a different set of cell and tissue-specific characteristics that will influence the behavior of the gasdermin.

For example, gasdermin A is predominantly expressed in keratinocytes within the skin. A keratinocyte is larger than most immune cells (meaning that the surface area-to-volume ratio is much smaller), and it has a scaffolding of cytokeratin intermediate filaments that provides increased mechanical strength to the cell[177]. Furthermore, as the keratinocyte differentiates and ultimately transitions into a corneocyte, its membrane composition shifts and stiffens as phospholipids and cholesterols are replaced by ceramides and saturated triglycerides[178]. Each of these unique characteristics could potentially affect the ability for gasdermin A to trigger cell lysis.

At the tissue level, a keratinocyte is physically interlocked with surrounding keratinocytes via desmosomes, meaning neighboring cells constantly exert force against a keratinocyte that may counter the expansive osmotic forces triggered by gasdermin pore formation (unlike immune cells that are usually found in relative isolation). Furthermore, the extracellular concentrations of salts are significantly elevated in the skin, and differences in salt concentrations in the intracellular and extracellular compartments ultimately drive cell swelling and lysis during pyroptosis[179]. Thus, future studies into gasdermin A as well as other members of the gasdermin family may need to take into account both the cellular and tissue characteristics that may sharply diverge from those of macrophages, the cell type in which inflammasomes and gasdermins are traditionally studied, and cultured HEK293T, the cell type in which gasdermins are often transfected into to study their pore-forming and lytic capabilities. Indeed, these differences in cell and tissue types may have been a force that helped drive the expansion of the gasdermin family.

Gasdermins were first identified as the effector of pyroptosis at the beginning of my thesis research. This discovery revolutionized our understanding of inflammasomes and pyroptosis. Through my focus on understanding the cell-specific roles of inflammasomes and gasdermins, my thesis research furthers our understanding of the gasdermin family and provides new avenues for research into the gasdermin family, members of which will likely prove to be valuable therapeutic targets.

APPENDIX: PROTEINS USED IN MOLECULAR PHYLOGENETICS

Gasdermin A

NCBI Accession ID	Organism	Abbreviation
NP_835465.2	Homo_sapiens	hGsdma
XP_014975037.1	Macaca_mulatta	
XP_023060010.1	Piliocolobus_tephrosceles	
XP_025218676.1	Theropithecus_gelada	
XP_008955035.1	Pan_paniscus	
XP_011723579.1	Macaca_nemestrina	
XP_001171222.1	Pan_troglodytes	
XP_024091062.1	Pongo_abelii	
XP_012658360.1	Otolemur_garnettii	
XP_021784852.1	Papio_anubis	
XP_008063364.1	Carlito_syrichta	
XP_012307501.1	Aotus_nancymaae	
XP_012621524.1	Microcebus_murinus	
XP_004041806.1	Gorilla_gorilla_gorilla	
XP_017724755.1	Rhinopithecus_bieti	
XP_017352685.1	Cebus_capucinus_imitator	
XP_005584115.1	Macaca_fascicularis	
XP_012516382.1	Propithecus_coquereli	
XP_011785254.1	Colobus_angolensis_palliatus	
XP_011854366.1	Mandrillus_leucophaeus	
XP_003942931.1	Saimiri_boliviensis_boliviensis	
XP_010373819.1	Rhinopithecus_roxellana	
XP_008580237.1	Galeopterus_variegatus	
XP_008011013.1	Chlorocebus_sabaeus	
NP_067322.1	Mus_musculus	mGsdma
NP_084003.2	Mus_musculus	mGsdma2
NP_001007462.1	Mus_musculus	mGsdma3
NP_001101767.1	Rattus_norvegicus	
XP_028745379.1	Peromyscus_leucopus	
XP_028611014.1	Grammomys_surdaster	
XP_027778953.1	Marmota_flaviventris	
XP_026645688.1	Microtus_ochrogaster	
XP_026242881.1	Urocitellus_parryii	
XP_004633937.1	Octodon_degus	

XP_013005065.1	Cavia_porcellus	
XP_005322019.1	Ictidomys_tridecemlineatus	
XP_021509099.1	Meriones_unguiculatus	
XP_004859525.1	Heterocephalus_glaber	
XP_012973102.1	Mesocricetus_auratus	
XP_020031928.1	Castor_canadensis	
XP_006971892.1	Peromyscus_maniculatus_bairdii	
XP_015351255.1	Marmota_marmota_marmota	
XP_013374647.1	Chinchilla_lanigera	
XP_012893237.1	Dipodomys_ordii	
XP_004655518.1	Jaculus_jaculus	
XP_012581601.1	Condylura_cristata	
XP_006833732.1	Chrysochloris_asiatica	
XP_029784118.1	Suricata_suricatta	
XP_012917953.1	Mustela_putorius_furo	
XP_014446163.1	Tupaia_chinensis	
XP_004608992.1	Sorex_araneus	
XP_017497970.1	Manis_javanica	
XP_002719393.1	Oryctolagus_cuniculus	
XP_004591216.1	Ochotona_princeps	
XP_007531080.1	Erinaceus_europaeus	
XP_007940243.1	Orycteropus_afer_afer	
XP_027984604.1	Eptesicus_fuscus	
XP_006924750.1	Pteropus_alecto	
XP_024429158.1	Desmodus_rotundus	
XP_019494184.1	Hipposideros_armiger	
XP_016057700.1	Miniopterus_natalensis	
XP_016020090.1	Rousettus_aegyptiacus	
XP_005861942.1	Myotis_brandtii	
XP_011381342.1	Pteropus_vampyrus	
XP_006774377.2	Myotis_davidii	
XP_025852001.1	Vulpes_vulpes	
XP_025296309.1	Canis_lupus_dingo	
XP_026889645.1	Acinonyx_jubatus	
XP_025773357.1	Puma_concolor	
XP_019673388.1	Felis_catus	
XP_019271588.1	Panthera_pardus	
XP_007085856.1	Panthera_tigris_altaica	
XP_004012902.1	Ovis_aries	

XP_005693821.2	Capra_hircus	
XP_011997233.1	Ovis_aries_musimon	
XP_015103368.1	Vicugna_pacos	
XP_026368703.1	Ursus_arctos_horribilis	
XP_019665612.1	Ailuropoda_melanoleuca	
XP_008687546.1	Ursus_maritimus	
NP_001071558.1	Bos_taurus	
XP_019836267.1	Bos_indicus	
XP_005898083.1	Bos_mutus	
XP_006068650.1	Bubalus_bubalis	
XP_010840931.1	Bison_bison_bison	
XP_001500838.3	Equus_caballus	
XP_014689408.1	Equus_asinus	
XP_008517125.1	Equus_przewalskii	
XP_004434607.1	Ceratotherium_simum_simum	
XP_006176398.1	Camelus_ferus	
XP_010990107.1	Camelus_dromedarius	
XP_010958761.1	Camelus_bactrianus	
XP_013835119.1	Sus_scrofa	
XP_020745726.1	Odocoileus_virginianus_texanus	
XP_027945757.1	Eumetopias_jubatus	
XP_027423431.1	Zalophus_californianus	
XP_025715235.1	Callorhinus_ursinus	
XP_021560076.1	Neomonachus_schauinslandi	
XP_012416038.1	Odobenus_rosmarus_divergens	
XP_006749918.1	Leptonychotes_weddellii	
XP_012411464.1	Trichechus_manatus_latirostris	
XP_020853178.1	Phascolarctos_cinereus	
XP_027729048.1	Vombatus_ursinus	
XP_012403791.1	Sarcophilus_harrisii	
XP_007654365.3	Ornithorhynchus_anatinus	
XP_028558572.1	Podarcis_muralis	
XP_015279010.1	Gekko_japonicus	
XP_008111551.1	Anolis_carolinensis	acGsdma
XP_019405871.1	Crocodylus_porosus	
XP_019362599.1	Gavialis_gangeticus	
XP_014451785.1	Alligator_mississippiensis	
XP_006022649.1	Alligator_sinensis	
XP_025022523.1	Python_bivittatus	pbGsdma

XP_015687751.1	Protobothrops_mucrosquamatus	
XP_013929683.1	Thamnophis_sirtalis	
XP_026573339.1	Pseudonaja_textilis	
XP_026535498.1	Notechis_scutatus	
XP_026510609.1	Terrapene_carolina_triunguis	
XP_006117469.1	Pelodiscus_sinensis	
XP_008160950.1	Chrysemys_picta_bellii	
XP_021388636.1	Lonchura_striata_domestica	
NP_001026532.1	Gallus_gallus	ggGsdma
XP_021233895.1	Numida_meleagris	
XP_015741468.1	Coturnix_japonica	
XP_025973622.1	Dromaius_novaehollandiae	
XP_029878858.1	Aquila_chrysaetos_chrysaetos	
XP_027763648.1	Empidonax_traillii	
XP_027603785.1	Pipra_filicauda	
XP_026720458.1	Athene_cunicularia	
XP_025928753.1	Apteryx_rowi	
XP_025897146.1	Nothoprocta_perdicaria	
XP_015506851.1	Parus_major	
XP_014813419.1	Calidris_pugnax	
XP_013800181.1	Apteryx_australis_mantelli	
XP_013057526.1	Anser_cygnoides_domesticus	
XP_011592385.1	Aquila_chrysaetos_canadensis	
XP_010583858.1	Haliaeetus_leucocephalus	
XP_019149421.2	Corvus_cornix_cornix	
XP_010007212.1	Chaetura_pelagica	
XP_009933676.1	Opisthocomus_hoazin	
XP_009897998.1	Picoides_pubescens	
XP_009883759.1	Charadrius_vociferus	
XP_009672097.1	Struthio_camelus_australis	
XP_009640852.1	Egretta_garzetta	
XP_009568865.1	Cuculus_canorus	
XP_009463179.1	Nipponia_nippon	
XP_009333228.1	Pygoscelis_adeliae	
XP_009288830.1	Aptenodytes_forsteri	
XP_009094796.1	Serinus_canaria	
XP_009082361.1	Acanthisitta_chloris	
XP_008634137.1	Corvus_brachyrhynchos	cbGsdma
XP_008503983.1	Calypte_anna	

XP_005531574.2	Pseudopodoces_humilis	
XP_005513819.1	Columba_livia	
XP_026655008.1	Zonotrichia_albicollis	
XP_014135543.1	Falco_cherrug	
XP_013150873.1	Falco_peregrinus	
XP_016159802.1	Ficedula_albicollis	
XP_027301037.1	Anas_platyrhynchos	
XP_012426589.1	Taeniopygia_guttata	
XP_030077862.1	Microcaecilia_unicolor	muGsdma
XP_029428328.1	Rhinatrema_bivittatum	

Gasdermin B

NCBI Accession ID	Organism	Abbreviation
NP_001159430.1	Homo_sapiens	hGsdmb
XP_009430521.1	Pan_troglodytes	
XP_018883925.1	Gorilla_gorilla_gorilla	
XP_008955037.1	Pan_paniscus	
XP_012658361.1	Otolemur_garnettii	
XP_003278296.2	Nomascus_leucogenys	
XP_002827669.2	Pongo_abelii	
XP_032019389.1	Hylobates_moloch	
XP_012973048.1	Mesocricetus_auratus	
XP_027279932.1	Cricetulus_griseus	
XP_006833730.1	Chrysochloris_asiatica	
XP_012581499.1	Condylura_cristata	
XP_007940378.1	Orycteropus_afer_afer	
XP_027630559.1	Tupaia_chinensis	
XP_023441904.1	Dasypus_novemcinctus	
XP_028377233.1	Phyllostomus_discolor	
XP_024429114.1	Desmodus_rotundus	
XP_016057754.1	Miniopterus_natalensis	mnGsdmb
XP_032947748.1	Rhinolophus_ferrumequinum	
XP_022279619.1	Canis_lupus_familiaris	
XP_025296608.1	Canis_lupus_dingo	
XP_015314316.2	Bos_taurus	btGsdmb
XP_010840944.1	Bison_bison_bison	
XP_005898079.1	Bos_mutus	
XP_025135973.1	Bubalus_bubalis	
XP_023508346.1	Equus_caballus	

XP_014689450.1	Equus_asinus	
XP_008517122.1	Equus_przewalskii	
XP_010990153.1	Camelus_dromedarius	
XP_010958860.1	Camelus_bactrianus	
XP_013827805.2	Capra_hircus	
XP_012041444.2	Ovis_aries	
XP_023409166.1	Loxodonta_africana	laGsdmb
XP_005653979.2	Sus_scrofa	
XP_004434611.1	Ceratotherium_simum_simum	
XP_016285970.1	Monodelphis_domestica	mdGsdmb
XP_023358160.1	Sarcophilus_harrisii	shGsdmb

Gasdermin C

NCBI Accession ID	Organism	Abbreviation
NP_113603.1	Homo_sapiens	hGsdmc
XP_028708741.1	Macaca_mulatta	
XP_005564120.1	Macaca_fascicularis	
XP_011758353.1	Macaca_nemestrina	
XP_001153860.1	Pan_troglodytes	
XP_032614393.1	Hylobates_moloch	
XP_032109296.1	Sapajus_apella	
XP_025250365.1	Theropithecus_gelada	
XP_023078764.2	Piliocolobus_tephrosceles	
XP_017725971.1	Rhinopithecus_bieti	
XP_017354851.1	Cebus_capucinus_imitator	
XP_011921019.1	Cercocebus_atys	
XP_011831848.1	Mandrillus_leucophaeus	
XP_011793570.1	Colobus_angolensis_palliatus	
XP_030793163.1	Rhinopithecus_roxellana	
XP_007999718.1	Chlorocebus_sabaeus	
XP_004047578.3	Gorilla_gorilla_gorilla	
XP_010342559.1	Saimiri_boliviensis_boliviensis	
XP_003903208.1	Papio_anubis	
XP_003820501.1	Pan_paniscus	
XP_012664852.2	Otolemur_garnettii	
XP_003256254.2	Nomascus_leucogenys	
XP_002819473.1	Pongo_abelii	
XP_008981514.1	Callithrix_jacchus	

NP_113555.1	Mus_musculus	mGsdmc1
NP_001161746.1	Mus_musculus	mGsdmc2
NP_899017.2	Mus_musculus	mGsdmc3
NP_083268.1	Mus_musculus	mGsdmc4
XP_017450238.1	Rattus_norvegicus	rnGsdmc
XP_032771866.1	Rattus_rattus	
XP_028629109.1	Grammomys_surdaster	
XP_032729332.1	Lontra_canadensis	
XP_029779186.1	Suricata_suricatta	
XP_032171903.1	Mustela_erminea	
XP_027804089.1	Marmota_flaviventris	
XP_026263122.1	Urocitellus_parryii	
XP_021501085.1	Meriones_unguiculatus	
XP_021073018.1	Mus_pahari	
XP_021039645.1	Mus_caroli	
XP_015341781.1	Marmota_marmota_marmota	
XP_010641186.1	Fukomys_damarensis	
XP_008843720.1	Nannospalax_galili	
XP_013376750.1	Chinchilla_lanigera	
XP_021578221.1	Ictidomys_tridecemlineatus	
XP_021107746.1	Heterocephalus_glaber	
XP_012578355.1	Condylura_cristata	
XP_004656383.1	Jaculus_jaculus	
XP_023419805.1	Cavia_porcellus	
XP_005078752.1	Mesocricetus_auratus	
XP_017197091.1	Oryctolagus_cuniculus	ocGsdmc
XP_027630809.1	Tupaia_chinensis	
XP_004602662.1	Sorex_araneus	
XP_007941614.1	Orycteropus_afer_afer	
XP_012377894.1	Dasypus_novemcinctus	
XP_028389399.1	Phyllostomus_discolor	
XP_024427836.1	Desmodus_rotundus	
XP_016071620.1	Miniopterus_natalensis	mnGsdmc
XP_023401449.1	Loxodonta_africana	laGsdmc
NP_001039469.1	Bos_taurus	btGsdmc
XP_019829042.1	Bos_indicus	
XP_005900062.1	Bos_mutus	
XP_010842633.1	Bison_bison_bison	
XP_006042923.1	Bubalus_bubalis	

XP_013843492.1	Sus_scrofa	ssGsdmc
XP_020730911.1	Odocoileus_virginianus_texanus	
XP_019650518.1	Ailuropoda_melanoleuca	
XP_026351145.1	Ursus_arctos_horribilis	
XP_008687605.1	Ursus_maritimus	
XP_022282826.1	Canis_lupus_familiaris	
XP_025306872.1	Canis_lupus_dingo	
XP_019678683.1	Felis_catus	fcGsdmc
XP_030160404.1	Lynx_canadensis	
XP_025778779.1	Puma_concolor	
XP_019315398.1	Panthera_pardus	
XP_026919714.1	Acinonyx_jubatus	
XP_031803207.1	Sarcophilus_harrisii	shGsdmc
XP_025726321.1	Callorhinus_ursinus	

Gasdermin D

NCBI Accession ID	Organism	Abbreviation
NP_001159709.1	Homo_sapiens	hGsdmd
XP_015001617.2	Macaca_mulatta	
XP_005564295.1	Macaca_fascicularis	
XP_001152706.2	Pan_troglodytes	
XP_008981331.1	Callithrix_jacchus	
XP_032616510.1	Hylobates_moloch	
XP_032111043.1	Sapajus_apella	
XP_025250524.1	Theropithecus_gelada	
XP_017738915.1	Rhinopithecus_bieti	
XP_017367031.1	Cebus_capucinus_imitator	
XP_012608366.1	Microcebus_murinus	
XP_012503394.1	Propithecus_coquereli	
XP_021527750.1	Aotus_nancymaae	
XP_011905474.1	Cercocebus_atys	
XP_011831038.1	Mandrillus_leucophaeus	
XP_011750785.1	Macaca_nemestrina	
XP_010383809.2	Rhinopithecus_roxellana	
XP_008581297.1	Galeopterus_variegatus	
XP_008054914.2	Carlito_syrichta	
XP_007999960.1	Chlorocebus_sabaeus	
XP_003942159.1	Saimiri_boliviensis_boliviensis	
XP_003903292.1	Papio_anubis	

XP_003819507.1	Pan_paniscus	
XP_003802420.1	Otolemur_garnettii	
XP_024106658.1	Pongo_abelii	
NP_081236.1	Mus_musculus	mGsdmd
NP_001124025.1	Rattus_norvegicus	rnGsdmd
XP_008832746.1	Nannospalax_galili	
XP_021078648.1	Mesocricetus_auratus	maGsdmd
XP_032772926.1	Rattus_rattus	
XP_031202285.1	Mastomys_coucha	
XP_027806786.1	Marmota_flaviventris	
XP_026265627.1	Urocitellus_parryii	
XP_021072889.1	Mus_pahari	
XP_021039083.1	Mus_caroli	
XP_015342041.1	Marmota_marmota_marmota	
XP_012889351.1	Dipodomys_ordii	
XP_010637563.1	Fukomys_damarensis	
XP_015863152.1	Peromyscus_maniculatus_bairdii	
XP_006830929.1	Chrysochloris_asiatica	
XP_005395830.1	Chinchilla_lanigera	
XP_005316153.1	Ictidomys_tridecemlineatus	
XP_021106782.1	Heterocephalus_glaber	
XP_004656438.1	Jaculus_jaculus	
XP_004639026.2	Octodon_degus	
XP_004618751.1	Sorex_araneus	
XP_004580923.1	Ochotona_princeps	
XP_003510483.1	Cricetulus_griseus	
XP_013001158.1	Cavia_porcellus	
XP_032171400.1	Mustela_erminea	
XP_032704245.1	Lontra_canadensis	
XP_029779202.1	Suricata_suricatta	
XP_006152136.1	Tupaia_chinensis	
XP_006879495.1	Elephantulus_edwardii	
XP_017525087.1	Manis_javanica	
XP_004480061.1	Dasypus_novemcinctus	
XP_008252155.1	Oryctolagus_cuniculus	ocGsdmd
XP_007954323.1	Orycteropus_afer_afer	
XP_016040631.1	Erinaceus_europaeus	eeGsdmd
XP_004697675.1	Echinops_telfairi	
XP_007488898.1	Monodelphis_domestica	

XP_028389413.1	Phyllostomus_discolor	
XP_019513341.1	Hipposideros_armiger	
XP_016075669.1	Miniopterus_natalensis	mnGsdmd
XP_015994746.1	Rousettus_aegyptiacus	
XP_011373217.1	Pteropus_vampyrus	
XP_008157982.1	Eptesicus_fuscus	
XP_006913014.1	Pteropus_alecto	
XP_015426878.1	Myotis_davidii	
NP_001039625.1	Bos_taurus	btGsdmd
XP_005888687.1	Bos_mutus	
XP_010852842.1	Bison_bison_bison	
XP_006045211.2	Bubalus_bubalis	
XP_010600015.1	Loxodonta_africana	laGsdmd
XP_014652722.1	Ceratotherium_simum_simum	
XP_022282557.1	Canis_lupus_familiaris	
XP_025843337.1	Vulpes_vulpes	
XP_025306643.1	Canis_lupus_dingo	
XP_031546305.1	Vicugna_pacos	
XP_017914166.1	Capra_hircus	
XP_020946165.1	Sus_scrofa	
XP_027829189.1	Ovis_aries	
XP_023504872.1	Equus_caballus	
XP_014713657.1	Equus_asinus	
XP_008534512.1	Equus_przewalskii	
XP_023104116.1	Felis_catus	fcGsdmd
XP_030160048.1	Lynx_canadensis	
XP_019290543.1	Panthera_pardus	
XP_026919519.1	Acinonyx_jubatus	
XP_032323580.1	Camelus_ferus	
XP_031295648.1	Camelus_dromedarius	
XP_010959450.1	Camelus_bactrianus	
XP_026344710.1	Ursus_arctos_horribilis	
XP_008682309.1	Ursus_maritimus	
XP_019658251.1	Ailuropoda_melanoleuca	
XP_020736699.1	Odocoileus_virginianus_texanus	
XP_032465962.1	Phocoena_sinus	
XP_032271700.1	Phoca_vitulina	
XP_030732008.1	Globicephala_melas	
XP_029059666.1	Monodon_monoceros	

XP_027949315.1	Eumetopias_jubatus	
XP_027467977.1	Zalophus_californianus	
XP_026988031.1	Lagenorhynchus_obliquidens	
XP_025727038.1	Callorhinus_ursinus	
XP_024596904.1	Neophocaena_asiaeorientalis_asiaeorientalis	
XP_022411150.1	Delphinapterus_leucas	
XP_021544405.1	Neomonachus_schauinslandi	
XP_007464679.1	Lipotes_vexillifer	
XP_007167001.1	Balaenoptera_acutorostrata_scammoni	
XP_007113167.2	Physeter_catodon	
XP_004265441.1	Orcinus_orca	
XP_023597400.1	Trichechus_manatus_latirostris	
XP_030875078.1	Leptonychotes_weddellii	
XP_020850599.1	Phascolarctos_cinereus	
XP_012397449.2	Sarcophilus_harrisii	shGsdmd
XP_028917767.1	Ornithorhynchus_anatinus	oaGsdmd

Gasdermin E

NCBI Accession ID	Organism	Abbreviation
NP_001120925.1	Homo_sapiens	hGsdme
XP_001096213.2	Macaca_mulatta	
XP_003318404.2	Pan_troglodytes	
XP_003270464.1	Nomascus_leucogenys	
XP_024105635.1	Pongo_abelii	
XP_009000514.1	Callithrix_jacchus	
XP_017719435.1	Rhinopithecus_bieti	
XP_017382493.1	Cebus_capucinus_imitator	
XP_012628783.1	Microcebus_murinus	
XP_012496187.1	Propithecus_coquereli	
XP_021525833.1	Aotus_nancymaae	
XP_011937000.1	Cercocebus_atys	
XP_011825996.1	Mandrillus_leucophaeus	
XP_011793945.1	Colobus_angolensis_palliatus	
XP_011729491.1	Macaca_nemestrina	
XP_010374233.1	Rhinopithecus_roxellana	
XP_008070518.1	Carlito_syrichta	
XP_007980048.1	Chlorocebus_sabaeus	
XP_005550020.1	Macaca_fascicularis	
XP_004045238.1	Gorilla_gorilla_gorilla	

XP_003935184.1	Saimiri_boliviensis_boliviensis	
XP_003896238.1	Papio_anubis	
XP_003807976.1	Pan_paniscus	
XP_003788653.1	Otolemur_garnettii	
XP_032615042.1	Hylobates_moloch	
XP_032142871.1	Sapajus_apella	
XP_025236017.1	Theropithecus_gelada	
XP_023081708.1	Piliocolobus_tephrosceles	
NP_001178678.1	Rattus_norvegicus	
NP_061239.1	Mus_musculus	mGsdme
XP_021109770.1	Heterocephalus_glaber	
XP_020034992.1	Castor_canadensis	
XP_027272248.1	Cricetulus_griseus	
XP_008839709.1	Nannospalax_galili	
XP_005087240.1	Mesocricetus_auratus	
XP_021486754.1	Meriones_unguiculatus	
XP_021046698.1	Mus_pahari	
XP_021020548.1	Mus_caroli	
XP_015345627.1	Marmota_marmota_marmota	
XP_012879848.1	Dipodomys_ordii	
XP_010626527.1	Fukomys_damarensis	
XP_006982246.1	Peromyscus_maniculatus_bairdii	
XP_006832344.1	Chrysochloris_asiatica	
XP_005366675.2	Microtus_ochrogaster	
XP_021577894.1	Ictidomys_tridecemlineatus	
XP_012576204.1	Condylura_cristata	
XP_004652861.1	Jaculus_jaculus	
XP_004626528.1	Octodon_degus	
XP_003467957.1	Cavia_porcellus	
XP_032762429.1	Rattus_rattus	
XP_031237728.1	Mastomys_coucha	
XP_028645887.1	Grammomys_surdaster	
XP_027788502.1	Marmota_flaviventris	
XP_026256023.1	Urocitellus_parryii	
XP_013366053.1	Chinchilla_lanigera	
XP_004604319.1	Sorex_araneus	
XP_006902459.1	Elephantulus_edwardii	
XP_004582613.1	Ochotona_princeps	
XP_002713872.1	Oryctolagus_cuniculus	

XP_032728909.1	Lontra_canadensis	
XP_004743370.1	Mustela_putorius_furo	
XP_032160672.1	Mustela_erminea	
XP_029786190.1	Suricata_suricatta	
XP_017506043.1	Manis_javanica	
XP_004447610.1	Dasypus_novemcinctus	
XP_007944697.1	Orycteropus_afer_afer	
XP_007529121.1	Erinaceus_europaeus	
XP_004702903.1	Echinops_telfairi	
XP_006912064.1	Pteropus_alecto	
XP_019507556.1	Hipposideros_armiger	
XP_016072537.1	Miniopterus_natalensis	
XP_016015049.1	Rousettus_aegyptiacus	
XP_023387299.1	Pteropus_vampyrus	
XP_028011374.1	Eptesicus_fuscus	
XP_006779071.1	Myotis_davidii	
XP_005872327.1	Myotis_brandtii	
XP_028381748.1	Phyllostomus_discolor	
XP_024418892.1	Desmodus_rotundus	
NP_001075358.1	Equus_caballus	
XP_008515297.1	Equus_przewalskii	
XP_014694495.1	Equus_asinus	
XP_020934334.1	Sus_scrofa	
NP_001180041.1	Bos_taurus	btGsdme
XP_005902937.1	Bos_mutus	
XP_019824428.1	Bos_indicus	
XP_010853670.1	Bison_bison_bison	
XP_006055333.1	Bubalus_bubalis	
XP_031310922.1	Camelus_dromedarius	
XP_010966934.1	Camelus_bactrianus	
XP_020733682.1	Odocoileus_virginianus_texanus	
XP_017902561.1	Capra_hircus	
XP_014950834.1	Ovis_aries	
XP_023400115.1	Loxodonta_africana	laGsdme
XP_004418969.1	Ceratotherium_simum_simum	
XP_015092757.1	Vicugna_pacos	
XP_853956.2	Canis_lupus_familiaris	
XP_025848911.1	Vulpes_vulpes	
XP_025320189.1	Canis_lupus_dingo	

XP_006929316.1	Felis_catus	
XP_019299169.1	Panthera_pardus	
XP_026930937.1	Acinonyx_jubatus	
XP_007089104.1	Panthera_tigris_altaica	
XP_030163969.1	Lynx_canadensis	
XP_025785639.1	Puma_concolor	
XP_019654189.1	Ailuropoda_melanoleuca	
XP_008684626.1	Ursus_maritimus	
XP_026363612.1	Ursus_arctos_horribilis	
XP_007466126.1	Lipotes_vexillifer	
XP_004397435.1	Odobenus_rosmarus_divergens	
XP_019782285.1	Tursiops_truncatus	
XP_004265687.1	Orcinus_orca	
XP_032257813.1	Phoca_vitulina	
XP_030713228.1	Globicephala_melas	
XP_029089784.1	Monodon_monoceros	
XP_027975160.1	Eumetopias_jubatus	
XP_027429302.1	Zalophus_californianus	
XP_026958176.1	Lagenorhynchus_obliquidens	
XP_025729082.1	Callorhinus_ursinus	
XP_022440687.1	Delphinapterus_leucas	
XP_004377520.1	Trichechus_manatus_latirostris	
XP_027728246.1	Vombatus_ursinus	
XP_031796450.1	Sarcophilus_harrisii	shGsdme
XP_020849090.1	Phascolarctos_cinereus	
XP_007505411.1	Monodelphis_domestica	
XP_028926176.1	Ornithorhynchus_anatinus	oaGsdme
XP_021393912.1	Lonchura_striata_domestica	
XP_021243122.1	Numida_meleagris	
XP_017679311.1	Lepidothrix_coronata	
XP_015709261.1	Coturnix_japonica	
XP_015473236.1	Parus_major	
XP_014749818.1	Sturnus_vulgaris	
XP_013027320.1	Anser_cygnoides_domesticus	
XP_010575897.1	Haliaeetus_leucocephalus	
XP_019141156.1	Corvus_cornix_cornix	
XP_010220413.1	Tinamus_guttatus	
XP_010199052.1	Colius_striatus	
XP_010183520.1	Mesitornis_unicolor	

XP_010165530.1	Antrostomus_carolinensis	
XP_010144987.1	Eurypyga_helias	
XP_010131040.1	Buceros_rhinoceros_silvestris	
XP_010116360.1	Chlamydotis_macqueenii	
XP_010072951.1	Pterocles_gutturalis	
XP_010009916.1	Nestor_notabilis	
XP_010005878.1	Chaetura_pelagica	
XP_009960564.2	Tyto_alba_alba	
XP_009960492.1	Leptosomus_discolor	
XP_009939657.1	Opisthocomus_hoazin	
XP_009928905.1	Haliaeetus_albicilla	
XP_009906998.1	Picoides_pubescens	
XP_009877840.1	Charadrius_vociferus	
XP_009863572.1	Apaloderma_vittatum	
XP_009808686.1	Gavia_stellata	
XP_009674755.1	Struthio_camelus_australis	
XP_009636961.1	Egretta_garzetta	
XP_009582421.1	Fulmarus_glacialis	
XP_009561166.1	Cuculus_canorus	
XP_009506330.1	Phalacrocorax_carbo	
XP_009489562.1	Pelecanus_crispus	
XP_009464781.1	Nipponia_nippon	
XP_009324004.1	Pygoscelis_adeliae	
XP_009280316.1	Aptenodytes_forsteri	
XP_030090516.1	Serinus_canaria	
XP_009076145.1	Acanthisitta_chloris	
XP_008933812.1	Merops_nubicus	
XP_017930682.2	Manacus_vitellinus	
XP_017586669.1	Corvus_brachyrhynchos	cbGsdme
XP_030301104.1	Calypte_anna	
XP_014104276.1	Pseudopodoces_humilis	
XP_005480924.2	Zonotrichia_albicollis	
XP_027670555.1	Falco_cherrug	
XP_014162807.1	Geospiza_fortis	
XP_027642249.1	Falco_peregrinus	
XP_005041048.1	Ficedula_albicollis	
XP_012955994.2	Anas_platyrhynchos	
XP_010711078.1	Meleagris_gallopavo	
XP_030120727.2	Taeniopygia_guttata	

NP_001006361.1	Gallus_gallus	ggGsdme
XP_032566913.1	Chiroxiphia_lanceolata	
XP_032037140.1	Aythya_fuligula	
XP_031965418.1	Corvus_moneduloides	
XP_031445980.1	Phasianus_colchicus	
XP_030799876.1	Camarhynchus_parvulus	
XP_030345602.1	Strigops_habroptila	
XP_029866133.1	Aquila_chrysaetos_chrysaetos	
XP_027751877.1	Empidonax_traillii	
XP_027594245.1	Pipra_filicauda	
XP_027531052.1	Neopelma_chrysocephalum	
XP_027495202.1	Corapipo_altera	
XP_026697503.1	Athene_cunicularia	
XP_025959584.1	Dromaius_novaehollandiae	
XP_025889163.1	Nothoprocta_perdicaria	
XP_023776256.1	Cyanistes_caeruleus	
XP_030909399.1	Melopsittacus_undulatus	
XP_020636651.1	Pogona_vitticeps	
XP_015285233.1	Gekko_japonicus	
XP_008110872.1	Anolis_carolinensis	acGsdme
XP_028605735.1	Podarcis_muralis	
XP_019390343.1	Crocodylus_porosus	
XP_019364145.1	Gavialis_gangeticus	
XP_019353382.1	Alligator_mississippiensis	
XP_025063881.1	Alligator_sinensis	
XP_015666066.1	Protobothrops_mucrosquamatus	
XP_013909822.1	Thamnophis_sirtalis	
XP_007433152.1	Python_bivittatus	pbGsdme
XP_032093603.1	Thamnophis_elegans	
XP_026562200.1	Pseudonaja_textilis	
XP_026529423.1	Notechis_scutatus	
XP_027689547.1	Chelonia_mydas	
XP_014436716.1	Pelodiscus_sinensis	
XP_023962559.1	Chrysemys_picta_bellii	
XP_032629745.1	Chelonoidis_abingdonii	
XP_030406666.1	Gopherus_evgoodei	
XP_029766858.1	Terrapene_carolina_triunguis	
XP_018431097.1	Nanorana_parkeri	
XP_012821030.1	Xenopus_tropicalis	xtGsdme

XP_030057926.1	Microcaecilia_unicolor	muGsdme
XP_029444983.1	Rhinatrema_bivittatum	
XP_014351702.1	Latimeria_chalumnae	
XP_022071512.1	Acanthochromis_polyacanthus	
XP_018544241.1	Lates_calcarifer	
XP_007233439.2	Astyanax_mexicanus	
XP_020565794.1	Oryzias_latipes	
XP_020793187.1	Boleophthalmus_pectinirostris	
XP_020492757.1	Labrus_bergylta	
XP_019948910.1	Paralichthys_olivaceus	
XP_019741943.1	Hippocampus_comes	
XP_017327120.1	Ictalurus_punctatus	
XP_017282053.1	Kryptolebias_marmoratus	
XP_016419594.1	Sinocyclocheilus_rhinocerous	
XP_016337634.1	Sinocyclocheilus_anshuiensis	
XP_016142929.1	Sinocyclocheilus_grahami	
XP_015259533.1	Cyprinodon_variegatus	
XP_014892308.1	Poecilia_latipinna	
XP_014859812.1	Poecilia_mexicana	
XP_012718094.1	Fundulus_heteroclitus	
XP_010773239.1	Notothenia_coriiceps	
XP_010740226.3	Larimichthys_crocea	
XP_017165221.1	Poecilia_reticulata	
XP_008289283.1	Stegastes_partitus	
XP_016536172.1	Poecilia_formosa	
XP_005934833.1	Haplochromis_burtoni	
XP_023186332.1	Xiphophorus_maculatus	
XP_005738539.1	Pundamilia_nyererei	
XP_004541527.2	Maylandia_zebra	
XP_003454487.2	Oreochromis_niloticus	
XP_031441875.1	Clupea_harengus	
XP_005170134.1	Danio_rerio	
NP_001001947.1	Danio_rerio	
XP_024123324.1	Oryzias_melastigma	
XP_022621341.1	Seriola_dumerili	
XP_032413990.1	Xiphophorus_hellerii	
XP_032375584.1	Etheostoma_spectabile	
XP_031709071.1	Anarrhichthys_ocellatus	
XP_031602092.1	Oreochromis_aureus	

XP_031432605.1	Clupea_harengus	
XP_031154890.1	Sander_lucioperca	
XP_030606161.1	Archocentrus_centrarchus	
XP_030248788.1	Sparus_aurata	
XP_030012894.1	Sphaeramia_orbicularis	
XP_029958404.1	Salarias_fasciatus	
XP_029927409.1	Myripristis_murdjan	
XP_029588348.1	Salmo_trutta	
XP_029360163.1	Echeneis_naucrates	
XP_029307874.1	Cottoperca_gobio	
XP_028983881.1	Betta_splendens	
XP_028835239.1	Denticeps_clupeoides	
XP_028674104.1	Erpetoichthys_calabaricus	
XP_028435836.1	Perca_flavescens	
XP_028326593.1	Gouania_willdenowi	
XP_028280814.1	Parambassis_ranga	
XP_027868606.1	Xiphophorus_couchianus	
XP_026855871.1	Electrophorus_electricus	
XP_026226820.1	Anabas_testudineus	
XP_026149143.1	Mastacembelus_armatus	
XP_026041600.1	Astatotilapia_calliptera	
XP_023658342.1	Paramormyrops_kingsleyae	
XP_023258886.1	Seriola_lalandi_dorsalis	
XP_023155220.1	Amphiprion_ocellaris	
XP_016893587.1	Cynoglossus_semilaevis	csGsdme
XP_011604087.2	Takifugu_rubripes	
XP_020468482.1	Monopterus_albus	
NP_001279331.1	Callorhinchus_milii	cmGsdme
XP_020389028.1	Rhincodon_typus	
XP_032903802.1	Amblyraja_radiata	
XP_022788280.1	Stylophora_pistillata	spGsdme
XP_020910515.1	Exaiptasia_pallida	epGsdme

Pejvakin

NCBI Accession ID	Organism	Abbreviation
NP_001036167.1	Homo_sapiens	hPjvk
XP_009442091.1	Pan_troglodytes	
XP_014965926.1	Macaca_mulatta	
XP_005573657.1	Macaca_fascicularis	

XP_002749314.1	Callithrix_jacchus	
XP_032611165.1	Hylobates_moloch	
XP_032148968.1	Sapajus_apella	
XP_025260082.1	Theropithecus_gelada	
XP_023068107.1	Piliocolobus_tephrosceles	
XP_017723775.1	Rhinopithecus_bieti	
XP_017388169.1	Cebus_capucinus_imitator	
XP_012641314.1	Microcebus_murinus	
XP_012506180.1	Propithecus_coquereli	
XP_012326893.1	Aotus_nancymaae	
XP_011902507.1	Cercocebus_atys	
XP_011847215.1	Mandrillus_leucophaeus	
XP_011799435.1	Colobus_angolensis_palliatus	
XP_011717756.1	Macaca_nemestrina	
XP_030772352.1	Rhinopithecus_roxellana	
XP_008565265.1	Galeopterus_variegatus	
XP_008053529.1	Carlito_syrichta	
XP_007963659.1	Chlorocebus_sabaeus	
XP_004032916.1	Gorilla_gorilla_gorilla	
XP_003921870.1	Saimiri_boliviensis_boliviensis	
XP_009180787.1	Papio_anubis	
XP_008966740.1	Pan_paniscus	
XP_030658207.1	Nomascus_leucogenys	
XP_009236151.1	Pongo_abelii	
NP_001074180.1	Mus_musculus	mPjvk
XP_006224560.1	Rattus_norvegicus	
XP_021050472.1	Mus_pahari	
XP_005065182.1	Mesocricetus_auratus	
XP_004868199.1	Heterocephalus_glaber	
XP_008853561.1	Nannospalax_galili	
XP_032757859.1	Rattus_rattus	
XP_031226566.1	Mastomys_coucha	
XP_028618841.1	Grammomys_surdaster	
XP_027801937.1	Marmota_flaviventris	
XP_026247819.1	Urocitellus_parryii	
XP_021505179.1	Meriones_unguiculatus	
XP_021012402.1	Mus_caroli	
XP_020033549.1	Castor_canadensis	
XP_015336589.1	Marmota_marmota_marmota	

XP_012883962.1	Dipodomys_ordii	
XP_010635075.1	Fukomys_damarensis	
XP_015843885.1	Peromyscus_maniculatus_bairdii	
XP_006866750.1	Chrysochloris_asiatica	
XP_005373436.1	Chinchilla_lanigera	
XP_005346676.1	Microtus_ochrogaster	
XP_005324712.1	Ictidomys_tridecemlineatus	
XP_004674538.1	Condylura_cristata	
XP_004660349.1	Jaculus_jaculus	
XP_004634773.1	Octodon_degus	
XP_003501070.1	Cricetulus_griseus	
XP_003478567.1	Cavia_porcellus	
XP_032712096.1	Lontra_canadensis	
XP_006151718.1	Tupaia_chinensis	
XP_004601427.1	Sorex_araneus	
XP_006878851.1	Elephantulus_edwardii	
XP_032211508.1	Mustela_erminea	
XP_004769035.1	Mustela_putorius_furo	
XP_029790180.1	Suricata_suricatta	
XP_007935422.1	Orycteropus_afer_afer	
XP_007534290.1	Erinaceus_europaeus	
XP_004701516.1	Echinops_telfairi	
XP_017517118.1	Manis_javanica	
XP_004476912.1	Dasypus_novemcinctus	
XP_002712360.1	Oryctolagus_cuniculus	
XP_004577070.1	Ochotona_princeps	
XP_005857693.1	Myotis_brandtii	
XP_028365357.1	Phyllostomus_discolor	
XP_024417351.1	Desmodus_rotundus	
XP_019509576.1	Hipposideros_armiger	
XP_016065696.1	Miniopterus_natalensis	
XP_016008059.1	Rousettus_aegyptiacus	
XP_032968392.1	Rhinolophus_ferrumequinum	
XP_011355082.1	Pteropus_vampyrus	
XP_008136734.1	Eptesicus_fuscus	
XP_006921303.1	Pteropus_alecto	
XP_006760637.1	Myotis_davidii	
XP_006083120.1	Myotis_lucifugus	
XP_535979.2	Canis_lupus_familiaris	

XP_025849734.1	Vulpes_vulpes	
XP_025316114.1	Canis_lupus_dingo	
XP_023115271.1	Felis_catus	
XP_030181704.1	Lynx_canadensis	
XP_025767998.1	Puma_concolor	
XP_019316325.1	Panthera_pardus	
XP_014942207.1	Acinonyx_jubatus	
XP_007083963.1	Panthera_tigris_altaica	
NP_001180112.1	Bos_taurus	btPjvk
XP_005907581.1	Bos_mutus	
XP_019825658.1	Bos_indicus	
XP_010858060.1	Bison_bison_bison	
XP_006059644.1	Bubalus_bubalis	
XP_001500909.3	Equus_caballus	
XP_014689590.1	Equus_asinus	
XP_008513713.1	Equus_przewalskii	
XP_002918869.3	Ailuropoda_melanoleuca	
XP_026348228.1	Ursus_arctos_horribilis	
XP_008685415.1	Ursus_maritimus	
XP_003406242.2	Loxodonta_africana	laPjvk
XP_004426736.1	Ceratotherium_simum_simum	
XP_020738717.1	Odocoileus_virginianus_texanus	
XP_017894275.1	Capra_hircus	
XP_004004594.1	Ovis_aries	
XP_006210278.1	Vicugna_pacos	
XP_010989669.1	Camelus_dromedarius	
XP_010958274.1	Camelus_bactrianus	
XP_006194628.1	Camelus_ferus	
XP_032494333.1	Phocoena_sinus	
XP_032275467.1	Phoca_vitulina	
XP_030706721.1	Globicephala_melas	
XP_029081400.1	Monodon_monoceros	
XP_027447016.1	Zalophus_californianus	
XP_026982887.1	Lagenorhynchus_obliquidens	
XP_025743405.1	Callorhinus_ursinus	
XP_024588595.1	Neophocaena_asiaeorientalis_asiaeorientalis	
XP_022425842.1	Delphinapterus_leucas	
XP_021558921.1	Neomonachus_schauinslandi	
XP_007450786.1	Lipotes_vexillifer	

XP_007190463.1	Balaenoptera_acutorostrata_scammoni	
XP_007130807.2	Physeter_catodon	
XP_006733299.1	Leptonychotes_weddellii	
XP_004403794.1	Odobenus_rosmarus_divergens	
XP_004311474.1	Tursiops_truncatus	
XP_004267423.1	Orcinus_orca	
XP_004375524.1	Trichechus_manatus_latirostris	
XP_027722001.1	Vombatus_ursinus	
XP_003764058.1	Sarcophilus_harrisii	shPjvk
XP_020846715.1	Phascolarctos_cinereus	
XP_001368857.1	Monodelphis_domestica	
XP_028928169.1	Ornithorhynchus_anatinus	oaPjvk
XP_426573.2	Gallus_gallus	ggPjvk
XP_032920040.1	Catharus_ustulatus	
XP_021145491.1	Columba_livia	
XP_032549672.1	Chiroxiphia_lanceolata	
XP_032046572.1	Aythya_fuligula	
XP_031970077.1	Corvus_moneduloides	
XP_031456993.1	Phasianus_colchicus	
XP_030808482.1	Camarhynchus_parvulus	
XP_030341457.1	Strigops_habroptila	
XP_029874976.1	Aquila_chrysaetos_chrysaetos	
XP_027752516.1	Empidonax_traillii	
XP_027587289.1	Pipra_filicauda	
XP_027534255.1	Neopelma_chrysocephalum	
XP_027493193.1	Corapipo_altera	
XP_026708820.1	Athene_cunicularia	
XP_025948212.1	Dromaius_novaehollandiae	
XP_025931524.1	Apteryx_rowi	
XP_025907871.1	Nothoprocta_perdicaria	
XP_023786694.1	Cyanistes_caeruleus	
XP_021408102.1	Lonchura_striata_domestica	
XP_021255407.1	Numida_meleagris	
XP_017691037.1	Lepidothrix_coronata	
XP_015723838.1	Coturnix_japonica	
XP_015491030.1	Parus_major	
XP_014809935.1	Calidris_pugnax	
XP_014745550.1	Sturnus_vulgaris	
XP_013816192.1	Apteryx_mantelli_mantelli	

XP_013027050.1	Anser_cygnoides_domesticus	
XP_010564222.1	Haliaeetus_leucocephalus	
XP_010405022.1	Corvus_cornix_cornix	
XP_010309352.1	Balearica_regulorum_gibbericeps	
XP_010285122.1	Phaethon_lepturus	
XP_010217678.1	Tinamus_guttatus	
XP_010198933.1	Colius_striatus	
XP_010178165.1	Mesitornis_unicolor	
XP_010173029.1	Antrostomus_carolinensis	
XP_010133399.1	Buceros_rhinoceros_silvestris	
XP_010123753.1	Chlamydotis_macqueenii	
XP_010079514.1	Pterocles_gutturalis	
XP_010021626.1	Nestor_notabilis	
XP_009994488.1	Chaetura_pelagica	
XP_009985399.1	Tauraco_erythrolophus	
XP_009964462.2	Tyto_alba_alba	
XP_009957273.1	Leptosomus_discolor	
XP_009932320.1	Opisthocomus_hoazin	
XP_009912995.1	Haliaeetus_albicilla	
XP_009897380.1	Picoides_pubescens	
XP_009883913.1	Charadrius_vociferus	
XP_009868885.1	Apaloderma_vittatum	
XP_009813285.1	Gavia_stellata	
XP_009694144.1	Cariama_cristata	
XP_009674596.1	Struthio_camelus_australis	
XP_009644325.1	Egretta_garzetta	
XP_009580620.1	Fulmarus_glacialis	
XP_009553924.1	Cuculus_canorus	
XP_009498492.1	Phalacrocorax_carbo	
XP_009491858.1	Pelecanus_crispus	
XP_009460604.1	Nipponia_nippon	
XP_009330652.1	Pygoscelis_adeliae	
XP_009276888.1	Aptenodytes_forsteri	
XP_009086279.1	Serinus_canaria	
XP_009082354.1	Acanthisitta_chloris	
XP_008945516.1	Merops_nubicus	
XP_017927185.1	Manacus_vitellinus	
XP_008632943.1	Corvus_brachyrhynchos	cbPjvk
XP_008503297.1	Calypte_anna	

XP_005519906.1	Pseudopodoces_humilis	
XP_005484170.1	Zonotrichia_albicollis	
XP_005442982.1	Falco_cherrug	
XP_005415947.1	Geospiza_fortis	
XP_005237060.1	Falco_peregrinus	
XP_005049151.1	Ficedula_albicollis	
XP_027317868.1	Anas_platyrhynchos	
XP_019472642.1	Meleagris_gallopavo	
XP_002199531.1	Taeniopygia_guttata	
XP_005152626.1	Melopsittacus_undulatus	
XP_032624383.1	Chelonoidis_abingdonii	
XP_030435617.1	Gopherus_evgoodei	
XP_024054274.1	Terrapene_carolina_triunguis	
XP_007069837.1	Chelonia_mydas	
XP_025038578.1	Pelodiscus_sinensis	
XP_028604312.1	Podarcis_muralis	
XP_020659760.1	Pogona_vitticeps	
XP_015269242.1	Gekko_japonicus	
XP_003225734.2	Anolis_carolinensis	acPjvk
XP_019410239.1	Crocodylus_porosus	
XP_019378569.1	Gavialis_gangeticus	
XP_014454831.1	Alligator_mississippiensis	
XP_006034600.1	Alligator_sinensis	
XP_032087879.1	Thamnophis_elegans	
XP_026552782.1	Pseudonaja_textilis	
XP_026523899.1	Notechis_scutatus	
XP_015674337.2	Protobothrops_mucrosquamatus	
XP_013916399.1	Thamnophis_sirtalis	
XP_007433246.1	Python_bivittatus	pbPjvk
XP_017953002.1	Xenopus_tropicalis	XtPjvk
XP_018417121.1	Nanorana_parkeri	
XP_030065796.1	Microcaecilia_unicolor	muPjvk
XP_029461755.1	Rhinatrema_bivittatum	
XP_014354128.1	Latimeria_chalumnae	
XP_021332701.1	Danio_rerio	drPjvk
XP_017336878.1	Ictalurus_punctatus	
XP_024144772.1	Oryzias_melastigma	
XP_030208891.1	Gadus_morhua	
XP_032412353.1	Xiphophorus_hellerii	

XP_032362115.1	Etheostoma_spectabile	
XP_031707545.1	Anarrhichthys_ocellatus	
XP_031605025.1	Oreochromis_aureus	
XP_031147629.1	Sander_lucioperca	
XP_030639171.1	Chanos_chanos	
XP_030610804.1	Archocentrus_centrarchus	
XP_030266265.1	Sparus_aurata	
XP_030014755.1	Sphaeramia_orbicularis	
XP_029941737.1	Salarias_fasciatus	
XP_029930250.1	Myripristis_murdjan	
XP_029377974.1	Echeneis_naucrates	
XP_029300217.1	Cottoperca_gobio	
XP_028984917.1	Betta_splendens	
XP_028809593.1	Denticeps_clupeoides	
XP_028663992.1	Erpetoichthys_calabaricus	
XP_028427897.1	Perca_flavescens	
XP_028322965.1	Gouania_willdenowi	
XP_028255869.1	Parambassis_ranga	
XP_027977177.1	Eumetopias_jubatus	
XP_027866688.1	Xiphophorus_couchianus	
XP_027015817.1	Tachysurus_fulvidraco	
XP_026874502.1	Electrophorus_electricus	
XP_026789215.1	Pangasianodon_hypophthalmus	
XP_026217304.1	Anabas_testudineus	
XP_024265015.1	Oncorhynchus_tshawytscha	
XP_023657402.1	Paramormyrops_kingsleyae	
XP_023282857.1	Seriola_lalandi_dorsalis	
XP_023125432.1	Amphiprion_ocellaris	
XP_022616901.1	Seriola_dumerili	
XP_022068643.1	Acanthochromis_polyacanthus	
XP_021428733.1	Oncorhynchus_mykiss	
XP_029133251.1	Labrus_bergylta	
XP_019746234.1	Hippocampus_comes	
XP_029112536.1	Scleropages_formosus	
XP_018516757.1	Lates_calcarifer	
XP_017295653.1	Kryptolebias_marmoratus	
XP_016304616.1	Sinocyclocheilus_anshuiensis	
XP_015813551.1	Nothobranchius_furzeri	
XP_015232892.1	Cyprinodon_variegatus	

XP_014847085.1	Poecilia_mexicana	
XP_014007857.1	Salmo_salar	
XP_013867462.1	Austrofundulus_limnaeus	
XP_012724997.1	Fundulus_heteroclitus	
XP_031414807.1	Clupea_harengus	
XP_028972406.1	Esox_lucius	
XP_019132545.1	Larimichthys_crocea	
XP_008422369.1	Poecilia_reticulata	
XP_008322774.1	Cynoglossus_semilaevis	csPjvk
XP_008291779.1	Stegastes_partitus	
XP_007553767.1	Poecilia_formosa	
XP_022530820.1	Astyanax_mexicanus	
XP_006636618.1	Lepisosteus_oculatus	
XP_005920274.1	Haplochromis_burtoni	
XP_014325563.1	Xiphophorus_maculatus	
XP_005742320.1	Pundamilia_nyererei	
XP_023009232.1	Maylandia_zebra	
XP_023819485.1	Oryzias_latipes	
XP_003966800.1	Takifugu_rubripes	
XP_003459969.1	Oreochromis_niloticus	
XP_026157845.1	Mastacembelus_armatus	
XP_020470942.1	Monopterus_albus	
XP_007888272.1	Callorhinchus_milii	cmPjvk
XP_032879750.1	Amblyraja_radiata	
XP_032813042.1	Petromyzon_marinus	

REFERENCES

1. Jorgensen, I., Rayamajhi, M. & Miao, E. A. Programmed cell death as a defence against infection. *Nature Publishing Group* **17,** 151–164 (2017).

2. Jorgensen, I. & Miao, E. A. Pyroptotic cell death defends against intracellular pathogens. *Immunol Rev* **265,** 130–142 (2015).

3. Jorgensen, I., Zhang, Y., Krantz, B. A. & Miao, E. A. Pyroptosis triggers pore-induced intracellular traps (PITs) that capture bacteria and lead to their clearance by efferocytosis. *J Exp Med* **213,** 2113–2128 (2016).

4. Jorgensen, I., Lopez, J. P., Laufer, S. A. & Miao, E. A. IL-1β, IL-18, and eicosanoids promote neutrophil recruitment to pore-induced intracellular traps following pyroptosis. *Eur. J. Immunol.* **46,** 2761–2766 (2016).

5. Moltke, von, J. *et al.* Rapid induction of inflammatory lipid mediators by the inflammasome in vivo. *Nature* **490,** 107–111 (2012).

6. Sauer, J.-D. *et al.* Listeria monocytogenes engineered to activate the Nlrc4 inflammasome are severely attenuated and are poor inducers of protective immunity. *Proc Natl Acad Sci USA* **108,** 12419 (2011).

7. Maltez, V. I. *et al.* Inflammasomes Coordinate Pyroptosis and Natural Killer Cell Cytotoxicity to Clear Infection by a Ubiquitous Environmental Bacterium. *Immunity* **43,** 987–997 (2015).

8. Aachoui, Y. *et al.* Canonical Inflammasomes Drive IFN-γ to Prime Caspase-11 in Defense against a Cytosol-Invasive Bacterium. *Cell Host and Microbe* **18,** 320–332 (2015).

9. Maltez, V. I. & Miao, E. A. Reassessing the Evolutionary Importance of Inflammasomes. *J. Immunol.* **196,** 956–962 (2016).

10. Shi, J. *et al.* Cleavage of GSDMD by inflammatory caspases determines pyroptotic cell death. *Nature* **526,** 660–665 (2015).

11. Kayagaki, N. *et al.* Caspase-11 cleaves gasdermin D for non-canonical inflammasome signalling. *Nature* **526,** 666–671 (2015).

12. He, W.-T. *et al.* Gasdermin D is an executor of pyroptosis and required for interleukin-1β secretion. *Cell Res* **25,** 1285–1298 (2015).

13. Saeki, N. *et al.* Distinctive expression and function of four GSDM family genes (GSDMA-D) in normal and malignant upper gastrointestinal epithelium. *Genes Chromosom. Cancer* **48,** 261–271 (2009).

14. Tamura, M. *et al.* Members of a novel gene family, Gsdm, are expressed exclusively in the epithelium of the skin and gastrointestinal tract in a highly tissue-specific manner. *Genomics* **89,** 618–629 (2007).

15. Ding, J. *et al.* Pore-forming activity and structural autoinhibition of the gasdermin family. *Nature* (2016). doi:10.1038/nature18590

16. Liu, X. *et al.* Inflammasome-activated gasdermin D causes pyroptosis by forming membrane pores. *Nature* **535,** 153–158 (2016).

17. Aglietti, R. A. *et al.* GsdmD p30 elicited by caspase-11 during pyroptosis forms pores in membranes. *Proceedings of the National Academy of Sciences* 201607769 (2016). doi:10.1073/pnas.1607769113

18. Sborgi, L. *et al.* GSDMD membrane pore formation constitutes the mechanism of pyroptotic cell death. *EMBO J.* **35,** 1766–1778 (2016).

19. Liu, Z. *et al.* Structures of the Gasdermin D C-Terminal Domains Reveal Mechanisms of Autoinhibition. *Structure/Folding and Design* 1–11 (2018). doi:10.1016/j.str.2018.03.002

20. Liu, Z. *et al.* Caspase-1 Engages Full-Length Gasdermin D through Two Distinct Interfaces That Mediate Caspase Recruitment and Substrate Cleavage. *Immunity* **53,** 106–114.e5 (2020).

21. Rogers, C. *et al.* Cleavage of DFNA5 by caspase-3 during apoptosis mediates progression to secondary necrotic/pyroptotic cell death. 1–14 (2017). doi:10.1038/ncomms14128

22. Hoffmann, E. K., Lambert, I. H. & Pedersen, S. F. Physiology of Cell Volume Regulation in Vertebrates. *Physiological Reviews* **89,** 193–277 (2009).

23. McNeil, P. L. & Kirchhausen, T. An emergency response team for membrane repair. *Nat Rev Mol Cell Biol* **6,** 499–505 (2005).

24. Jimenez, A. J. *et al.* ESCRT machinery is required for plasma membrane repair. *Science* **343,** 1247136 (2014).

25. Rühl, S. *et al.* ESCRT-dependent membrane repair negatively regulates pyroptosis downstream of GSDMD activation. *Science* **362,** 956–960 (2018).

26. Gong, Y.-N. *et al.* ESCRT-III Acts Downstream of MLKL to Regulate Necroptotic Cell Death and Its Consequences. *Cell* **169,** 286–300.e16 (2017).

27. Guo, Y. *et al.* Mitochondrial DNA drives noncanonical inflammation activation via cGAS–STING signaling pathway in retinal microvascular endothelial cells. 1–12 (2020). doi:10.1186/s12964-020-00637-3

28. Rauch, I. *et al.* NAIP-NLRC4 Inflammasomes Coordinate Intestinal Epithelial Cell Expulsion with Eicosanoid and IL-18 Release via Activation of Caspase-1 and -8. *Immunity* **46,** 649–659 (2017).

29. Martín-Sánchez, F. *et al.* Inflammasome-dependent IL-1β release depends upon membrane permeabilisation. *Cell Death Differ* **23,** 1219–1231 (2016).

30. Brough, D. & Rothwell, N. J. Caspase-1-dependent processing of pro-interleukin-1beta is cytosolic and precedes cell death. *Journal of Cell Science* **120,** 772–781 (2007).

31. Russo, H. M. *et al.* Active Caspase-1 Induces Plasma Membrane Pores That Precede Pyroptotic Lysis and Are Blocked by Lanthanides. *J. Immunol.* **197,** 1353–1367 (2016).

32. Chen, K. W. *et al.* The Neutrophil NLRC4 Inflammasome Selectively Promotes IL-1β Maturation without Pyroptosis during Acute Salmonella Challenge. *Cell Reports* **8,** 570–582 (2014).

33. Gaidt, M. M. *et al.* Human Monocytes Engage an Alternative Inflammasome Pathway. *Immunity* **44,** 833–846 (2016).

34. Shi, C.-S. *et al.* Activation of autophagy by inflammatory signals limits IL-1β production by targeting ubiquitinated inflammasomes for destruction. *Nat Immunol* **13,** 255–263 (2012).

35. Wang, J.-G. *et al.* Monocytic microparticles activate endothelial cells in an IL-1β-dependent manner. *Blood* **118,** 2366–2374 (2011).

36. MacKenzie, A. *et al.* Rapid secretion of interleukin-1beta by microvesicle shedding. *Immunity* **15,** 825–835 (2001).

37. Miao, E. A. *et al.* Caspase-1-induced pyroptosis is an innate immune effector mechanism against intracellular bacteria. *Nat Immunol* **11,** 1136–1142 (2010).

38. Yu, J. *et al.* Inflammasome activation leads to Caspase-1-dependent mitochondrial damage and block of mitophagy. *Proceedings of the National Academy of Sciences* **111,** 15514–15519 (2014).

39. Bergsbaken, T., Fink, S. L., Hartigh, den, A. B., Loomis, W. P. & Cookson, B. T. Coordinated host responses during pyroptosis: caspase-1-dependent lysosome exocytosis and inflammatory cytokine maturation. *The Journal of Immunology* **187,** 2748–2754 (2011).

40. Saeki, N. & Sasaki, H. Gasdermin Superfamily: A Novel Gene Family Functioning in Epithelial Cells in *Endothelium and Epithelium*, 193-211 (2012).

41. Wang, Y. *et al.* Chemotherapy drugs induce pyroptosis through caspase-3 cleavage of a gasdermin. *Nature* **547,** 99–103 (2017).

42. Wu, C. *et al.* BioGPS: an extensible and customizable portal for querying and organizing gene annotation resources. *Genome Biol* **10,** (2009).

43. Tanaka, S., Mizushina, Y., Kato, Y., Tamura, M. & Shiroishi, T. Functional conservation of Gsdma cluster genes specifically duplicated in the mouse genome. *G3 (Bethesda)* **3,** 1843–1850 (2013).

44. Runkel, F. *et al.* The dominant alopecia phenotypes Bareskin, Rex-denuded, and Reduced Coat 2 are caused by mutations in gasdermin 3. *Genomics* **84,** 824–835 (2004).

45. Saeki, N., Kuwahara, Y., Sasaki, H., Satoh, H. & Shiroishi, T. Gasdermin (Gsdm) localizing to mouse Chromosome 11 is predominantly expressed in upper gastrointestinal tract but significantly suppressed in human gastric cancer cells. *Mamm Genome* **11,** 718–724 (2000).

46. Lunny, D. P. *et al.* Mutations in Gasdermin 3 Cause Aberrant Differentiation of the Hair Follicle and Sebaceous Gland. *J Invest Dermatol* **124,** 615 (2005).

47. Tanaka, S. *et al.* A new Gsdma3 mutation affecting anagen phase of first hair cycle. *Biochemical and Biophysical Research Communications* **359,** 902–907 (2007).

48. Li, J. *et al.* Gsdma3 is required for hair follicle differentiation in mice. *Biochemical and Biophysical Research Communications* **403,** 18–23 (2010).

49. Zhou, Y. *et al.* Gsdma3 mutation causes bulge stem cell depletion and alopecia mediated by skin inflammation. *American Journal Of Pathology* **180,** 763–774 (2012).

50. Kumar, S. *et al.* Gsdma3(I359N) is a novel ENU-induced mutant mouse line for studying the function of Gasdermin A3 in the hair follicle and epidermis. *J. Dermatol. Sci.* **67,** 190–192 (2012).

51. Shi, P. *et al.* Loss of conserved Gsdma3 self-regulation causes autophagy and cell death. *Biochem J* **468,** 325–336 (2015).

52. Guo, H. Gsdma3 is required for mammary gland development in mice. *Histochem Cell Biol* **0,** 0–0 (2017).

53. Yu, J. *et al.* Polymorphisms in GSDMA and GSDMB are associated with asthma susceptibility, atopy and BHR. *Pediatr. Pulmonol.* **46,** 701–708 (2011).

54. Hao, K. *et al.* Lung eQTLs to Help Reveal the Molecular Underpinnings of Asthma. *PLoS Genet* **8,** e1003029–11 (2012).

55. Wu, H. *et al.* Genetic variation in ORM1-like 3 (ORMDL3) and gasdermin-like (GSDML) and childhood asthma. *Allergy* **64,** 629–635 (2009).

56. Moffatt, M. F. *et al.* Genetic variants regulating ORMDL3 expression contribute to the risk of childhood asthma. *Nature* **448,** 470–473 (2007).

57. Moffatt, M. F. *et al.* A large-scale, consortium-based genomewide association study of asthma. *N Engl J Med* **363,** 1211–1221 (2010).

58. Das, S. *et al.* GSDMB induces an asthma phenotype characterized by increased airway responsiveness and remodeling without lung inflammation. *Proc. Natl. Acad. Sci. U.S.A.* **113,** 13132–13137 (2016).

59. Chao, K. L., Kulakova, L. & Herzberg, O. Gene polymorphism linked to increased asthma and IBD risk alters gasdermin-B structure, a sulfatide and phosphoinositide binding protein. *Proc. Natl. Acad. Sci. U.S.A.* **114,** E1128–E1137 (2017).

60. Zihlif, M. *et al.* Association Between Gasdermin A and Gasdermin B Polymorphisms and Susceptibility to Adult and Childhood Asthma Among Jordanians. *Genet Test Mol Biomarkers* gtmb.2015.0174 (2016). doi:10.1089/gtmb.2015.0174

61. Qiu, R. *et al.* Genetic variants on 17q21 are associated with ankylosing spondylitis susceptibility and severity in a Chinese Han population. *Scand. J. Rheumatol.* **42,** 469–472 (2013).

62. Kiani, A. K. *et al.* Genetic link of type 1 diabetes susceptibility loci with rheumatoid arthritis in Pakistani patients. *Immunogenetics* **67,** 277–282 (2015).

63. Li, X. *et al.* Genome-wide association studies of asthma indicate opposite immunopathogenesis direction from autoimmune diseases. *J. Allergy Clin. Immunol.* **130,** 861–8.e7 (2012).

64. Hirschfield, G. M. *et al.* Variants at IRF5-TNPO3, 17q12-21 and MMEL1 are associated with primary biliary cirrhosis. *Nat Genet* **42,** 655–657 (2010).

65. Kurreeman, F. A. S. *et al.* Use of a multiethnic approach to identify rheumatoid-arthritis-susceptibility loci, 1p36 and 17q12. *Am J Hum Genet* **90,** 524–532 (2012).

66. Witsø, E. *et al.* Genetic Determinants of Enterovirus Infections: Polymorphisms in Type 1 Diabetes and Innate Immune Genes in the MIDIA Study. *Viral Immunol.* **28,** 556–563 (2015).

67. Crosslin, D. R. *et al.* Genetic variants associated with the white blood cell count in 13,923 subjects in the eMERGE Network. *Hum Genet* **131,** 639–652 (2012).

68. Zhou, Z. *et al.* Granzyme A from cytotoxic lymphocytes cleaves GSDMB to trigger pyroptosis in target cells. *Science* **368,** (2020).

69. Watabe, K. *et al.* Structure, expression and chromosome mapping of MLZE, a novel gene which is preferentially expressed in metastatic melanoma cells. *Jpn. J. Cancer Res.* **92,** 140–151 (2001).

70. Bischoff, A. M. L. C. *et al.* A novel mutation identified in the DFNA5 gene in a Dutch family: a clinical and genetic evaluation. *Audiol. Neurootol.* **9,** 34–46 (2004).

71. Yu, C. *et al.* A 3-nucleotide deletion in the polypyrimidine tract of intron 7 of the DFNA5 gene causes nonsyndromic hearing impairment in a Chinese family. *Genomics* **82,** 575–579 (2003).

72. Van Laer, L. *et al.* Nonsyndromic hearing impairment is associated with a mutation in DFNA5. *Nat Genet* **20,** 194–197 (1998).

73. de Beeck, K. O., Van Laer, L. & Van Camp, G. DFNA5, a gene involved in hearing loss and cancer: a review. *Ann Otol Rhinol Laryngol* **121,** 197–207 (2012).

74. Van Laer, L. *et al.* Mice lacking Dfna5 show a diverging number of cochlear fourth row outer hair cells. *Neurobiology of Disease* **19,** 386–399 (2005).

75. Delmaghani, S. *et al.* Mutations in the gene encoding pejvakin, a newly identified protein of the afferent auditory pathway, cause DFNB59 auditory neuropathy. *Nat Genet* **38,** 770–778 (2006).

76. Schwander, M. *et al.* A forward genetics screen in mice identifies recessive deafness traits and reveals that pejvakin is essential for outer hair cell function. *Journal of Neuroscience* **27,** 2163–2175 (2007).

77. Delmaghani, S. *et al.* Hypervulnerability to Sound Exposure through Impaired Adaptive Proliferation of Peroxisomes. *Cell* **163,** 894–906 (2015).

78. Defourny, J. *et al.* Pejvakin-mediated pexophagy protects auditory hair cells against noise-induced damage. *Proc Natl Acad Sci USA* **116,** 8010 (2019).

79. Hettema, E. H., Erdmann, R., van der Klei, I. & Veenhuis, M. ScienceDirect Evolving models for peroxisome biogenesis. *Current Opinion in Cell Biology* **29,** 25–30 (2014).

80. Harris, S. L. *et al.* Conditional deletion of pejvakin in adult outer hair cells causes progressive hearing loss in mice. *Neuroscience* **344,** 380–393 (2017).

81. Kelley, N., Jeltema, D., Duan, Y. & He, Y. The NLRP3 Inflammasome: An Overview of Mechanisms of Activation and Regulation. *IJMS* **20,** (2019).

82. Kovacs, S. B. *et al.* Neutrophil Caspase-11 Is Essential to Defend against a Cytosol-Invasive Bacterium. *CellReports* **32,** 107967 (2020).

83. Liu, F. & Whitton, J. L. Cutting edge: re-evaluating the in vivo cytokine responses of CD8+ T cells during primary and secondary viral infections. *The Journal of Immunology* **174,** 5936–5940 (2005).

84. Weizman, O.-E. *et al.* ILC1 Confer Early Host Protection at Initial Sites of Viral Infection. *Cell* **171,** 795–808.e12 (2017).

85. Mazet, J. M., Chiodetti, A. L., Mahale, J. N. & Gérard, A. Imaging of In Situ Interferon Gamma Production in the Mouse Spleen following Listeria monocytogenes Infection. *JoVE* 1–12 (2019). doi:10.3791/59819

86. Dinarello, C. A. Overview of the IL-1 family in innate inflammation and acquired immunity. *Immunol Rev* **281,** 8–27 (2017).

87. Mukai, K., Tsai, M., Saito, H. & Galli, S. J. Mast cells as sources of cytokines, chemokines, and growth factors. *Immunol Rev* **282,** 121–150 (2018).

88. Bouabe, H. Cytokine Reporter Mice: The Special Case of IL-10. *Scandinavian Journal of Immunology* **75,** 553–567 (2012).

89. Corish, P. & Tyler-Smith, C. Attenuation of green fluorescent protein half-life in mammalian cells. *Protein Eng Des Sel* **12,** 1035–1040 (1999).

90. Mohrs, M., Shinkai, K., Mohrs, K. & Locksley, R. M. Analysis of type 2 immunity in vivo with a bicistronic IL-4 reporter. *Immunity* **15,** 303–311 (2001).

91. Sun, J., Madan, R., Karp, C. L. & Braciale, T. J. Effector T cells control lung inflammation during acute influenza virus infection by producing IL-10. *Nat Med* **15,** 277–284 (2009).

92. Artis, D. & Spits, H. The biology of innate lymphoid cells. *Nature* **517,** 293–301 (2015).

93. Seyda, M., Elkhal, A., Quante, M., Falk, C. S. & Tullius, S. G. T Cells Going Innate. *Trends in Immunology* **37,** 546–556 (2016).

94. Aachoui, Y., Sagulenko, V., Miao, E. A. & Stacey, K. J. Inflammasome-mediated pyroptotic and apoptotic cell death, and defense against infection. *Curr. Opin. Microbiol.* **16,** 319–326 (2013).

95. Franchi, L. *et al.* Cytosolic flagellin requires Ipaf for activation of caspase-1 and interleukin 1beta in salmonella-infected macrophages. *Nat Immunol* **7,** 576–582 (2006).

96. Miao, E. A. *et al.* Cytoplasmic flagellin activates caspase-1 and secretion of interleukin 1beta via Ipaf. *Nat Immunol* **7,** 569–575 (2006).

97. Ren, T., Zamboni, D. S., Roy, C. R., Dietrich, W. F. & Vance, R. E. Flagellin-Deficient Legionella Mutants Evade Caspase-1- and Naip5-Mediated Macrophage Immunity. *PLoS Pathog* **2,** e18–9 (2006).

98. Molofsky, A. B. *et al.* Cytosolic recognition of flagellin by mouse macrophages restricts Legionella pneumophila infection. *J Exp Med* **203,** 1093–1104 (2006).

99. Miao, E. A. *et al.* Innate immune detection of the type III secretion apparatus through the NLRC4 inflammasome. *Proceedings of the National Academy of Sciences* **107,** 3076–3080 (2010).

100. Ramirez, M. L. G. *et al.* Extensive peptide and natural protein substrate screens reveal that mouse caspase-11 has much narrower substrate specificity than caspase-1. *J Biol Chem* **293,** 7058–7067 (2018).

101. Wiersinga, W. J., van der Poll, T., White, N. J., Day, N. P. & Peacock, S. J. Melioidosis: insights into the pathogenicity of Burkholderia pseudomallei. *Nat. Rev. Microbiol.* **4,** 272–282 (2006).

102. Ceballos-Olvera, I., Sahoo, M., Miller, M. A., Barrio, L. D. & Re, F. Inflammasome-dependent Pyroptosis and IL-18 Protect against Burkholderia pseudomallei Lung Infection while IL-1β Is Deleterious. *PLoS Pathog* **7,** e1002452–13 (2011).

103. Aachoui, Y. *et al.* Caspase-11 protects against bacteria that escape the vacuole. *Science* **339,** 975–978 (2013).

104. Wang, J. *et al.* Caspase-11-dependent pyroptosis of lung epithelial cells protects from melioidosis while caspase-1 mediates macrophage pyroptosis and production of IL-18. *PLoS Pathog* **14,** e1007105–19 (2018).

105. Harly, C., Cam, M., Kaye, J. & Bhandoola, A. Development and differentiation of early innate lymphoid progenitors. *J Exp Med* **215,** 249–262 (2018).

106. Robinette, M. L. *et al.* IL-15 sustains IL-7R-independent ILC2 and ILC3 development. *Nat Commun* **8,** 14601–13 (2017).

107. Tsuchiya, K. *et al.* Caspase-1 initiates apoptosis in the absence of gasdermin D. *Nat Commun* **10,** 2091–19 (2019).

108. Wang, J., Deobald, K. & Re, F. Gasdermin D Protects from Melioidosis through Pyroptosis and Direct Killing of Bacteria. *J. Immunol.* **202,** 3468–3473 (2019).

109. Bossaller, L. *et al.* Cutting edge: FAS (CD95) mediates noncanonical IL-1β and IL-18 maturation via caspase-8 in an RIP3-independent manner. *J. Immunol.* **189,** 5508–5512 (2012).

110. Afonina, I. S., Müller, C., Martin, S. J. & Beyaert, R. Proteolytic Processing of Interleukin-1 Family Cytokines: Variations on a Common Theme. *Immunity* **42,** 991–1004 (2015).

111. Chen, K. W. *et al.* Noncanonical inflammasome signaling elicits gasdermin D-dependent neutrophil extracellular traps. *Sci. Immunol.* **3,** eaar6676 (2018).

112. Zhao, Y. *et al.* The NLRC4 inflammasome receptors for bacterial flagellin and type III secretion apparatus. *Nature* 1–7 (2011). doi:10.1038/nature10510

113. Hagar, J. A., Powell, D. A., Aachoui, Y., Ernst, R. K. & Miao, E. A. Cytoplasmic LPS activates caspase-11: implications in TLR4-independent endotoxic shock. *Science* **341,** 1250–1253 (2013).

114. Abram, C. L., Roberge, G. L., Hu, Y. & Lowell, C. A. Comparative analysis of the efficiency and specificity of myeloid-Cre deleting strains using ROSA-EYFP reporter mice. *Journal of Immunological Methods* **408,** 89–100 (2014).

115. Sollberger, G. *et al.* Gasdermin D plays a vital role in the generation of neutrophil extracellular traps. *Sci. Immunol.* **3,** eaar6689 (2018).

116. Kupz, A. *et al.* NLRC4 inflammasomes in dendritic cells regulate noncognate effector function by memory CD8+ T cells. *Nat Immunol* **13,** 162–169 (2012).

117. Kayagaki, N. *et al.* Noncanonical inflammasome activation by intracellular LPS independent of TLR4. *Science* **341,** 1246–1249 (2013).

118. Hagar, J. A. *et al.* Lipopolysaccharide Potentiates Insulin-Driven Hypoglycemic Shock. *The Journal of Immunology* 3634–3643 (2017). doi:10.4049/jimmunol.1700820

119. Karmakar, M. *et al.* N-GSDMD trafficking to neutrophil organelles facilitates IL-1β release independently of plasma membrane pores and pyroptosis. *Nat Commun* 1–14 (2020). doi:10.1038/s41467-020-16043-9

120. Fernandes-Alnemri, T. *et al.* The pyroptosome: a supramolecular assembly of ASC dimers mediating inflammatory cell death via caspase-1 activation. *Cell Death Differ* **14,** 1590–1604 (2007).

121. Sahillioglu, A. C., Sumbul, F., Ozören, N. & Haliloglu, T. Structural and Dynamics Aspects of ASC Speck Assembly. *Structure/Folding and Design* **22,** 1722–1734 (2014).

122. Kayagaki, N. *et al.* Non-canonical inflammasome activation targets caspase-11. *Nature* **479,** 117–121 (2011).

123. Kuida, K. *et al.* Altered cytokine export and apoptosis in mice deficient in interleukin-1 beta converting enzyme. *Science* **267,** 2000–2003 (1995).

124. Cheng, K. T. *et al.* Caspase-11–mediated endothelial pyroptosis underlies endotoxemia-induced lung injury. *J. Clin. Invest.* **127,** 4124–4135 (2017).

125. Rayamajhi, M., Zhang, Y. & Miao, E. A. Detection of pyroptosis by measuring released lactate dehydrogenase activity. *Methods Mol Biol* **1040,** 85–90 (2013).

126. Mitchell, P. S. *et al.* NAIP-NLRC4-deficient mice are susceptible to shigellosis. *Elife* **9,** (2020).

127. Lee, S., Hirohama, M., Noguchi, M., Nagata, K. & Kawaguchi, A. Influenza A Virus Infection Triggers Pyroptosis and Apoptosis of Respiratory Epithelial Cells through the Type I Interferon Signaling Pathway in a Mutually Exclusive Manner. *J. Virol.* **92,** e00396–18 (2018).

128. Zhuang, J. *et al.* Bronchial epithelial pyroptosis promotes airway inflammation in a murine model of toluene diisocyanate-induced asthma. *Biomed Pharmacother* **125,** 109925 (2020).

129. Pinteaux, E. *et al.* Cell-specific conditional deletion of interleukin-1 (IL-1) ligands and its receptors: a new toolbox to study the role of IL-1 in health and disease. *J Mol Med (Berl)* **98,** 923–930 (2020).

130. Functional Conservation of Gsdma Cluster Genes Specifically Duplicated in the Mouse Genome. 1–8 (2013). doi:10.1534/g3.113.007393/-/DC1

131. Lin, P.-H., Lin, H.-Y., Kuo, C.-C. & Yang, L.-T. N-terminal functional domain of Gasdermin A3 regulates mitochondrial homeostasis via mitochondrial targeting. *J. Biomed. Sci.* **22,** 44 (2015).

132. Brittle, E. E., Wang, F., Lubinski, J. M., Bunte, R. M. & Friedman, H. M. A replication-competent, neuronal spread-defective, live attenuated herpes simplex virus type 1 vaccine. *J. Virol.* **82,** 8431–8441 (2008).

133. McGraw, H. M., Awasthi, S., Wojcechowskyj, J. A. & Friedman, H. M. Anterograde spread of herpes simplex virus type 1 requires glycoprotein E and glycoprotein I but not Us9. *J. Virol.* **83,** 8315–8326 (2009).

134. Schwartz, O. & Albert, M. L. Biology and pathogenesis of chikungunya virus. *Nat. Rev. Microbiol.* 1–10 (2010). doi:10.1038/nrmicro2368

135. Long, K. M. *et al.* γδ T Cells Play a Protective Role in Chikungunya Virus-Induced Disease. *J. Virol.* **90,** 433–443 (2015).

136. Long, K. M. *et al.* Dendritic cell immunoreceptor regulates Chikungunya virus pathogenesis in mice. *J. Virol.* **87,** 5697–5706 (2013).

137. Hise, A. G. *et al.* An essential role for the NLRP3 inflammasome in host defense against the human fungal pathogen Candida albicans. *Cell Host and Microbe* **5,** 487–497 (2009).

138. Solis, N. V. & Filler, S. G. Mouse model of oropharyngeal candidiasis. *Nat Protoc* **7,** 637–642 (2012).

139. Schmidt, E., Torre, della, R. & Borradori, L. Clinical Features and Practical Diagnosis of Bullous Pemphigoid. *Immunology and Allergy Clinics of NA* **32,** 217–232 (2012).

140. Ujiie, H., Nishie, W. & Shimizu, H. Pathogenesis of Bullous Pemphigoid. *Immunology and Allergy Clinics of NA* **32,** 207–215 (2012).

141. Iwata, H. & Kitajima, Y. Bullous pemphigoid: role of complement and mechanisms for blister formation within the lamina lucida. *Exp Dermatol* **22,** 381–385 (2013).

142. Liu, Z. *et al.* The role of complement in experimental bullous pemphigoid. *J. Clin. Invest.* **95,** 1539–1544 (1995).

143. Liu, Z. *et al.* A critical role for neutrophil elastase in experimental bullous pemphigoid. *J. Clin. Invest.* **105,** 113–123 (2000).

144. Liu, Z. *et al.* A major role for neutrophils in experimental bullous pemphigoid. *J. Clin. Invest.* **100,** 1256–1263 (1997).

145. Liu, Z. *et al.* Subepidermal Blistering Induced by Human Autoantibodies to BP180 Requires Innate Immune Players in a Humanized Bullous Pemphigoid Mouse Model. *Journal of autoimmunity* **31,** 331–338 (2008).

146. Lin, L. *et al.* Eosinophils Mediate Tissue Injury in the Autoimmune Skin Disease Bullous Pemphigoid. *J Investig Dermatol* **138,** 1032–1043 (2018).

147. Li, C. *et al.* Experimental atopic dermatitis depends on IL-33R signaling via MyD88 in dendritic cells. *Nature Publishing Group* 1–11 (2017). doi:10.1038/cddis.2017.90

148. Ahmad, M. *et al.* Identification and characterization of murine caspase-14, a new member of the caspase family. *Cancer Res* **58,** 5201–5205 (1998).

149. Mikolajczyk, J., Scott, F. L., Krajewski, S., Sutherlin, D. P. & Salvesen, G. S. Activation and Substrate Specificity of Caspase-14 †. *Biochemistry* **43,** 10560–10569 (2004).

150. Chowdhury, D. & Lieberman, J. Death by a Thousand Cuts: Granzyme Pathways of Programmed Cell Death. *Annu. Rev. Immunol.* **26,** 389–420 (2008).

151. Lin, L. *et al.* Dual targets for mouse mast cell protease-4 in mediating tissue damage in experimental bullous pemphigoid. *J. Biol. Chem.* **286,** 37358–37367 (2011).

152. Tomimori, Y. *et al.* Role of mast cell chymase in allergen-induced biphasic skin reaction. *Biochem Pharmacol* **64,** 1187 (2002).

153. Terakawa, M., Tomimori, Y., Goto, M. & Fukuda, Y. Mast cell chymase induces expression of chemokines for neutrophils in eosinophilic EoL-1 cells and mouse peritonitis eosinophils. *Eur J Pharmacol* **538,** 175–181 (2006).

154. de Veer, S. J. *et al.* Selective Substrates and Inhibitors for Kallikrein-Related Peptidase 7 (KLK7) Shed Light on KLK Proteolytic Activity in the Stratum Corneum. *J Investig Dermatol* **137,** 430–439 (2017).

155. Naik, S. M. *et al.* Human Keratinocytes Constitutively Express Interleukin-18 and Secrete Biologically Active Interleukin-18 After Treatment with Pro-Inflammatory Mediators and Dinitrochlorobenzene. *J Investig Dermatol* **113,** 766–772 (1999).

156. Abu-Humaidan, A. H. Persistent Intracellular Staphylococcus aureus in Keratinocytes Lead to Activation of the Complement System with Subsequent Reduction in the Intracellular Bacterial Load. 1–14 (2018). doi:10.3389/fimmu.2018.00396&domain=pdf&date_stamp=2018-03-01

157. Arkwright, P. D. Staphylococcus aureus Internalized by Skin Keratinocytes Evade Antibiotic Killing. *fmicb-10-02242.tex* 1–10 (2019). doi:10.3389/fmicb.2019.02242

158. Prabhakara, R. *et al.* Epicutaneous model of community-acquired Staphylococcus aureus skin infections. *Infect Immun* **81,** 1306–1315 (2013).

159. Hu, J., Cladel, N. M., Budgeon, L. R., Balogh, K. K. & Christensen, N. D. The Mouse Papillomavirus Infection Model. *Viruses* **9,** 246 (2017).

160. MacLeod, D. T., Nakatsuji, T., Wang, Z., di Nardo, A. & Gallo, R. L. Vaccinia virus binds to the scavenger receptor MARCO on the surface of keratinocytes. *J Investig Dermatol* **135,** 142–150 (2015).

161. Laureti, M., Narayanan, D., Rodriguez-Andres, J., Fazakerley, J. K. & Kedzierski, L. Flavivirus Receptors: Diversity, Identity, and Cell Entry. *Front. Immunol.* **9,** 2180–2180 (2018).

162. Lim, P.-Y., Behr, M. J., Chadwick, C. M., Shi, P.-Y. & Bernard, K. A. Keratinocytes are cell targets of West Nile virus in vivo. *J. Virol.* **85,** 5197–5201 (2011).

163. Nestle, F. O., Di Meglio, P., Qin, J.-Z. & Nickoloff, B. J. Skin immune sentinels in health and disease. *Nature Reviews Immunology* 1–13 (2009). doi:10.1038/nri2622

164. Jiang, S., Gu, H., Zhao, Y. & Sun, L. Teleost Gasdermin E Is Cleaved by Caspase 1, 3, and 7 and Induces Pyroptosis. *The Journal of Immunology* **203,** 1369–1382 (2019).

165. Jiang, S., Zhou, Z., Sun, Y., Zhang, T. & Sun, L. Coral gasdermin triggers pyroptosis. *Sci. Immunol.* **5,** (2020).

166. Saeki, N. & Sasaki, H. in *Endothelium and Epithelium* (eds. Carrasco, J. & Mota, A.) 193–211 (Nova Science Publishers, 2011).

167. Wilmanski, J. M., Petnicki-Ocwieja, T. & Kobayashi, K. S. NLR proteins: integral members of innate immunity and mediators of inflammatory diseases. *J Leukoc Biol* **83,** 13–30 (2008).

168. Seaman, J. E. *et al.* Cacidases: caspases can cleave after aspartate, glutamate and phosphoserine residues. *Cell Death Differ* 1–10 (2016). doi:10.1038/cdd.2016.62

169. Panganiban, R. A. *et al.* A functional splice variant associated with decreased asthma risk abolishes the ability of gasdermin B to induce epithelial cell pyroptosis. *J Allergy Clin Immunol* **142,** 1469–1478.e2 (2018).

170. Hou, J. *et al.* PD-L1-mediated gasdermin C expression switches apoptosis to pyroptosis in cancer cells and facilitates tumour necrosis. *Nat Cell Biol* **22,** 1264–1275 (2020).

171. Li, J.-Y. *et al.* The zebrafish NLRP3 inflammasome has functional roles in ASC-dependent interleukin-1β maturation and gasdermin E–mediated pyroptosis. *J. Biol. Chem.* **295,** 1120–1141 (2020).

172. Wang, Z. *et al.* Zebrafish GSDMEb Cleavage-Gated Pyroptosis Drives Septic Acute Kidney Injury In Vivo. *The Journal of Immunology* **204,** 1929–1942 (2020).

173. LaRock, C. N. *et al.* IL-1β is an innate immune sensor of microbial proteolysis. *Sci. Immunol.* **1,** (2016).

174. Pang, I. K. & Iwasaki, A. Inflammasomes as mediators of immunity against influenza virus. *Trends in Immunology* **32,** 34–41 (2011).

175. De Schutter, E. *et al.* Punching Holes in Cellular Membranes: Biology and Evolution of Gasdermins. *Trends in Cell Biology* (2021).

176. Upham, N. S., Esselstyn, J. A. & Jetz, W. Inferring the mammal tree: Species-level sets of phylogenies for questions in ecology, evolution, and conservation. *PLOS Biology* **17,** e3000494 EP – (2019).

177. Yoon, S. & Leube, R. E. Keratin intermediate filaments: intermediaries of epithelial cell migration. *Essays Biochem* **63,** 521–533 (2019).

178. Gutowska-Owsiak, D., Podobas, E. I., Eggeling, C., Ogg, G. S. & Bernardino de la Serna, J. Addressing Differentiation in Live Human Keratinocytes by Assessment of Membrane Packing Order. *Frontiers in Cell and Developmental Biology* **8,** 1078 (2020).

179. Olde Engberink, R. H. G., Selvarajah, V. & Vogt, L. Clinical impact of tissue sodium storage. *Pediatr Nephrol* **35,** 1373–1380 (2020).